INFORMATION TO USERS

UNIVERSITY OF OKLAHOMA

GRADUATE COLLEGE

CALCITE-WATER REACTION RATES
AT RESERVOIR CONDITIONS

A Dissertation

SUBMITTED TO THE GRADUATE FACULTY

in partial fulfillment of the requirements for the

degree of

Doctor of Philosophy

By

SATAVISA SARKAR
Norman, Oklahoma
2002

UMI Number: 3034885

UMI®

CALCITE-WATER REACTION RATES
AT RESERVOIR CONDITIONS

A Dissertation APPROVED FOR THE
SCHOOL OF GEOLOGY AND GEOPHYSICS

BY

James M. Forgotson

ACKNOWLEDGEMENTS

TABLE OF CONTENTS

LIST OF TABLES

LIST OF FIGURES

LIST OF APPENDICES

ABSTRACT

Calcite dissolution rates were experimentally investigated at elevated temperatures to determine the effects of temperature, hydrodynamics, solution pH, P_{CO_2}, and saturation state. Based on the data, a master rate equation was derived that describes dissolution rates over the entire range of conditions in these experiments. The results were compared to other published dissolution rates at elevated temperatures.

The study was further extended to dissolution of calcite in high ionic strength solutions at elevated temperatures. The experiments were performed for a range of solution ionic strengths, hydrodynamic conditions, P_{CO_2}, and temperatures. A rate law based on the solution saturation state was fit to the results from batch experiments. The temperature dependence of rates was determined from the flow-through experiments and the ionic strength dependence was determined from the batch experiments. These experimental results yield insights into calcite reactions in formation brines.

A numerical model was developed for predicting calcite scale precipitation in near-wellbore regions during water flooding and petroleum recovery operations. Rate equations based on the experimental studies were used to calculate the precipitation of calcite scale. Precipitation of scale, in time and space, was predicted as a function of temperature, formation brine chemistry,

and solution flow rate. Existing models for predicting calcite scale precipitation are often based only on equilibrium assumptions. The model proposed in this study is a simplistic formulation that includes kinetic considerations.

Attempts were made to express calcite reactions in terms of surface complexation occurring at the calcite-water interface for dissolution at elevated temperatures. This would permit an interpretation of calcite-water reaction in terms of actual surface species acting as intermediaries or "activated complexes" in the reaction steps. Surface speciations were done for solutions of various chemistries (solution chemistries used in the experiments in this study). Rate data and the surface densities were fit to surface complexation-based rate equations and rate constants were determined using multiple linear regression. The study suggests that further investigation is necessary to identify the surface complexes that can satisfactorily describe dissolution rates at elevated temperatures.

CHAPTER 1

Overview

Calcite dissolution kinetics has been well-studied at surface temperature and pressure conditions addressing various aspects of physical and chemical parameters that influence calcite-water reaction rates (Berner and Morse, 1974; Plummer et al., 1978, 1979; Morse, 1983; Sjoberg and Rickard, 1984; Chou et al., 1989; Van Cappellen et al., 1993; Arakaki and Mucci, 1995; Dreybrodt et al., 1996, Nilsson and Sternbeck, 1999; Teng et al., 2000). These studies provide the theoretical background and database necessary to understand processes such as karst development and certain aspects of the earth's carbon cycle. However, relatively few studies have been done on calcite-water reaction rates at elevated temperatures (Talman, et al., 1990; Shiraki and Brantley, 1995). In addition, the influence of ionic strength on calcite reaction rates in aqueous solution is not well understood (Zuddas and Mucci, 1998), especially at elevated temperatures. Investigations of these aspects can lead to a better understanding of reservoir diagenesis, production conditions from sub-salt reservoirs and scale formation in industrial processes involving water heating-cooling and degassing of CO_2. It may also contribute to a better understanding of the effects of geothermal activities and their possible applications to energy resources.

Calcite Dissolution at Elevated Temperatures

It is recognized that in addition to temperature and pressure, solution pH, P_{CO_2}, ionic strength, saturation state, hydrodynamic conditions and the presence of inhibiting inorganic species or organic ligands all play significant roles in calcite dissolution (Plummer et al., 1978, 1979). In the present study, dissolution rates at elevated temperatures were experimentally investigated as a function of temperature-pressure, solution pH, P_{CO_2}, saturation, and hydrodynamics (Chapter 2).

These experiments illustrated the relative importance of diffusional transport versus surface reaction in limiting calcite reaction rates at higher temperatures. A master rate equation encompassing the entire range of conditions in these experiments was derived. The results were compared with extrapolations of models, based on calcite growth in supersaturated regime at elevated temperatures. This tests the assumption that similar mechanisms are operative for dissolution and precipitation. Results were also compared with other dissolution data at elevated temperatures.

Calcite Reaction in Hot Brines

Calcite dissolution rates were also studied in saline solutions at elevated temperatures. Production wells and pipelines in sub-salt oil fields, which produce saline water, are often damaged by scaling. Calcite, one of the common scaling minerals, forms a relatively insoluble coating on the available metallic surfaces, restricting fluid flow significantly, increasing maintenance costs. Calcite reaction

2

rates in high ionic strength (0.1 to 0.9 molal) solutions have been studied at 25°C (Zuddas and Mucci, 1994, 1998). In the present study, dissolution at 70°C-150°C and in 0.7, 1, 2, and 4 molal sodium chloride solutions under varying conditions of P_{CO_2} and disc spinning rates, were investigated (Chapter 3). Two different experimental designs were used to conduct this part of the study— batch experiments and mixed-flow experiments. These designs will be discussed in Chapter 2 and 3.

An integrated form of rate law, based on the degree of solution saturation, was fit to the results from the batch experiments at varying salinities. Dissolution rates were obtained directly from steady-state experiments (mixed flow reactor setting) done using 0.7 m solutions at varying temperatures.

Reaction-Transport Model

Based on experimental results, a numerical model was developed for predicting calcite precipitation in near-wellbore regions during water flooding and petroleum recovery operations (Chapter 4). The geochemical program PHREEQC Interactive 2.4.2 (Parkhurst and Appelo, 2001) was used for this purpose. PHREEQCI can model solution speciation and one-dimensional transport in conjunction with locally occurring kinetically controlled reactions. Precipitation of calcite scale was predicted as a function of temperature, formation brine chemistry, and solution flow rate in time and space.

Surface Complexation

An attempt was made to express calcite-water reaction rates in terms of surface densities of complexes, which form as an intermediate step in the overall reaction (Chapter 5).

It is often necessary to specify pH-P_{CO_2} ranges over which a rate law may be valid. Integrating reaction rates with surface complexation allows the rate expressions to be comprehensive and applicable over a wide range of physical and chemical conditions instead of being restricted to a specific range of pH and P_{CO_2}. This is because the formation of complexes is reflective of these conditions and consequently any rate law expressed in terms of surface complexes will have these dependencies embedded in them.

Surface speciations were done for all solutions and experimental conditions in this study. The surface densities of complexes were determined based on a surface complexation model for carbonate minerals proposed by Van Cappellen et al. (1993). For calculating the solution speciation, participating reactions and surface complexations were modeled using PHREEQCI 2.4.2 (Parkhurst and Appelo, 2001). The observed dissolution rates and the surface densities determined using PHREEQCI were fit to a surface complexation-based rate equation and rate constants were determined using multiple linear regression. The results suggest that the rate equation may not be appropriate for expressing dissolution rates at elevated temperatures. Further investigation is necessary to identify the complexes, which can satisfactorily describe rates at these conditions.

Diagenetic Implications

The rates and rate equations obtained from this study are valid at reservoir temperatures. Due to constraints of the experimental apparatus pressures were lower than typical burial diagenetic (about 50 Mpa) conditions. However, effect of pressures on reaction kinetics is not significant in this range (between 7 and 50 Mpa) and these results should be valid at diagenetic conditions as well. Pressure does increase solubility and impact buried rocks significantly in terms of pore collapse, increase of pore pressure, remobilization of pore fluids, pressure solutions etc. Some of these are more in the domain of mechanical impacts than chemical. The most significant parameter in calcite precipitation-dissolution will probably be partial pressure of CO_2. Since Pco_2 is variable from basin to basin, or even within a basin, and more importantly on the timing of hydrocarbon migration, if any, or proximity to such migration pathways, such effects will have to be considered on an individual basis. The segments of the basins will need to be considered with a view to the particular burial history and fluid migration history of the area to evaluate these effects on its diagenetic evolution.

Diagenetic history of a rock is often deciphered from the petrographic observations. The two reaction mechanisms that are discussed in this study – transport control and surface reaction control, may be reflected in the rock texture. Reactions controlled by surface reaction rates occur when mineral is not at equilibrium with the surrounding fluid. Dissolutions under such conditions may lead to an uneven surface with a more corroded appearance. Whereas,

5

transport-controlled reactions are more likely to give rise to a smooth dissolution surface. However, it may be necessary to look at SEM (Scanning Electron Micrograph) to observe such textural expressions. It is also important to note that diagenetic changes occur over geologic periods of time. Kinetics is more relevant when there is a change in conditions within a short timeframe when the mineral is out of equilibrium with the surrounding fluid.

CHAPTER 2

Calcite Dissolution Rates at Elevated Temperatures as a Function of pH, Pco_2, Saturation, and Hydrodynamics

ABSTRACT

Calcite dissolution kinetics at temperatures near 100°C and 6.9 MPa was investigated focusing on the interrelated variables of saturation state, hydrodynamics, pH, and Pco_2. Experiments were performed in a mixed flow/ rotating disc reactor under constant flow-through, temperature, and pressure conditions. Influent solutions were prepared by bubbling double distilled water with mixtures of CO_2 and N_2 gas, and in some cases with HCl or NaOH, resulting in an inlet pH range of 3.9 to 8, and Pco_2 from 0.0 to 0.1 MPa. Carrara Marble discs were mounted on an Inconel stir bar inside a titanium reactor with a magnetic stirring housing, and spun from 50 to 900 rpm. Rates were determined directly from differences in Ca^{2+} concentration between influent and effluent solutions. By examining how rates of dissolution vary with spinning rate, one can assess the degree to which transport through a hydrodynamic boundary layer is rate limiting for the reaction kinetics. Degree of saturation Ω (defined as the ratio of ion activity product to equilibrium constant) of effluent solutions varied from 0.01-0.40.

Results indicate that the rate of calcite dissolution has a nonlinear dependence on saturation state for all the pH regimes at moderate to high P_{CO_2}. A mixed transport-surface reaction control (i.e. a rate dependence on both interfacial solid-fluid reaction and transport through the hydrodynamic boundary layer) was observed for solutions with higher P_{CO_2} and lower pH. For reactions at similar pH but low P_{CO_2}, rates were transport controlled. At near neutral to alkaline regions, reaction at higher P_{CO_2} displayed mixed rate control. All experiments with low P_{CO_2} showed transport controlled kinetics. These results indicate that as P_{CO_2} increases, surface reaction and transport become competing processes in determining the overall rate of calcite dissolution. No change in reaction mechanism was evidenced in response to temperature increases between 70 -130°C.

The mechanistic model of Plummer et al. (1978), which is often used to describe calcite reaction at low temperature and ionic strength, was able to capture the quantitative form of the saturation dependence of dissolution rates at a given stirring rate. However, the Plummer model did not account for the obvious transport influence observed in all experiments. An alternative model that best fits this data is derived from considering a surface saturation state determined from a balance of reactive and diffusive fluxes at the calcite-water interface. The resulting rate equation

$$R = k_t \left[1 - \Omega_b^{\pm} + \zeta \left\{ 1 - \sqrt{(1 + 2(1 - \Omega_b^{\pm})/\zeta)} \right\} \right]$$

Is valid at 100°C, pH from 4 to 8, Pco_2 from 10^{-5} to 0.3 MPa, and spinning rates from 50 to 900 rpm, and predicts experimental rates to an excellent degree. In the above equation, k_t is $(Dm_{eq})/\delta$, D is the diffusion coefficient, m_{eq} is the mean ionic molal equilibrium concentration and δ is the thickness of the hydrodynamic boundary layer. $\Omega_b^{\pm}$ is the mean ionic bulk saturation and ζ represents $(Dm_{eq})/2\delta k^{+}$, and k^{+} equals $k_2 Pco_2 + k_3$, where k_2 and k_3 are constant at a given temperature. The resulting fit parameters are $k_t = 3.488e{-}7 * m_{eq} * (Spin)^{1/2}$ mole/cm^2-s, $k_2 = 2.15e{-}7$ mole/cm^2-MPa-s, and $k_3 = 9.409e{-}8$ mole/cm^2-s.

INTRODUCTION

Calcite is one of the most abundant rock-forming minerals in the upper crust and its reactive nature allows it to precipitate and dissolve extensively at surface conditions as well as at higher temperatures and pressures. Reaction of calcite in seawater is an important control on global carbon cycling (Berner and Morse, 1974; Berner, 1995; Zuddas and Mucci, 1998). Numerous studies have been done in the past few decades to identify the chief factors controlling the reaction rates of calcite at or near surface conditions (Nancollas and Reddy, 1971; Plummer et al., 1978 and 1979; Reddy et al., 1981; Morse, 1983; Nielsen, 1983; Sjoberg and Rickard, 1984; Compton and Daly, 1984 and 1987; Inskeep and Bloom, 1985 and 1986; Busenberg and Plummer, 1986; Chou et al., 1989; Compton and Pritchard, 1990; Wollast, 1990; Brown et al., 1993; Dove and Hochella, 1993; Van Cappellen, 1993; Arakaki and Mucci, 1995; Dreybrodt et al.,

1996; Lebron and Suarez, 1998; Zuddas and Mucci, 1998; Kile et al., 2000; Davis et al., 2000; Teng et al., 2000).

Few investigations have examined rates of calcite reaction at elevated temperatures, presumably because the rapid kinetics favors equilibration of calcite-water systems over time scales of interest. Interest in diverse areas such as reservoir diagenesis, problems of scale formation in industrial processes involving water heating-cooling and degassing of CO_2, hydrothermal activities at mid-oceanic ridges, geothermal applications, and CO_2 sequestration have prompted some studies on calcite-water reaction kinetics at elevated temperatures (Talman et al., 1990; Shiraki and Brantley, 1995). Rate data is relevant for such cases when rapid change in conditions may not allow for mineral-fluid equilibrium to be established. The current study investigates calcite dissolution kinetics at conditions near 100°C and 6.9 MPa, focusing on the effects of saturation state, hydrodynamics, Pco_2 and pH. The construction of a rate equation valid over these conditions enables assessment of the validity of local equilibrium assumptions.

THEORETICAL BACKGROUND

Lower Temperature and Pressure

Previous investigations on calcite-water reactions that are most relevant to the current study are discussed in detail in this section. Plummer et al. (1978; 1979) studied calcite dissolution kinetics at 5°-60°C, a pH of 2–7 and 0.0 to 0.1 MPa Pco_2. Crushed Iceland Spar grains were used as solid reactants in batch

reactors under pH-stat and free-drift methods. They suggested a mechanistic model for the dissolution of calcite that proceeds via three parallel elementary reactions:

$$CaCO_3 + H^+ \overset{k_1}{=} Ca^{2+} + HCO_3^- \qquad (1)$$

$$CaCO_3 + H_2CO_3^* \overset{k_2}{=} Ca^{2+} + 2HCO_3^- \qquad (2)$$

$$CaCO_3 + H_2O \overset{k_3}{=} Ca^{2+} + HCO_3^- + OH^- \qquad (3)$$

At far-from-equilibrium conditions and low pH, Plummer et al. (1978) reported a first-order dependence on bulk fluid H^+ activity. Described by reaction (1), rates under these conditions were found to vary as a function of stirring rate, implying that diffusive transport of protons through a boundary layer existing at solid-fluid interfaces was rate limiting. With increasing Pco_2, a linear dependence on Pco_2 was reported for far-from-equilibrium conditions, represented by reaction (2). At near-neutral pH with very little to no dissolved CO_2, rates were found to be independent of either pH or Pco_2, as represented by reaction (3).

The overall rate of dissolution is given by the rate law:

$$R = k_1 aH^+ + k_2 aH_2CO_3^* + k_3 aH_2O - k_4 aCa^{2+} aHCO_3^- \qquad (4)$$

where k_1, k_2 and k_3 are forward rate constants dependent on temperature and k_4 accounts for the backward reaction and is a function of both temperature and Pco_2. k_1 has an additional stirring rate-dependence, reflecting the transport control at low pH. At near-equilibrium conditions, the rate of backward reaction

11

becomes important in rate determination. It is driven by interaction of Ca^{2+} and HCO_3^- with the surface adsorption layer.

Calcite dissolution in aqueous KCl solutions under far-from-equilibrium conditions was studied using a rotating disc experimental design, between 1-62°C at a pH of 2.7 to 8.4 (Sjoberg and Rickard, 1984). The benefit of this design in controlling hydrodynamics near the solid-solution interface is discussed in a later section. A mixed reaction-transport control of rates was observed for neutral and alkaline solutions with transport-control behavior dominating for acidic conditions. They describe this "mixed kinetics" behavior using a rate law expressed as a combination of transport controlled and surface-controlled rate equations.

Dreybrodt and Buhmann (1991) considered hydrodynamics as a key influence on rates under some conditions. They calculated calcite dissolution rates for varying flow velocities, using a specified thickness for the diffusion boundary layer (also known as the hydrodynamic boundary layer). These are thin layers of solution at the mineral-fluid interface arising from friction between the solid and moving fluid. Concentration gradients can exist across the layer if diffusion is slow relative to surface reaction, and can limit the overall reaction rates. Dreybrodt and Buhmann (1991) observed good agreement between their predicted rates and dissolution rates observed by Herman (1982) for rotating-disc experiments at 25°C, 0.1 MPa over a boundary layer thickness of up to 0.02 cm.

Alkattan et al. (1998) studied calcite dissolution as a function of pH and temperature within a pH range of −1 to 3 and a temperature of 25 − 80°C. Single

calcite crystals were dissolved in hydrochloric acid solutions with a free-drift rotating disc setup. Logarithms of overall calcite dissolution rates for a constant disc rotation speed were found to be inversely proportional to the bulk solution pH. Rate constants and H^+ diffusion coefficients were found to increase with temperature.

Another approach in deriving a rate model for calcite reaction in aqueous solution has been to relate it to surface speciation at the mineral-fluid interface (Van Cappellen et al., 1993; Arakaki and Mucci, 1995; Nilsson and Sternbeck. 1999). Due to complexities of multiple interacting factors such as pH, P_{CO_2}, and temperatures in controlling rates, rate models are usually specific to a certain range of conditions instead of a single model encompassing the entire gamut of conditions over which calcite growth and dissolution occurs. It is widely held that the rates of surface complexation reactions limit the surface attachment (precipitation) and detachment (dissolution) kinetics. Surface complexation reactions are true elementary reactions, and as such, rates may be expressed as a simple linear function of surface concentrations (Morse, 1986; Chou et al, 1989; Arakaki and Mucci, 1995; Brady et al, 1996; Nilsson and Sternbeck 1999).

It is of relevance to also make a note of some recent studies on calcite growth, which have attempted to relate microscopic surface processes with macroscopic rates described by overall rate laws for calcite-fluid reactions (Dove and Hochella, 1993; Teng et al., 2000). In situ Atomic Force Microscopy was used to quantify calcite growth rates from measured advancements of steps and surface slopes under varying degrees of supersaturation. The variation in surface

structure triggered differences in growth mechanisms. These workers argue that for identification of the true nature of the growth mechanism, formulation of rate laws and better prediction of rates, such microscopic level observations are critical.

Elevated Temperature and Pressure

Talman et al. (1990) investigated calcite dissolution at temperatures between 100° and $210^{\circ}C$ under varying stirring rates and P_{CO_2}. Iceland spar rhombs mounted in a stirred batch reactor were used as solid reactants. They observed good agreement with the Plummer et al. (1978 and 1979) model, especially at low pH conditions for which a stirring influence was dominant. Reactions under high dissolved CO_2 displayed an apparent change in reaction mechanism at temperatures above $100^{\circ}C$. They were unable to propose a mechanism with any degree of confidence based on their data. A linear dependence on P_{CO_2} for high dissolved CO_2 conditions was also reported.

Calcite precipitation kinetics at $100^{\circ}C$ and 10.0 MPa was studied by Shiraki and Brantley (1995). They described their data with respect to degree of saturation Ω (ratio of ion activity product and solubility product) and proposed rate models for surface-reaction controlled rates based on known mineral growth mechanisms. The reactant solutions had pH ranges of 6.8 – 7.6 and a P_{CO_2} of 3 $\times 10^{-4}$ to 1 $\times 10^{-2}$ MPa. At stirring speeds of 1200 rpm, experiments with low P_{CO_2} and saturation states showed a parabolic rate dependence on Ω corresponding to a spiral growth mechanism (Blum and Lasaga, 1987). For higher P_{CO_2}, rates

increased linearly with saturation and a surface adsorption growth mechanism was interpreted for this series. The Plummer et al. (1978) model could describe the observed parabolic dependence. However, data at higher CO_2 concentrations were not described well by this model.

Summarizing studies on calcite-fluid reactions in terms of the aforementioned approaches and findings, three major categories of rate laws have been proposed based on experimental results of macroscopic rate determination. These can categorized as elementary reaction-based, saturation state-based, and surface complexation-based rate expressions. The rate expressions are determined based on experiments using different experimental designs. For example, stirred reactors with calcite powders are used in one setup whereas rotating disc of single crystals are used in another. Mixed flow systems have been used as against batch experiments. Key roles are assigned to solution pH, P_{CO_2}, hydrodynamics, saturation state, and the presence of rate-inhibiting organic or inorganic species. Microscopic studies attempt to obtain a better grasp on reaction mechanism and provide a link with macroscopic rate laws.

The current study is directed towards extending the database for dissolution behavior at elevated temperatures over a broader range of chemical conditions than previously studied. Polished marble in a rotating disc setup, similar to Sjoberg and Rickard (1984) was used for this study. This is chosen in lieu of the more common powder experiments, which suffer from poorly defined hydrodynamics at crystal-fluid interfaces (Compton and Daly, 1984; Dreybrodt and Buhmann, 1991). Furthermore, the large exposed surface area of powdered

solid allows rapid reaction and consequently large changes in reactive surface area concomitant with reaction progress. Studies on the effect of particle size in rate determination indicate that initial dissolution rate for coarser (e.g. > 62 μm) particles may be 1% that for finer (< 62 μm) particles. The change with extent of reaction is consequently much larger for finer particles and this is not accounted for simply by normalizing to BET surface area (Morse, 1978). A mixed-flow system was used instead of batch reactor so that reaction rates could be determined directly rather than using an integrated form of an assumed rate law (Talman et al., 1990).

The experiments showed the relative importance of transport versus surface reaction in limiting calcite reaction rates at higher temperatures. A master equation was derived that describes rates over the entire range of conditions in these experiments. Finally, these results are compared with other rates reported in the literature for elevated temperatures.

EXPERIMENTAL METHODS

The experiments were performed in a mixed flow/ rotating disc reactor. In this set-up, the disc was mounted on an Inconel™ stir bar inside a titanium reactor fitted with a magnetic stirring housing and was immersed in reactive fluid (Figure 2.1). An impeller was also attached to the shaft to ensure that the solution was well-mixed and fresh reactive solution was continuously directed towards the mineral surface. The reactant solution, contained in a Nalgene™ tank, was continuously fed into the reactor via a high pressure liquid

chromatography (HPLC) pump. Depending on the desired saturation and/ or pH condition of the reactive fluid, carbon dioxide and/ or nitrogen gas was bubbled into this tank prior to and during the experiments. All valves, tubing, reactor components, and pump-wetted parts that the solution contacts prior to reaction with calcite are composed of reactively inert material (PEEK^{TM}, titanium, Inconel^{TM}, gold, Nalgene^{TM}). Disc spinning rates and solution flow rates were held constant during each experiment. The disc spinning rate determines the hydrodynamic condition at the mineral-fluid interface. The solution flow rate controls the degree of saturation, as faster flow results in a solution that is more undersaturated. The effluent solution was collected for analysis after approximately four residence times (one residence time equals reactor volume divided by solution volumetric flow rate). Pressure inside the reactor and constant flow conditions were maintained downstream of the reactor by a backpressure regulator. Chemical analysis of the outlet solution for Ca^{2+} concentration was performed in triplicate using standard atomic absorption techniques. The pH of influent solutions was measured with a ROSS^{TM} Combination electrode.

Carrara Marble was used as the solid reactant for all the dissolution experiments. Marble slabs were cored into 4 cm diameter cylinders, which were then sliced into 0.75 cm thick discs. The discs were cast in epoxy, keeping one surface exposed. The exposed surface was polished successively down to 5 μm grit and all other surfaces were coated with PFA Teflon. After polishing, the samples were kept in hot water overnight for annealing. Quantitative electron

microprobe analysis for elemental composition indicates the sample to be relatively pure with impurities constituting less than 0.5% by weight (Table 2.A.1).

This study utilized a range of reactive solutions. Double-deionized water equilibrated with atmospheric CO_2, distilled water continuously bubbled with N_2, CO_2, or N_2-CO_2 mixtures, and gas-bubbled solutions with added NaOH or HCl were used to investigate a variety of P_{CO_2} and pH conditions (Table 2.1).

The total inorganic carbon (TIC) of the inlet solutions was determined from alkalinity and measured in situ pH using SOLMINEQ88 (Kharaka et. al., 1988). The TIC of the effluent solutions is given by $TIC_{out} = TIC_{in} + \Delta Ca$ (Shiraki and Brantley, 1995), where ΔCa is the difference in Ca^{2+} concentration of outlet and inlet solutions. The solution pH is given by the negative logarithm of mH^+. The mH^+ was calculated using alkalinity and TIC_{out} by simultaneous solution of the following equations:

$$Alkalinity = mHCO_3^- + 2mCO_3^{2-} + mOH^- - mH^+ \qquad (5)$$

$$TIC = mH_2CO_3 + mHCO_3^- + mCO_3^{2-} \qquad (6)$$

plus mass action constraints for carbonic acid and water dissociation.

The alkalinity was determined using the charge balance equation above. Using the above inputs, saturation index (log of saturation) was determined by the geochemical programs SOLMINEQ88 (Kharaka et. al., 1988), PHREEQC (Parkhurst, et al, 1995) and PHREEQC Interactive Alpha Version 2.4.2 (Parkhurst and Appelo, 2001). The results from the programs matched closely

Figure 2.1 Experimental design: mixed flow/ rotating disc reactor
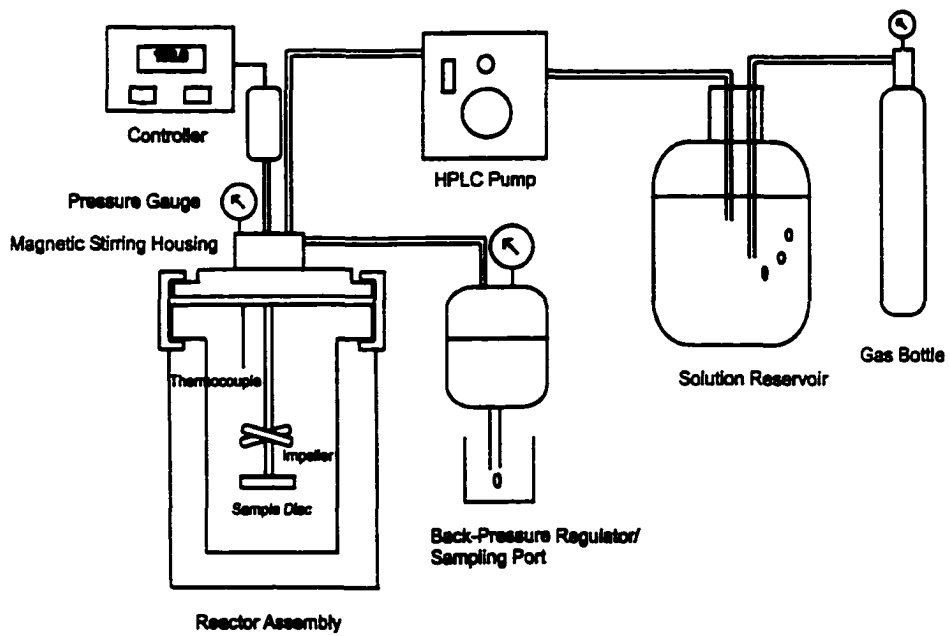
Figure 2.2 (1 – Ω) given by saturation index (SI) modeled using SOLMINEQ88 and PHREEQCI are in close agreement.
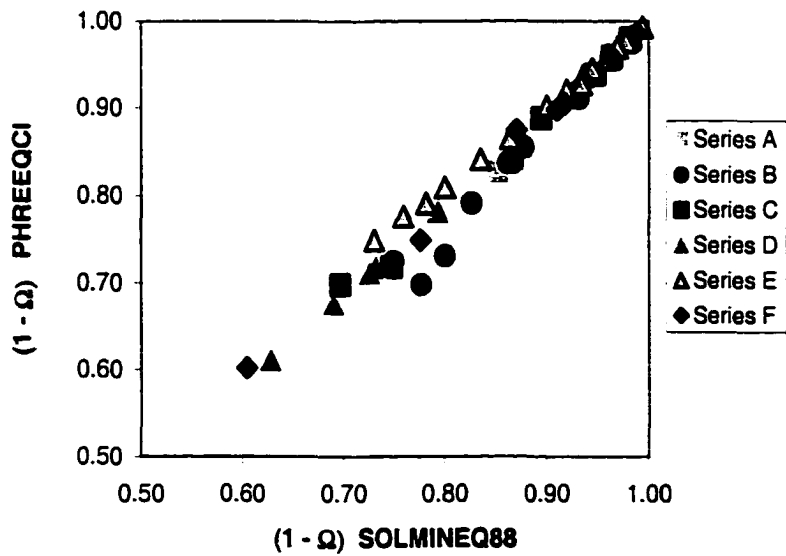
Table 2.1 Inlet solution and gas bubbled for all the series and their respective inlet pH and inlet TIC

Series	Inlet Solution-Gas head	Inlet pH	Inlet TIC (mole/ kg)
A	Double deionized water — N_2	7.5	None
B	Double deionized water	5.5	2.6×10^{-5}
C	Double deionized water — CO_2–N_2 mixture	4.5	$1.5 - 3 \times 10^{-3}$
D	NaOH solution — CO_2	7.0	$2.15 - 2.2 \times 10^{-1}$
E	Double deionized water — CO_2	3.9 – 4.0	$3 - 3.5 \times 10^{-2}$
F	Dilute hydrochloric acid solution — N_2	4.0	None

Table 2.2 Experimental parameters and results

Series	Spin (rpm)	Flow rate (g/ min)	ΔCa2+ (mole/ kg)	pH out (calculated)	Alkalinity (mole/ kg)	Total TIC (mole/ kg)	Dissolution Rate (mole/ cm^2-s)
A	302	4.74	7.54E-05	8.10	1.51E-04	7.54E-05	5.31E-10
	601	9.35	6.07E-05	8.01	1.21E-04	6.07E-05	8.43E-10
	301	9.33	4.92E-05	7.92	9.85E-05	4.92E-05	6.82E-10
	901	9.25	9.35E-05	8.19	1.87E-04	9.35E-05	1.28E-09
	301	3.14	9.62E-05	8.20	1.92E-04	9.62E-05	4.48E-10
B	301	8.61	7.59E-05	7.94	1.52E-04	1.02E-04	9.56E-10
	599	8.57	9.61E-05	8.07	1.92E-04	1.22E-04	1.20E-09
	904	8.63	9.23E-05	8.06	1.85E-04	1.18E-04	1.17E-09
	901	9.15	9.58E-05	8.07	1.92E-04	1.22E-04	1.28E-09
	300	4.87	9.27E-05	8.06	1.85E-04	1.18E-04	6.60E-10
	300	2.15	1.16E-04	8.18	2.31E-04	1.41E-04	3.63E-10
	300	7.37	7.86E-05	7.96	1.57E-04	1.04E-04	8.60E-10
	300	3.46	1.05E-04	8.12	2.10E-04	1.31E-04	5.39E-10
	301	2.19	1.19E-04	8.20	2.39E-04	1.45E-04	3.88E-10
	301	5.06	1.14E-04	8.17	2.27E-04	1.39E-04	8.53E-10
C	300	8.89	2.80E-04	6.07	5.59E-04	1.71E-03	3.63E-09
	301	1.45	6.18E-04	6.57	1.24E-03	2.04E-03	1.31E-09
	301	5.00	3.94E-04	6.25	7.88E-04	1.85E-03	2.88E-09
	601	8.69	3.76E-04	5.82	7.52E-04	3.50E-03	4.77E-09
	902	8.67	3.91E-04	6.10	7.81E-04	2.27E-03	4.95E-09
	300	1.08	7.03E-04	6.58	1.41E-03	2.13E-03	1.11E-09
	300	3.11	5.05E-04	6.37	1.01E-03	1.97E-03	2.30E-09
	300	0.61	8.89E-04	6.76	1.78E-03	2.35E-03	7.97E-10
D	300	8.62	1.90E-05	6.95	1.72E-01	2.18E-01	2.39E-10
	599	8.66	2.36E-05	6.97	1.72E-01	2.16E-01	2.99E-10
	902	8.70	2.72E-05	6.98	1.72E-01	2.15E-01	3.46E-10
	300	4.31	2.51E-05	6.95	1.72E-01	2.18E-01	1.59E-10
	300	1.57	3.13E-05	6.99	1.72E-01	2.14E-01	7.18E-11
E	301	8.33	8.70E-04	5.10	1.74E-03	3.54E-02	1.08E-08
	601	8.30	1.18E-03	5.23	2.36E-03	3.57E-02	1.43E-08
	900	8.36	1.32E-03	5.29	2.65E-03	3.50E-02	1.64E-08
	300	4.10	1.47E-03	5.36	2.94E-03	3.37E-02	8.81E-09
	300	1.67	2.08E-03	5.52	4.16E-03	3.43E-02	5.15E-09
	300	6.05	1.29E-03	5.36	2.59E-03	3.00E-02	1.14E-08
	300	8.71	9.05E-04	5.15	1.81E-03	3.24E-02	1.15E-08
	301	9.33	8.94E-04	5.20	1.79E-03	2.89E-02	1.22E-08
	300	8.11	1.04E-03	5.22	2.08E-03	3.25E-02	1.23E-08
	301	2.79	1.55E-03	5.41	3.10E-03	3.23E-02	6.31E-09

Series	Spin (rpm)	Flow rate (g/ min)	ΔCa2+ (mole/ kg)	pH out (calculated)	Alkalinity (mole/ kg)	Total TIC (mole/ kg)	Dissolution Rate (mole/ cm^2-s)
	600	3.25	2.03E-03	5.50	4.06E-03	3.50E-02	9.65E-09
	601	4.93	1.65E-03	5.44	3.30E-03	3.24E-02	1.19E-08
	600	2.62	1.97E-03	5.52	3.94E-03	3.27E-02	7.53E-09
	900	2.89	2.13E-03	5.59	4.26E-03	3.08E-02	9.01E-09
	900	4.86	1.85E-03	5.49	3.69E-03	3.26E-02	1.31E-08
	599	2.10	2.11E-03	5.55	4.23E-03	3.29E-02	6.48E-09
	53	8.00	5.87E-04	4.98	1.17E-03	3.06E-02	6.86E-09
	50	1.30	1.76E-03	5.45	3.52E-03	3.32E-02	3.35E-09
F	301	8.56	1.19E-04	7.77	1.50E-04	1.19E-04	1.06E-09
	601	8.53	1.03E-04	7.56	1.18E-04	1.03E-04	1.29E-09
	901	8.58	1.22E-04	7.77	1.55E-04	1.22E-04	1.53E-09
	301	4.30	1.27E-04	7.83	1.64E-04	1.27E-04	7.95E-10
	301	1.75	1.67E-04	8.11	2.44E-04	1.67E-04	4.28E-10
	301	1.62	1.49E-04	8.01	2.08E-04	1.49E-04	3.53E-10
	300	8.50	8.80E-05	7.22	8.70E-05	8.80E-05	1.09E-09

with each other (Table 2.A.2; Figure 2.2). Saturation Ω is given as a ratio of ion

activity product for calcium and carbonate ions, to the solubility product of calcite.

Rates were determined using the following equation (Table 2.2).

$$R = \frac{(Ca^{2+}_{out} - Ca^{2+}_{in}) \cdot Flow\ rate}{Disc\ surface\ area} \quad \frac{moles/\ Kg\ \cdot\ Kg/\ sec}{cm^2} \tag{7}$$

RESULTS AND DISCUSSION

Reactive Surface Area

Surface roughening due to dissolution produces an increase in the

reactive surface area of solid, thereby increasing dissolution. This in turn, might

lead to an overestimation of reaction rates. To determine the effect on rates,

samples for several experiments were collected at the end of each residence

time and analyzed for Ca^{2+} concentration. A typical concentration-time profile

shows that the rates (proportional to concentration for our experimental design)

rise and plateau after three residence times, indicating a steady state within 3 to

4 residence times (Figure 2.3). This suggests surface area increase was not

significant enough over the experimental time scale to affect the rate calculation.

The discs were discarded after a number of experiments if polishing did

not restore the surface back to its original condition. This ensured that samples

used were comparable in surface roughness (area) between experiments.

Pco₂, pH, Ionic Strength and Temperature

The solution chemistry at experimental conditions, including Pco_2 and ionic strength, were modeled using SOLMINEQ88 (Table 2.3 and 2.4). pH of the effluent solutions were calculated as described earlier (Experimental Methods). Dissolution data varying over a range of conditions, and a constant disc-spinning rate of 300 rpm, are plotted with respect to Pco_2, pH, and ionic strength (Figure 2.4 – 2.6). The rates are found to increase linearly from low to high Pco_2 series (Figure 2.4). The spread of rate values for each experimental series reflects a variation in saturation. Dissolution rates reported for 25°C within similar Pco_2 range (Plummer et al., 1978) are shown for comparison. Below a Pco_2 of 3.2 x 10^{-2} to 1 x 10^{-2} bar, rates were reported to be independent of Pco_2 (Berner and Morse, 1974; Plummer et al., 1978). Rates from the present study appear to display a similar general trend with respect to Pco_2, but they are higher as expected, due to elevated temperatures. When plotted as a function of in situ pH, dissolution rates are seen to increase with decreasing pH (Figure 2.5a). In Figure 2.5b, data from this study at 100°C, is compared to the dissolution rates observed at 25°C from several sources (Plummer et al., 1978; Sjoberg, 1978; Chou et al., 1989). The same overall trend for pH dependence is observed in all results although the rates are higher due to temperature. The observed rates also increase measurably with increasing ionic strength as rates increase from series A ($I = 10^{-4}$ molal) to series E ($I = 10^{-2}$ molal in Figure 2.6). Within each series, rates drop as solutions get higher in ionic strength, reflecting an increase in total dissolved solids and saturation. The effect of ionic strength has been

24

Table 2.3 SOLMINEQ88 output

Series	TDS (mg/L)	Ionic Strength (molal)	P_{CO_2} (bar)	$aH_2CO_3^*{}_{out}$	ΔG	Rate (mole/cm^2-s)
A	7.53	0.00022	1.13E-04	1.39E-06	-1.952	5.31E-10
	6.05	0.00018	1.14E-04	1.40E-06	-2.401	8.43E-10
	4.89	0.00015	1.16E-04	1.41E-06	-2.845	6.82E-10
	9.36	0.00028	1.13E-04	1.39E-06	-1.496	1.28E-09
	9.63	0.00028	1.17E-04	1.43E-06	-1.418	4.48E-10
B	9.09	0.00023	2.21E-04	2.72E-06	-1.997	9.56E-10
	11.14	0.00028	1.99E-04	2.43E-06	-1.467	1.20E-09
	11	0.00027	1.97E-04	2.41E-06	-1.535	6.60E-10
	13	0.00034	1.81E-04	2.20E-06	-1.031	3.63E-10
	8.98	0.00022	2.19E-04	2.68E-06	-1.992	8.60E-10
	11.85	0.00030	1.91E-04	2.34E-06	-1.297	5.39E-10
	12.72	0.00031	1.72E-04	2.13E-06	-1.109	3.88E-10
	12.91	0.00033	1.76E-04	2.17E-06	-1.103	8.53E-10
C	45	0.00083	9.37E-02	1.15E-03	-2.985	3.63E-09
	99	0.00180	6.52E-02	7.92E-04	-1.023	1.31E-09
	62	0.00116	8.74E-02	1.06E-03	-2.194	2.88E-09
	106	0.00200	6.67E-02	8.10E-04	-0.886	1.11E-09
	78	0.00146	8.15E-02	9.90E-04	-1.670	2.30E-09
	135	0.00251	5.54E-02	6.72E-04	-0.262	7.97E-10
D	14136.62	0.16024	2.71E+00	3.31E-02	-1.167	2.39E-10
	14129.62	0.16018	2.71E+00	3.32E-02	-0.958	1.59E-10
	14134.34	0.15955	2.46E+00	3.01E-02	-0.732	7.18E-11
E	138.49	0.00263	2.764	3.36E-02	-3.023	1.08E-08
	187.39	0.00356	2.696	3.32E-02	-2.397	1.43E-08
	209.23	0.00398	2.626	3.22E-02	-2.143	1.64E-08
	230.82	0.00441	2.506	3.07E-02	-1.869	8.81E-09
	326.52	0.00623	2.447	2.99E-02	-1.127	5.15E-09
	206.06	0.00390	2.230	2.73E-02	-2.039	1.14E-08
	142.51	0.00272	2.497	3.06E-02	-2.897	1.15E-08
	141.46	0.00269	2.212	2.71E-02	-2.824	1.22E-08
	167.15	0.00315	2.458	3.03E-02	-2.581	1.23E-08
	245.97	0.00467	2.374	2.90E-02	-1.707	6.31E-09
	321.06	0.00610	2.510	3.07E-02	-1.192	9.65E-09
	260.49	0.00494	1.108	1.36E-02	-1.037	1.19E-08
	312.34	0.00586	0.532	6.51E-03	-0.142	7.53E-09
	338.24	0.00641	2.147	2.63E-02	-0.972	9.01E-09
	293.21	0.00557	2.345	2.87E-02	-1.334	1.31E-08

Series	TDS (mg/L)	Ionic Strength (molal)	P_{CO2} (bar)	$aH_2CO_3^{*}{}_{out}$	ΔG	Rate (mole/cm^2-s)
	333.35	0.00634	2.324	2.84E-02	-1.055	6.48E-09
	92.27	0.00173	2.405	2.94E-02	-3.788	6.86E-09
	274.96	0.00527	2.416	2.96E-02	-1.477	3.35E-09
	105	0.00195	5.30E-01	6.49E-03	-2.591	4.93E-09
	125.9	0.00239	5.21E-01	6.37E-03	-1.988	4.96E-09
F	14.98	0.00036	3.95E-04	4.83E-06	-1.852	1.06E-09
	13.07	0.00031	5.22E-04	6.39E-06	-2.439	1.29E-09
	15.38	0.00037	3.99E-04	4.88E-06	-1.786	1.53E-09
	15.76	0.00038	2.98E-04	3.64E-06	-1.511	7.95E-10
	19.87	0.00050	2.14E-04	2.62E-06	-0.686	4.28E-10
	18	0.00044	2.79E-04	3.41E-06	-1.110	3.53E-10
	11.35	0.00026	9.26E-04	1.13E-05	-3.278	1.09E-09

Table 2.4 Calculated in situ solution pH and P_{CO_2}

Series	Inlet Solution-Gas head	pH	P_{CO_2} (bar)
A	Double deionized water – N_2	8.0	1.15×10^{-4}
B	Double deionized water	8.0	2×10^{-4}
C	Double deionized water – CO_2–N_2 mixture	6.0 – 6.5	$6.5 – 9.5 \times 10^{-2}$
E	Double deionized water – CO_2	5.0 – 5.5	0.5 – 2.7
F	Dilute hydrochloric acid solution – N_2	7.0	$2 – 9 \times 10^{-4}$

Figure 2.3 Concentration-time profile. [Residence time = Reactor Volume/ Volumetric Flow Rate of Solution]
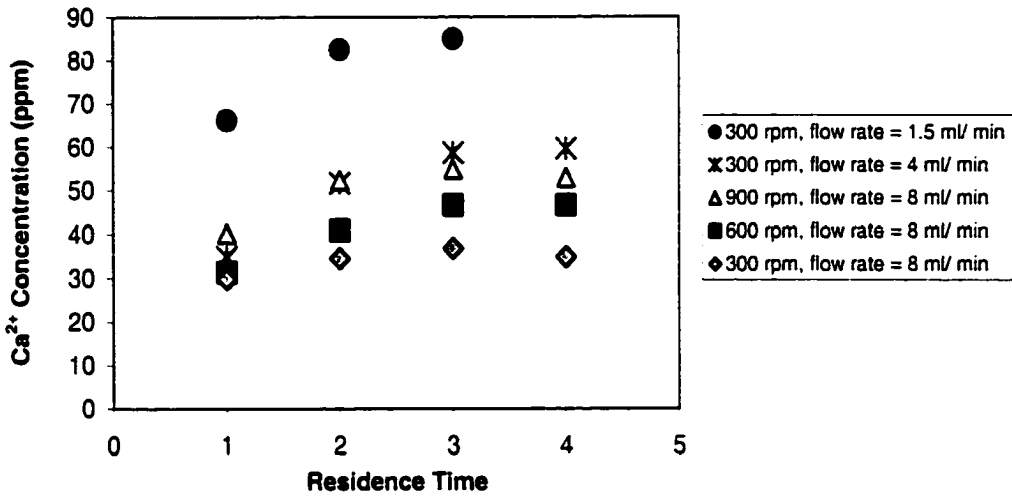
Figure 2.4 Dissolution rates for calcite with respect to Pco_2 for all series at 300 rpm spinning rates compared with rates at 25°C reported by Plummer et al. (1978)
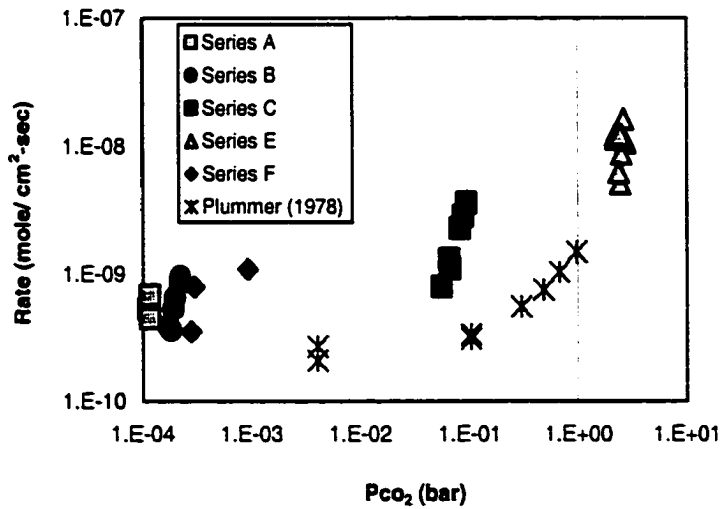
Figure 2.5a Dissolution rates for entire range of pH conditions for all series at 300 rpm spinning rate
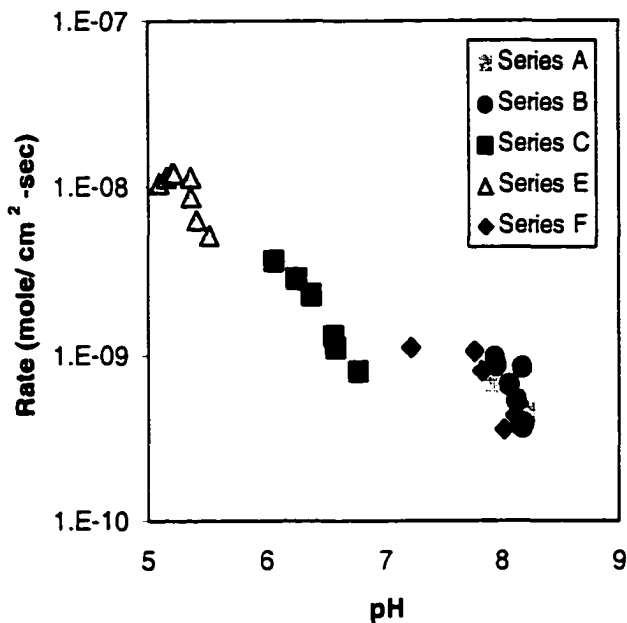
Figure 2.5b Dissolution rate data at 25°C compared to data at 100°C from this study. (Rate data from fig. 2.5a is replotted on a log axis for comparison with published data from several sources)

Series A	X Plummer et al., 1978; Pco2 0 atm
Series B	Plummer et al., 1978; Pco2 0.3 atm
Series C	Plummer et al., 1978 Pco2 1 atm
Series E	+ Chou et al., 1989
Series F	O Sjoberg, 1978
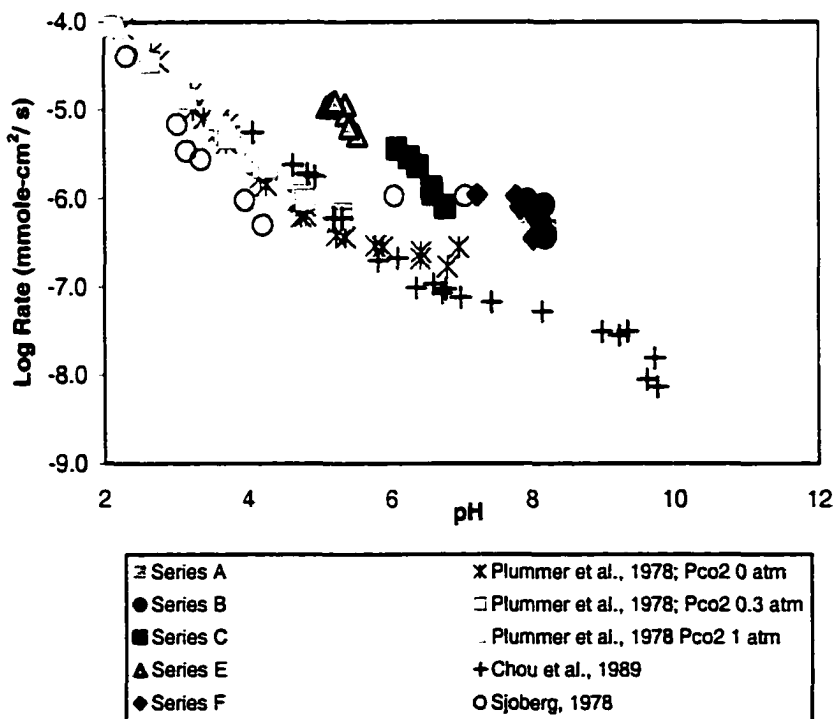
Figure 2.6 Dissolution rates with respect to ionic strength for all series at 300 rpm spinning rate
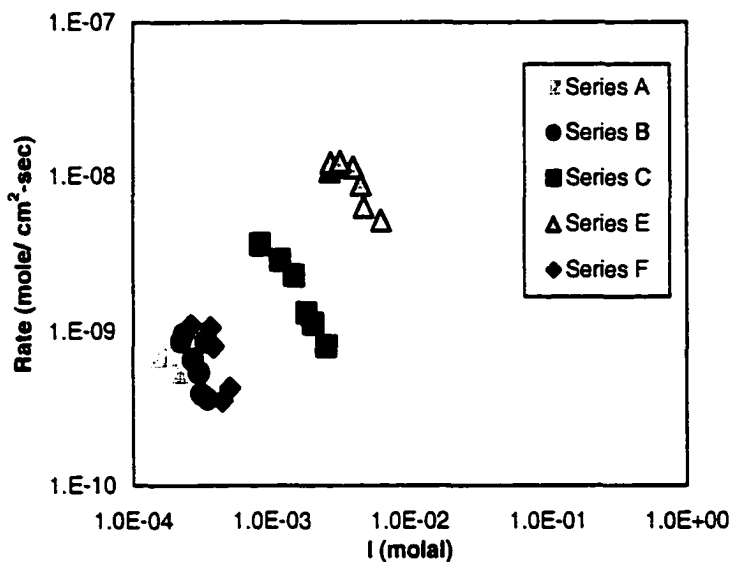
Figure 2.7   Temperature dependence of rate with respect to spinning rate. Rate data (Ω = 0.02 – 0.10) from experiments using double deionized water in atmospheric CO_2
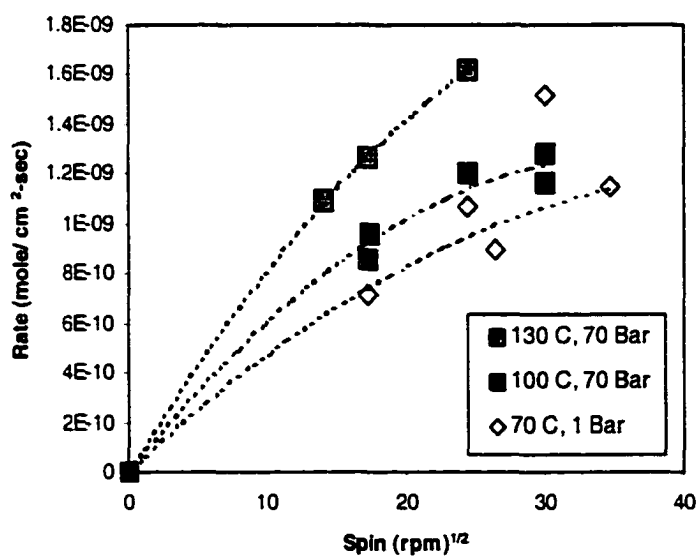
studied for calcite precipitation rates by Zuddas and Mucci (1998). At 25°C, precipitation rate was reported to increase by two orders of magnitude for a two-fold increase in ionic strength, for solution ionic strength ranging between 0.1 and 0.9 molal. The dependence observed in the present study is close to linear for solution ionic strength ranging between 10^{-4} and 10^{-2} molal.

The influence of temperature on calcite-water dissolution was studied using double-deionized reactant solution at 130°C and 70°C and rates were compared to those at 100°C (series B). For disc spinning rates varying between 300 and 1200 rpm, dissolution rates are plotted with respect to the square root of spinning rate (Figure 2.7). The curved nature of the fits in this plot suggests that the reaction mechanism is not purely transport controlled; rather it is mixed-kinetic controlled (Sjoberg and Rickard, 1984). This implies that the reaction mechanism does not change in response to temperature between 70 to 130°C (reaction mechanisms will be discussed in further detail in the following sections). A linear fit in this plot would indicate that rates are controlled entirely by the rate of transport across the hydrodynamic boundary layer. The rates at 130°C are possibly approaching transport control, as the fit is nearly linear. Also, there is some scatter in the 70°C data that calls for further study before concluding if dependence is purely transport controlled or mixed kinetic controlled. Dissolution rates at 300 rpm disc spinning rates for solutions at 100°C and 130°C are plotted with respect to $(1-\Omega^{1/2})$ to illustrate the influence of saturation state (Figure 2.8). A second order dependence on saturation is observed at both temperatures.

Disc Spinning Rate

Calcite dissolution occurs in multiple steps.

1. Transport of reactants from the bulk fluid towards active sites on the mineral surface, across a hydrodynamic boundary layer

2. Complexation or speciation of reactive precursors

3. Surface chemical reaction and detachment from the mineral surface

4. Transport of the reaction products away from the active site, by diffusion through a hydrodynamic or diffusional boundary layer into the well-mixed bulk fluid

Any of the above four steps may be rate limiting. If two or more steps occur at similar rates both are competing processes and may be rate determining. At certain conditions (e.g. high H^+ ion activity) the reaction at the surface is very rapid and transport is the rate-limiting step, making the reaction transport-controlled. For transport-controlled dissolution, the rate is proportional to the concentration gradient and has a first order dependence with respect to concentration (Sjoberg and Rickard, 1984; Casey, 1987; Shiraki and Brantley, 1995; Dreybrodt et al, 1996; Raines and Dewers, 1997).

$$R = k_T (C^t_s - C^t_b) \qquad (10)$$

where R is the dissolution rate in mole/ area-time, and k_T is the transport rate constant given by D/δ, D being the diffusion coefficient through a boundary layer and δ the boundary layer thickness. With substitution of k_T this becomes

$$R = D \; (C^{\pm}_s - C^{\pm}_b)/\delta \tag{11}$$

$C^{\pm}$ indicates mean ionic concentration of Ca^{2+} and CO_3^{2-}.

$$C^{\pm} = C_{Ca^{2+}}^{1/2} C_{CO_3^{2-}}^{1/2} \tag{12}$$

The subscripts s and b refer to concentrations at the mineral surface and within the bulk solution, respectively.

In a rotating disc experimental setup an increase in disc spinning rate, representing an increase in fluid flow velocity at the mineral-water interface, results in a decrease in the boundary layer thickness δ. As indicated by the transport-controlled rate equation above, the dissolution rate is inversely proportional to δ. For purely transport-controlled reactions, rates increase linearly with the square root of disc spinning rates, as has been illustrated for transport dependent dissolution (Sjoberg and Rickard, 1984; Compton et al, 1989; Dreybrodt and Buhmann, 1991).

For conditions in this study, transport-controlled behavior was observed in two distinct pH regimes. The solutions at both high pH (inlet pH above 7) and low pH (inlet pH 4) are characterized by a low $aH_2CO_3^*$. At high pH, series A and D were linear with the square root of disc spinning rate indicating entirely transport-

controlled rate dependence (Figure 2.9). At the other extreme, series F (dilute hydrochloric acid solution) also shows a linear trend when plotted against the square root of spinning rate, suggesting transport control (Figure 2.10). Transport control at lower pH is in agreement with data reported for lower temperatures (Plummer et al., 1978). At higher pH, mixed kinetics is reported at lower temperatures (Sjoberg and Rickard, 1984). However, transport is thought to become increasingly dominant as the temperature increases. This has been confirmed in the present study and is attributable to a lower activation energy for diffusion compared to surface reaction kinetics.

Within the lower pH regime, series E displays a mixed kinetic behavior. It is noted that higher $aH_2CO_3^*$ induced a higher rate of dissolution. The rates were greater than the acidic series by an order of magnitude (Figure 2.10). It is also important to recognize that as P_{CO_2} (or $aH_2CO_3^*$) increases, both transport and surface reaction are rapid and competing processes in which either of the two may be the rate-determining mechanism for the overall reaction.

Saturation State

For surface reaction controlled kinetics empirical models and rate laws have been put forward which consider the influence of saturation state or degree of disequilibrium on rates (Morse, 1983; Shiraki and Brantley, 1995). The linear rate laws are of the general form:

$$R \propto [1 - exp(-n\Delta G/ RT)] \qquad (13)$$

Figure 2.8 Temperature dependence of rate with respect to saturation. Rate data from experiments using double deionized water in atmospheric CO_2
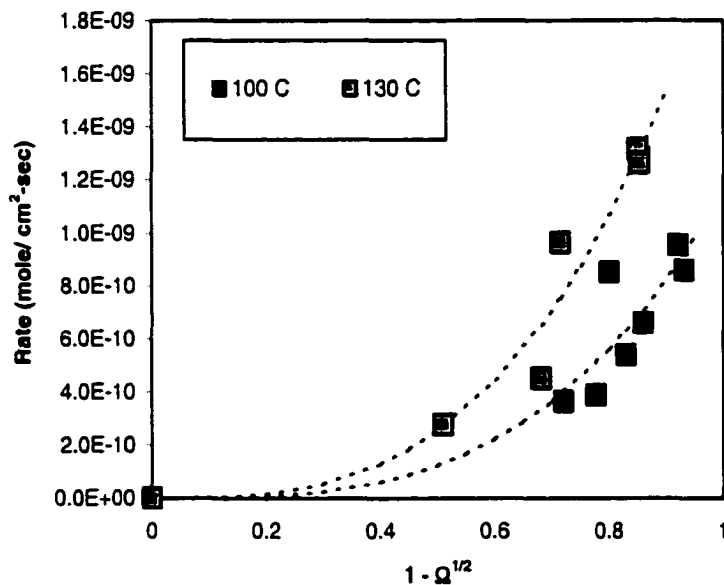
Figure 2.9 Spinning dependence of rate ($\Omega = 0.02 - 0.10$) for neutral to alkaline pH conditions
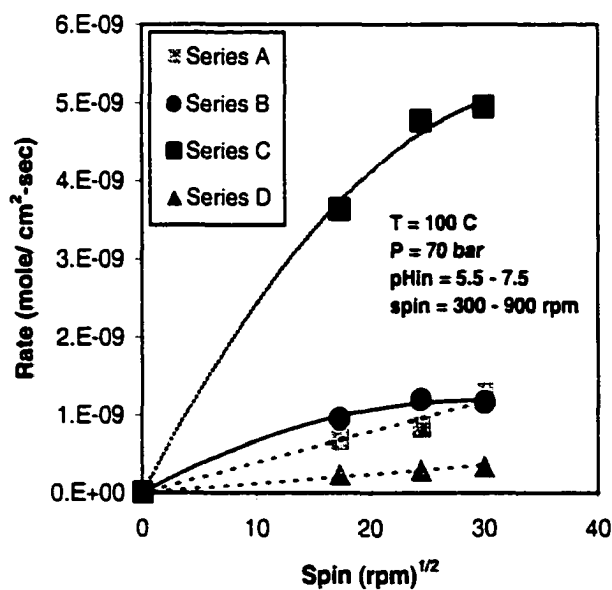
Figure 2.10 Spinning dependence for low pH regime. Three subsets of series E are displayed; set I experiments were performed at flow rates above 8 ml/ minute, set II at around 5 ml/ minute, set III at less than 3 ml/ minute. Flow rate is significant because higher the flow rate, less saturated the solution. Series F rates are for experiments at flow rates above 8 ml/ minute
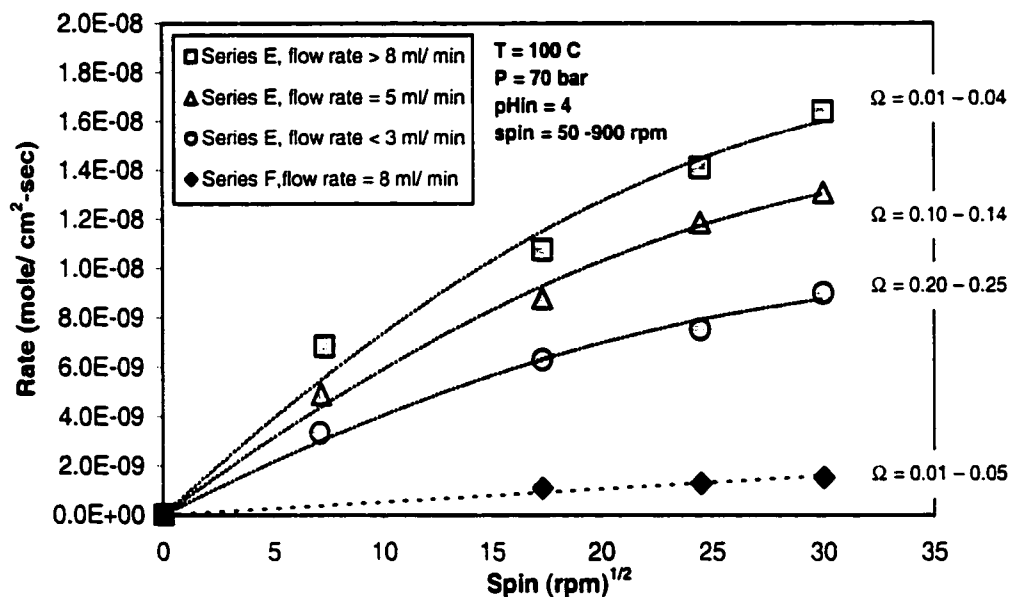
Figure 2.11 Saturation dependence for neutral to alkaline regime
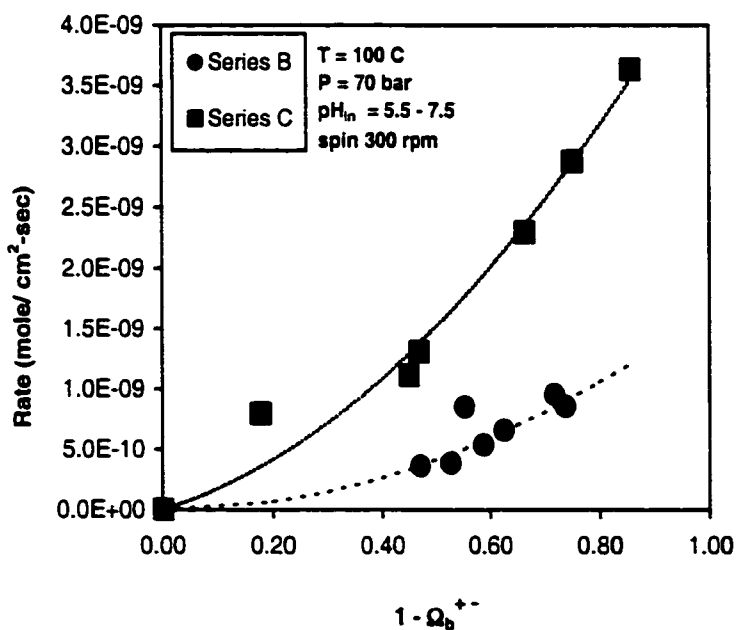
where R is gas constant, T is absolute temperature, and ΔG is the change in Gibbs free energy for calcite dissolution (Kazmierczak et al, 1982; Sjoberg and Rickard, 1984). This is equivalent to a rate law expressed in terms of saturation Ω as follows:

$$R = k\,(1 - \Omega) \qquad (14)$$

where k is the dissolution rate constant, $\Omega = a_{Ca2+}a_{CO32-}/K_{sp}$, a_i referring to activity of species i and K_{sp} is the solubility product for the calcite-water reaction. Rate laws that are nonlinear with respect to saturation or ΔG have been used to describe calcite reaction behavior. A general equation suggested by Lasaga (1981) for rates controlled by crystal defects is as follows:

$$R = k\,(1 - [\,exp(\Delta G/RT)]^m)^n \qquad (15)$$

As $\Omega = exp\,(\Delta G/RT)^m$, in terms of saturation it is expressed in a general form:

$$R_d = k_d\,(1 - \Omega^m)^n \qquad (16)$$

R_d and k_d are the rate and the rate constant respectively. The terms m and n are fit parameters. For calcite dissolution in seawater, Morse (1978) used an empirical expression of a similar form, using $m = 1$ and n varying for different natural calcite samples (Shiraki and Brantley, 1995).

Attempts to fit experimental data to the above rate law have shown that n is a function of the reaction mechanism and hydrodynamics (Reddy and

Nancollas, 1973; Morse, 1978; Kazmierczak et al., 1982; Rickard and Sjoberg, 1983; Nielsen, 1983; MacInnis and Brantley, 1992; Shiraki and Brantley, 1995). For n approximating 1 (linear rate law), adsorption/ desorption related reactions have been suggested, whereas for n of about 2, the reaction is considered to be occurring by a spiral growth at screw dislocation mechanism (Nielsen, 1983; Blum and Lasaga, 1987; Shiraki and Brantley, 1995).

To observe dissolution as function of saturation state, the rates (mole/ cm^2-sec) at a constant disc spinning rate of 300 rpm were plotted against $(1 - \Omega_b^{\pm})$. $\Omega_b^{\pm}$, also known as mean ionic bulk saturation, is given by the square root of saturation $(\Omega^{1/2})$ and has been used to describe saturation dependence (Nielsen, 1983). Two series (series B and C) at near neutral to alkaline pH are plotted (Figure 2.11). For both series B and C a second or higher order increase in rate, in response to change in saturation state, was observed.

A progressive increase in rates was observed due to an increase in P_{CO_2} and a corresponding lowering of pH. The nonlinear dependence of the reaction rate with saturation state, coupled with an obvious spinning rate dependence, suggests a mixed kinetics. The observations were made based on series C and E experiments. The dissolution rates were plotted with respect to $(1 - \Omega_b^{\pm})$ (Figure 2.11 and 2.12). A rate expression describing this dependence is derived in the following section.

Rate Laws for Calcite Dissolution at Elevated Temperatures

Plummer model

All data at 300 rpm disc spinning rates were fit to the elementary reaction-based mechanistic model proposed by Plummer et al. (1978). According to this model, dissolution behavior is described in terms of three regions in pH-P_{CO_2} domain that are dominated by three elementary reactions. At a fixed P_{CO_2} and temperature, the overall rate is described by equation (4), which takes into account these three reactions as well as a back reaction for precipitation at close to equilibrium conditions. The rates observed in the present study fall within region 2 (high pH, high P_{CO_2}) and 3 (high pH, low P_{CO_2}) described by Plummer et al. (1978). Rates at elevated temperatures show pH and P_{CO_2} dependence similar to those at lower temperatures. Series E represents sections in region 2 and is dominated by $aH_2CO_3^*$. However, conditions are close to those near the boundary between region 1 (low pH, low P_{CO_2}) and 2 and the effect of pH is apparent. Series C represents an area in which H^+, $H_2CO_3^*$ and H_2O all are thought to contribute significantly. This is also true for rates obtained in the present study. All other series are within the limits of region 3 and do not show significant dependence on either pH or P_{CO_2}. The Plummer model was able to predict the rates at elevated temperatures to a fair degree. However, the model predicts no transport dependence in region 3, which is dominated by the reaction of calcite with H_2O. In contrast, transport controlled behavior for low $aH_2CO_3^*$ solutions across all pH domains, was observed in this study (Figure 2.9 and

2.10). The curve-fit parameters determined by fitting the present data at 300 rpm disc spinning rates, to the Plummer rate equation, are shown in Table 2.5 (Figure 2.13).

Mixed Kinetics Model

As shown by previous studies, both transport controlled and surface reaction controlled kinetics influence calcite dissolution (Kazmierczak et al., 1982; Sjoberg and Rickard, 1984; Dreybrodt et al., 1996). It is pertinent to elaborate on mixed kinetic behavior to interpret the experimental results. An overall reaction for calcite dissolution in aqueous solution occurs through a number of steps proceeding in series. The overall reaction is limited by the rate at which the slowest step occurs. For example, surface reaction involving detachment of ions from exposed calcite surface can occur only when reactant species such as H^+, $H_2CO_3^*$ etc. which are primarily responsible for triggering calcite dissolution, are transported towards an active reaction site on the calcite surface. Also, surface reaction cannot occur faster than the rate at which dissolution products are transported away from the calcite-solution interface into the bulk solution. Similarly, the rate of transport is limited by the rate at which dissolved ions are detached by surface reaction. Kinetics is considered to display a mixed control when surface reaction and transport occur at about the same speed.

Transport controlled dissolution is described by equation (11). Similarly, the rate law for surface reaction controlled dissolution has been described by a

Figure 2.12 Dissolution rates for solutions at low pH and high P_{CO_2}. Data fitted to a rate equation describing mixed kinetic control. (R = 0.97)
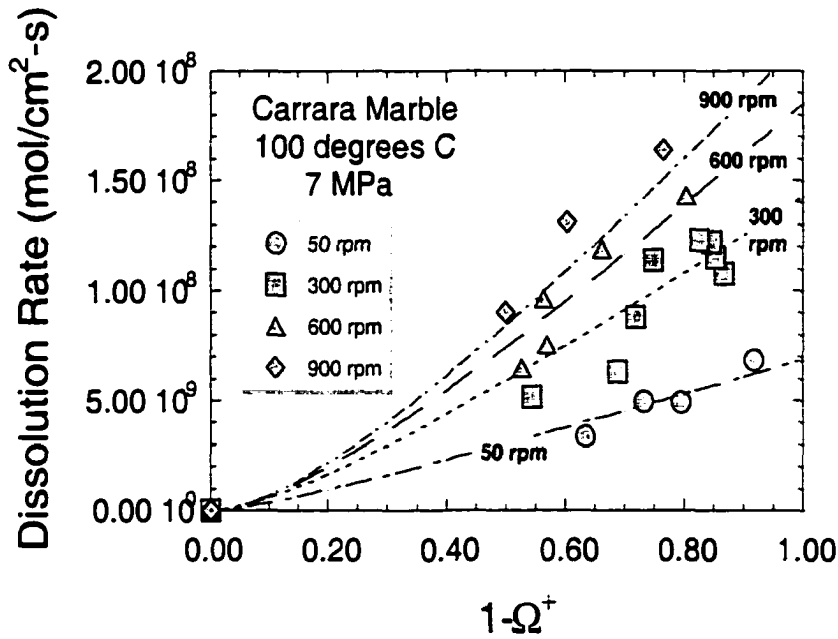
Figure 2.13 All 300 rpm data fit to Plummer Model (Plummer et. al., 1978). (R = 0.96)
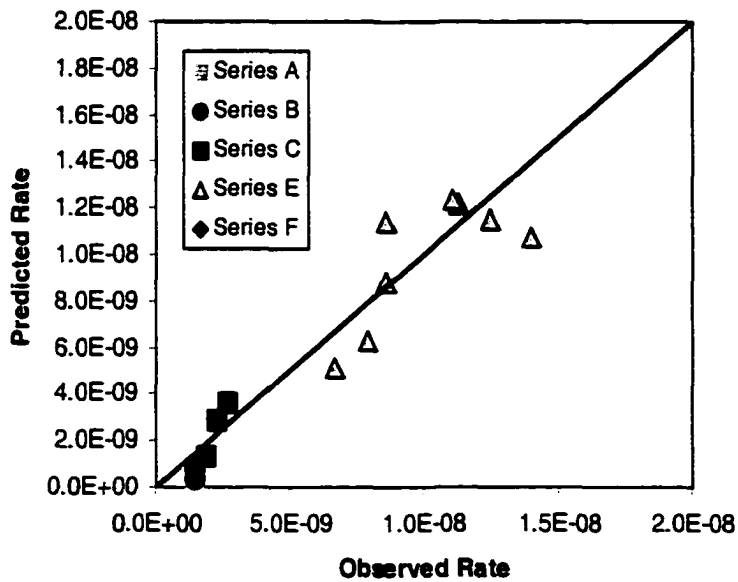
general form that is second order in concentration (Davies and Jones, 1955; Liu and Nancollas, 1971; Shiraki and Brantley, 1995; Raines and Dewers, 1997). When expressed in terms of mean ionic concentration, $C^{\pm}$, as defined by equation (12), the surface reaction rate law becomes:

$$R = k^{+}(C_{eq}{}^{\pm} - C_{b}{}^{\pm})^{2} \qquad (17)$$

where k^{+} is the rate constant for surface controlled dissolution, $C_{eq}{}^{\pm}$ is the mean ionic bulk concentration at equilibrium and $C_{b}{}^{\pm}$ is the mean ionic bulk concentration. Since mixed kinetic control implies that the surface reaction and the transport rates are occurring at about the same rate and fluxes from surface reaction and transport are equivalent, Casey (1987) and Murphy et al. (1989) combined surface and transport control rate laws to express mixed kinetic rates. By balancing the surface reaction flux and diffusive flux, one obtains

$$D \, (C_{s}{}^{\pm} - C_{b}{}^{\pm}) / \, \delta = k^{+} \, (C_{s}{}^{\pm} - C_{eq}{}^{\pm})^{2} \qquad (18)$$

Solving Eq. (18) for $C_{s}{}^{\pm}$ and substituting into Eq. (10) with some algebraic manipulations results in

$$R = k_{t} \, [1 - \Omega_{b}{}^{\pm} + \zeta \, \{1 - (1 + 2 \, (1 - \Omega_{b}{}^{\pm}) / \zeta \,)^{1/2} \, \}] \qquad (19)$$

where $k_{t} \, (= Dm_{eq} / \, \delta)$ is the rate coefficient for transport control, D represents the diffusion coefficient, m_{eq} is the mean ionic molal equilibrium concentration, δ is

42

the thickness of the hydrodynamic boundary layer, Ω_b^z is the mean ionic bulk saturation, the dimensionless parameter $\zeta = Dm_{eq} / 2\delta k^+$, and k^+ is the second order rate coefficient for surface reaction control. ζ is a measure of relative dominance between transport and surface control. Results of the fits are given in Table 2.5. Plummer rate law and mixed kinetic rate law, both seem to fit the data well but equation (19) appears to give a better fit and represents data for all disc spinning rates (Figure 2.13 and 2.14). This equation has also been used to describe mixed kinetic behavior observed for gypsum dissolution (Raines and Dewers, 1997).

Comparison to Other Studies at Elevated Temperatures

Calcite precipitation data (Shiraki and Brantley, 1995) and dissolution data (Talman et. al., 1990) at high temperature have been compared in terms of rate with respect to ΔG. Shiraki and Brantley (1995) have extrapolated the regression curve for their data on precipitation in order to test the predictive ability of their model in dissolution regime. Their extrapolation curve for growth at screw dislocation (their curve A) and growth by adsorption mechanism (their curve B) are shown (Figure 2.15). In this study, solutions at lower $aH_2CO_3^*$ (series A, B, D and F) are comparable to curve A in solution pH and P_{CO_2} conditions and the current results seem to match well. It follows the plateauing trend predicted by the Shiraki and Brantley model. Data at higher $aH_2CO_3^*$ (series C and E) show rates higher than the rates predicted by curve B as shown (Figure 2.15). This

43

Table 2.5 Rate models fit to the experimental data

$R = k_1 \, aH^+ + k_2 \, aH_2CO_3^* + k_3 - k_4 \, aCa^+ . aHCO_3^-$

$k_4 = K_2/K_C \, (k_1^{\cdot} + 1/\,aH^+_{surf}) \, (k_2 \, aH_2CO_3^* + k_3)$

Disc spinning rate = 300 rpm

$K_2/K_C = 0.1372$
$k_1 = .0014392$
$k_2 = 3.79e\text{-}10$
$k_3 = 1.418e\text{-}9$

$R = .96$

$R = k_t \, [1 - \Omega_b^{\pm} + \zeta \, \{1 - (1 + 2\,(1 - \Omega_b^{\pm})/\zeta)^{1/2} \}]$

$k_t = Dm_{eq}/\delta \qquad \zeta = Dm_{eq}/2\delta k^*$
$k^* = k_2 Pco_2 + k_3$

$k_t = 3.488\ E\text{-}7\ m_{eq}(spin)^{1/2}\ mole/cm^2\text{-}s$
$k_2 = 2.179\ E\text{-}8\ mole/cm^2\text{-}atm\text{-}s$
$k_3 = 9.409\ E\text{-}8\ mole/cm^2\text{-}s$

$R = 0.97$

Figure 2.14 All data fit to mixed kinetic model (R = 0.97)
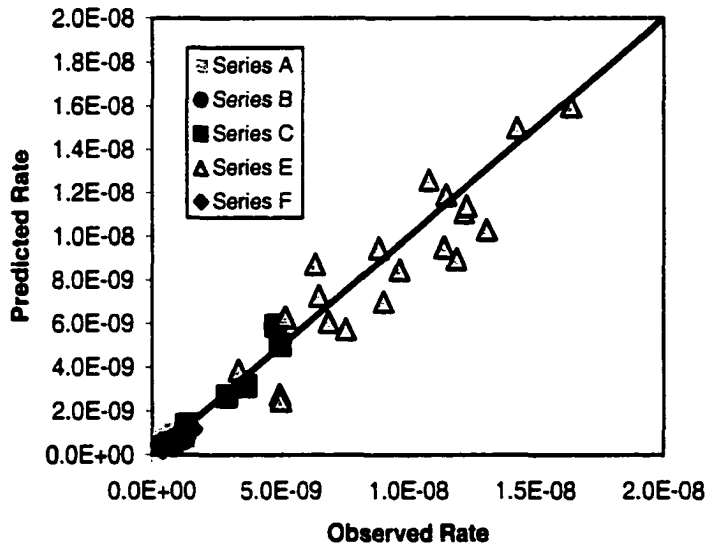
Figure 2.15 Dissolution rate (Talman et. al., 1990) and extrapolation of precipitation rate at 100°C as a function of ΔG (Shiraki and Brantley, 1995)
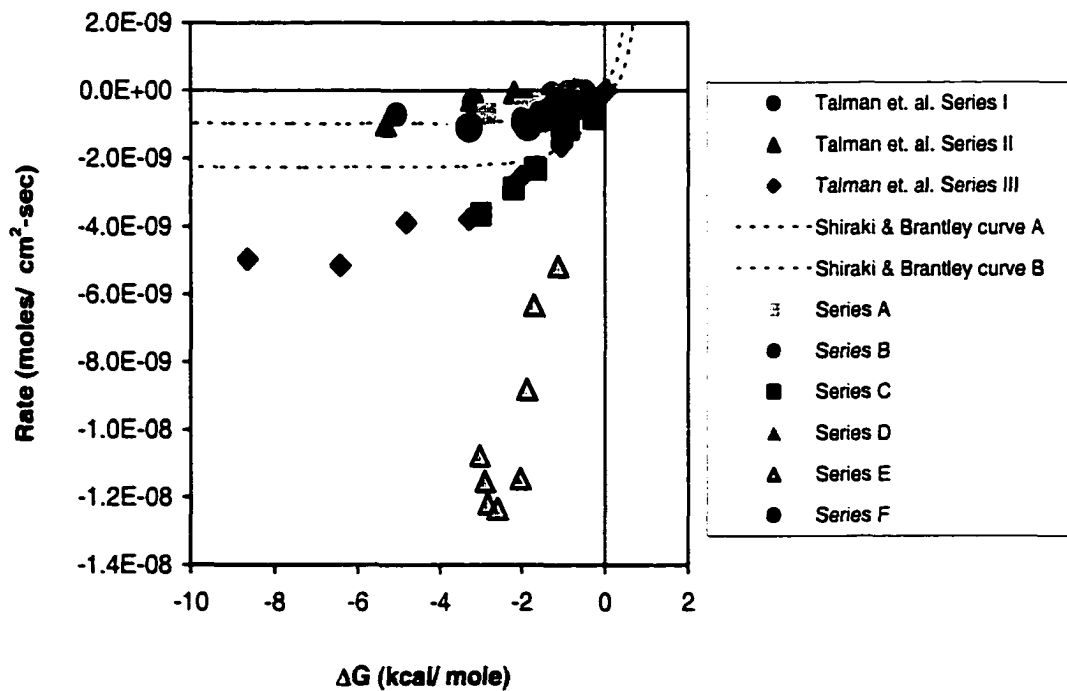
may be interpreted as the effect of higher dissolved CO_2 content in solution in the present study.

Calcite dissolution at elevated temperatures has been reported by Talman et al. (1990). However, their solution chemistry and experimental designs are not identical to the present study. Series A, B, D and F in this study are similar to series I and II in their experiments, although series I and II are, in fact, somewhat higher in Pco_2. Similarly, series C in the current study exhibits rates that are equal to series III reported by Talman and others, although series III is higher in Pco_2 (Figure 2.15). In summary, rates observed in the present study are higher than rates reported by Talman et al. (1990) at equivalent Pco_2 conditions for dissolution at 100°C.

Dissolution Textures

SEM photomicrographs of reacted samples suggest dissolution may not actually be occurring at all sites on the exposed surface to the same extent (Figure 2.16 to 2.18). Rather some weak planes, twins, fractures etc. may be more prone to reaction than others. The degree to which densities of such active sites in the form of point defects, dislocations, microfractures, kinks, grain boundaries, twins, corners, and edges impact rate calculation, has been studied by Schott et al. (1989). It was observed that the impact was not significant unless defect density in the initial sample was above a critical limit of about 10^7 cm^{-2}. This is also consistent with a theoretical study on quartz where such critical dislocation density for quartz was predicted to be on the order of 10^9 cm^{-2} (Blum

46

Figure 2.16 Unreacted polished (5 μm) Carrara marble showing an overall uniform surface. [150 μm X 150 μm]

Figure 2.17. Surface dissolution texture on sample disc reacted at 100°C, 6.9 MPa, in double deionized water and CO_2 -N_2 atmosphere. [75 μm X 75 μm]
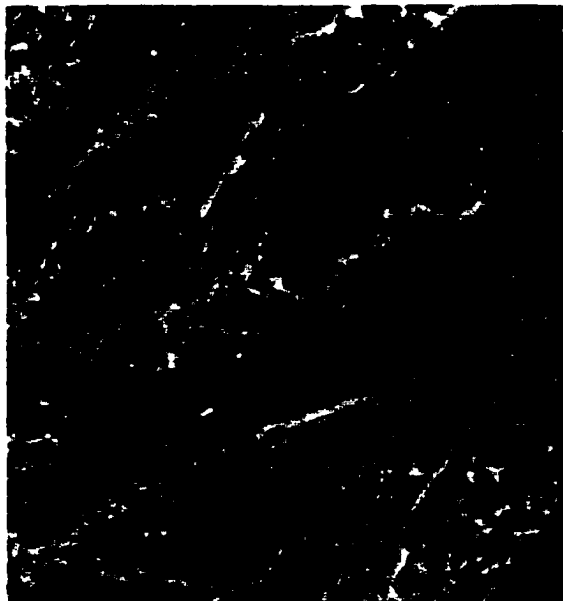
Figure 2.18 Dissolution texture on sample disc reacted at $100^{\circ}C$, 6.9 MPa, in double deionized water and CO_2 -N_2 atmosphere. Image shows active sites at which reaction has occurred preferentially. [100 μm X 100 μm]

and Lasaga, 1987). This may be due to the fact that point defects and dislocations dissolve at a higher rate but contribute a small mass to the solution because activities at such sites occur only at a submicroscopic scale. This suggests that meaningful parameterization of a rate expression is possible based on studies with relatively undeformed samples such as those used in this study.

Surface Complexation

Chemical structure and reactivity at the mineral-water interface has been described for carbonate minerals by a surface complexation model proposed by Van Cappellen et al. (1993). Attempts were made to extend a rate equation based on this model, to encompass surface speciation under these experimental conditions at elevated temperatures. The results are reported in Chapter 5.

CONCLUSIONS

Based on dissolution experiments at elevated temperatures, transport controlled behavior is observed at and above $100^{\circ}C$, for all pH regimes at low $aH_2CO_3^*$ conditions. Mixed kinetic control is indicated for all series with moderate to high $aH_2CO_3^*$. For the low $aH_2CO_3^*$ series, data agree well with projections based on extrapolations from a precipitation model. Dissolution rates increase linearly with $aH_2CO_3^*$. Data suggest transport control at low $aH_2CO_3^*$ conditions for all pH regimes unlike other dissolution data at lower temperatures. The Plummer et. al. (1978) model is able to predict the present rates but does

not account for the transport-controlled behavior for systems with low $aH_2CO_3^*$.

A mixed kinetic model derived by Raines and Dewers (1997) describes this data more closely.

High $aH_2CO_3^*$ may play a much more significant role in calcite dissolution at elevated temperatures than apparent from results at lower temperatures or precipitation at elevated temperatures. This needs to be taken into account for systems in which high dissolved CO_2 may be present at elevated temperatures, such as conditions prevailing in oil and gas production pipelines. This may have important implications for estimation of formation damage potential or designing remediation methods for scaling problems in production wellbores.

APPENDIX A

Table 2.A.1 Quantitative electron microprobe analysis for elemental composition of Carrara marble

Analytical Conditions: 20 kV, 10 nA, 20 um spot; 45 s on peak for all elements										
Weight Percents of the Elements (C & O calculated by stoichiometry)										
Label	Fe	Mn	Mg	Ca	Sr	Al	Si	C	O	Total
MDL:	0.025	0.021	0.011	0.013	0.039	0.015	0.011	---	---	
Marble Sample										
Marble-1	0.012	0.014	0.314	39.573	0.034	0.008	0.005	12.029	48.069	100.058
Marble-2	0.001	0.000	0.370	39.575	0.011	0.006	0.007	12.051	48.155	100.175
Marble-3	0.013	0.010	0.346	39.776	0.021	0.002	0.007	12.104	48.370	100.648
Marble-4	0.000	0.013	0.350	39.609	0.024	0.000	0.009	12.056	48.178	100.239
Marble-5	0.017	0.002	0.384	39.429	0.025	0.000	0.004	12.017	48.019	99.896
Marble-6	0.000	0.011	0.325	39.330	0.020	0.002	0.012	11.963	47.803	99.466
Marble-7	0.003	0.017	0.365	39.765	0.041	0.000	0.004	12.110	48.392	100.696
Marble-8	0.002	0.005	0.319	39.534	0.059	0.000	0.003	12.018	48.023	99.963
Marble-9	0.000	0.001	0.332	39.730	0.031	0.000	0.009	12.082	48.281	100.466
Marble-10	0.009	0.000	0.353	39.135	0.031	0.003	0.008	11.915	47.613	99.067
Marble-11	0.015	0.015	0.320	39.583	0.018	0.000	0.002	12.031	48.076	100.059
Marble-12	0.006	0.007	0.355	39.498	0.000	0.001	0.005	12.019	48.028	99.918
Marble-13	0.007	0.019	0.350	39.688	0.048	0.000	0.003	12.081	48.278	100.475
Marble-14	0.001	0.019	0.345	39.765	0.000	0.000	0.002	12.093	48.326	100.552
Marble-15	0.000	0.001	0.353	39.622	0.044	0.000	0.004	12.057	48.181	100.261
Marble-16	0.000	0.000	0.354	39.594	0.051	0.004	0.004	12.050	48.153	100.208
Marble-17	0.001	0.002	0.379	39.460	0.032	0.001	0.011	12.026	48.059	99.970
Marble-18	0.004	0.000	0.359	39.476	0.003	0.000	0.005	12.013	48.004	99.864
Marble-19	0.000	0.000	0.370	39.597	0.039	0.000	0.009	12.062	48.200	100.277
Marble-20	0.000	0.006	0.348	39.689	0.000	0.000	0.012	12.078	48.264	100.398
Marble-21	0.000	0.000	0.385	39.291	0.009	0.000	0.006	11.971	47.838	99.500
Marble-22	0.002	0.000	0.384	39.760	0.040	0.000	0.007	12.116	48.417	100.726
Marble-23	0.000	0.000	0.336	39.351	0.036	0.000	0.005	11.968	47.824	99.520
Marble-24	0.000	0.005	0.361	39.312	0.016	0.000	0.008	11.969	47.829	99.498
Marble-25	0.000	0.000	0.345	39.512	0.001	0.004	0.009	12.019	48.030	99.921
Average	0.004	0.006	0.352	39.546	0.025	0.001	0.006	12.036	48.096	100.073
Std Dev	0.005	0.007	0.020	0.170	0.017	0.002	0.003	0.051	0.205	0.429

Table 2.A.2 Saturation index from modeling by SOLMINEQ88 and PHREEQCI

Series	Log (AP/KT) SOLMNQ	1–Ω	Log (AP/KT) PHREEQC	1–Ω	Deviation	Deviation%
A	-1.146	0.93	-1.06	0.91	0.02	2
	-1.406	0.96	-1.34	0.95	0.01	1
	-1.662	0.98	-1.61	0.98	0.00	0
	-0.878	0.87	-0.8	0.84	0.03	3
	-0.83	0.85	-0.76	0.83	0.03	3
B	-1.173	0.93	-1.1	0.92	0.01	1
	-0.859	0.86	-0.79	0.84	0.02	3
	-0.911	0.88	-0.84	0.86	0.02	2
	-0.874	0.87	-0.79	0.84	0.03	3
	-0.899	0.87	-0.84	0.86	0.02	2
	-0.602	0.75	-0.56	0.72	0.03	3
	-1.166	0.93	-1.05	0.91	0.02	2
	-0.759	0.83	-0.68	0.79	0.03	4
	-0.651	0.78	-0.52	0.7	0.08	10
	-0.699	0.80	-0.57	0.73	0.07	9
C	-1.748	0.98	-1.69	0.98	0.00	0
	-0.598	0.75	-0.55	0.72	0.03	4
	-1.282	0.95	-1.21	0.94	0.01	1
	-1.755	0.98	-1.7	0.98	0.00	0
	-1.446	0.96	-1.39	0.96	0.00	1
	-0.518	0.7	-0.52	0.7	0.00	0
	-0.976	0.89	-0.95	0.89	0.01	1
	-0.153	0.3	-0.17	0.32	-0.03	-9
D	-0.684	0.79	-0.66	0.78	0.01	1
	-0.572	0.73	-0.55	0.72	0.01	2
	-0.508	0.69	-0.49	0.68	0.01	2
	-0.561	0.73	-0.54	0.71	0.01	2
	-0.429	0.63	-0.41	0.61	0.02	3
E	-1.771	0.98	-1.76	0.98	0.00	0
	-1.408	0.96	-1.41	0.96	0.00	0
	-1.259	0.94	-1.26	0.95	0.00	0
	-1.095	0.92	-1.1	0.92	0.00	0
	-0.66	0.78	-0.68	0.79	-0.01	-1
	-1.194	0.94	-1.2	0.94	0.00	0
	-1.697	0.98	-1.67	0.98	0.00	0
	-1.654	0.98	-1.63	0.98	0.00	0
	-1.516	0.97	-1.52	0.97	0.00	0
	-1	0.9	-1.01	0.9	0.00	0
	-0.698	0.8	-0.72	0.81	-0.01	-1
	-0.569	0.73	-0.6	0.75	-0.02	-3

Series	Log (AP/ KT) SOLMNQ	1−Ω	Log (AP/ KT) PHREEQC	1−Ω	Deviation	Deviation%
	-0.781	0.83	-0.8	0.84	-0.01	-1
	-0.618	0.76	-0.65	0.78	-0.02	-2
	-2.218	0.99	-2.17	0.99	0.00	0
	-0.865	0.86	-0.87	0.87	0.00	0
	-1.422	0.96	-1	0.96	0.00	1
	-1.184	0.93	-1	0.93	0.01	1
F	-1.084	0.92	-1.02	0.9	0.01	1
	-1.429	0.96	-1.39	0.96	0.00	0
	-1.046	0.91	-0.99	0.9	0.01	1
	-0.885	0.87	-0.9	0.87	0.00	-1
	-0.402	0.6	-0.4	0.6	0.00	0
	-0.65	0.78	-0.6	0.75	0.03	4
	-1.92	0.99	-1.85	0.99	0.00	0

CHAPTER 3

Calcite Dissolution in High Ionic Strength Solutions at 70°C to 150°C

ABSTRACT

Calcite dissolution was studied over a range of ionic strengths and hydrodynamic conditions between 70 – 150°C in aqueous solutions of varying P_{CO_2}. A series of experiments were done at 70°C, in which Carrara marble was reacted to saline solutions ranging in ionic strength between 0.7 – 4 molal (28,000 – 160,000 ppm). The experiments were done in batch reactors under nitrogen and carbon dioxide atmospheres. Rate coefficients were determined by integrating an expression for concentration differential over time. To observe the effect of temperature, another series of experiments were performed at 70, 100 and 150°C using 0.7 molal NaCl solutions in a mixed-flow reactor. Rates at steady-state were determined directly from the change in calcium concentration between the inlet and outlet solutions.

The rate law fitted to the batch experimental results was used in a scale prediction model proposed in this study (Chapter 4).

INTRODUCTION

Calcite dissolution and growth kinetics in aqueous systems have been investigated extensively (Nancollas and Reddy, 1971; Berner and Morse, 1974; Plummer et al., 1978 and 1979; Sjoberg and Rickard, 1984; Compton and Daly, 1984; Inskeep and Bloom, 1985; Busenberg and Plummer, 1986; Chou et al., 1989; Dove and Hochella, 1993; Dreybrodt et al., 1996; Teng et al., 2000) at surface conditions to further the understanding of karstification, diagenesis of calcareous deep-sea sediments, evolution of water chemistry in carbonate terrain, the global carbon dioxide cycle and other biogeochemical processes. Data applicable to calcite-water reactions in concentrated solutions at elevated temperatures are scarce. Calcite scale precipitation occurring in water treatment and desalination facilities or petroleum production pipelines, are areas where such data may be useful.

In the current study, the effect of ionic strength on calcite dissolution rate was investigated over a range of ionic strengths at elevated temperatures. This part is an extension of the investigation of calcite dissolution rates at elevated temperatures and pressures (Chapter 2). The present set of experiments cover a range of temperature, salinity, Pco_2 and hydrodynamic conditions. A rate law fit to the experimental data was used in a scale prediction model (Chapter 4).

THEORETICAL BACKGROUND

The activated complex theory or transition state theory provides a theoretical framework on which the understanding of reaction mechanisms, rates

55

and the controlling factors are founded (Langmuir, 1997; Stumm and Morgan, 1996). According to this theory, the activated complex, a high-energy ground-state species, forms from the reactants and is a transition state between the reactant and the final product. The formation of the activated complex is the rate limiting reaction step. For example in a reaction between reactants A and B to form the solid AB,

$$A + B \xrightarrow{k^+} AB^{\ddagger} \rightarrow AB \tag{1}$$

$AB^{\ddagger}$ represents the activated complex and k^+ is the forward rate coefficient for this reaction. Based on this idea, an equation describing the effect of ionic strength on reaction rates was first derived by Brønsted and Bjerrum and is known as Brønsted-Bjerrum equation (Castellan, 1971; Brezonik, 1994; Stumm and Morgan, 1996; Langmuir, 1997). For reactions in aqueous solution, if k^+ gives the reaction rate at any ionic strength, and k_o represents the reaction rate at the reference state i.e. the rate in an infinitely dilute solution, then k^+ is given by

$$k^+ = k^+_o \left(\gamma_A \, \gamma_B / \gamma^{\ddagger} \right) \tag{2}$$

where γ_A and γ_B are activity coefficients of the reactants A and B, and $\gamma^{\ddagger}$ gives the activity coefficient of the activated complex. Taking the logarithm on both sides and rearranging equation (2) gives

$$\log \left(k / k_o \right) = \log \left(\gamma_A \, \gamma_B / \gamma^{\ddagger} \right) \tag{3}$$

The activity coefficients γ_i are a function of the ionic strength and are given by various equations thought to be valid over some range in ionic strength. If the Debye-Hückel limiting law (Langmuir, 1997) is used to compute the activity coefficients, then

$$log\ \gamma_i = -A\ z_i^2\ I^{1/2} \tag{4}$$

where z_i is the charge of species i and I is the molal ionic strength. The charge of activated complex z_i must equal the sum of charges of species A and B. Substitution of equation (4) into equation (3) and simplification results in the form

$$log\ (k/\ k_o) = 1.02\ (z_A\ z_B)\ I^{1/2} \tag{5}$$

Equation (5) indicates that $log\ k$ is linearly related to the square root of the ionic strength. It should be noted that applicability of this law is limited to ionic strengths up to 10^{-3} molal. If an extended Debye-Hückel equation is used to compute γ, application of this law is valid up to an ionic strength of 10^{-1} molal. However, the equations are often used with lower accuracy above these limits (Brezonik, 1994). The best estimate of activity coefficients at high ionic strengths is given by the Pitzer model, which has been shown to be valid for electrolyte solutions up to 6 molal (Pitzer, 1987). The *interaction parameters* in Pitzer models take into account the electrostatic effects due to interaction between similarly charged ions, which is significant for concentrated solutions (Langmuir, 1997).

The effect of ionic strength on rates of calcite reaction in saline solutions has been studied by several workers (Badiozamani et al., 1977; Chen et al., 1979; Kazmierczak et al., 1982; Walter, 1986; Zhong and Mucci, 1989; Zuddas and Mucci, 1994 and 1998). Early experimental investigations using seawater or artificial seawater suggested that calcite-water reaction kinetics displayed little or no dependence of rates on ionic strength (Badiozamani et al., 1977; Chen et al., 1979; Kazmierczak et al., 1982; Walter, 1986; Zhong and Mucci, 1989). Investigations on the influence of salinity on the calcite-water system have always been focused more on solubility rather than reaction rates (Millero, 1979, Patterson et al., 1982, 1984; Harvie et al., 1984; Pabalan and Pitzer, 1987; He and Morse, 1993).

More recent investigations have reported an ionic strength influence on the kinetic parameters and mechanisms of calcite growth (Zuddas and Mucci, 1994, 1998). The dependence of the rate constant on solution ionic strength (0.1 m to 0.9 m) was studied for calcite growth at 25°C by Zuddas and Mucci (1998). The logarithm of rate constants were reported to increase linearly with ionic strength by several orders of magnitude. The influence on rates was attributed to catalysis induced by the presence of an inert electrolyte (Bischoff, 1968). In accordance with the Brønsted-Bjerrum theory, the polar properties of the solvent are believed to play a role in reaction kinetics (Lasaga, 1995). In high ionic strength solution the activity of water is reduced. Hydrated ions available to participate in the surface reactions are smaller in dimension, as fewer water molecules are attached to the ions. The surface reactions are facilitated by

smaller ions, which may be incorporated into the lattice with greater ease. The increase in reaction order was attributed to a change in the reaction mechanism as a result of ion interactions at the mineral-solution interface in high ionic strength solutions. It was suggested that the ionic strength might be governing the development of nonequivalent kink sites thereby impacting reaction mechanisms (Zuddas and Mucci, 1998). Based on the observations, a model reflecting the dependence of growth rate on ionic strength was proposed.

Zuddas and Mucci (1998) also report a variation in the dissolution rate constant with an increase in ionic strength (Figure 3.1). Their data suggests that ionic strength dependence is somewhat complex. The rate constant increases initially (up to 0.6 m) followed by a drop at higher ionic strengths. Some of these conditions, which impact growth rates, are expected to influence the dissolution rate and mechanism in a similar fashion.

In summary, the ionic strength influences dissolution in three respects. A change in ionic strength impacts the solubility of calcite. Dissolution rate constants are reported to change in response to an increase in ionic strength. In addition, microtopography of mineral surfaces may change, implying a change in reaction mechanism with an increase in ionic strength.

EXPERIMENTAL METHODS

Solid and Fluid Reactants

Carrara Marble was used as the solid reactant for all of the dissolution experiments. Marble slabs were cored into 4 cm diameter cylinders, which were

then sliced into 0.75 cm thick discs. The discs were cast in epoxy keeping one surface exposed. The exposed surface was polished successively down to 5 μm grit and all other surfaces were coated with PFA Teflon. Quantitative electron microprobe analysis for elemental composition indicates the sample to be relatively pure with impurities constituting less than 0.5% by weight. The result of this analysis is reported in Chapter 2 (Table 2.A.1). Reagent grade (ACS) NaCl was used to prepare the nutrient solutions of various ionic strengths. A constant volume of 1000 ml NaCl solution was used for each experiment. To determine the effect of P_{CO_2}, experiments were performed under nitrogen and carbon dioxide atmospheres.

To test the validity of experiments, and to ensure that no Ca^{2+} is released or absorbed by the epoxy or any other reactor parts, an epoxy disc was made without any marble embedded in it. A blank experiment was run using 0.7 m NaCl solution at 150°C under flow-through conditions over a period of 4 residence times. Chemical analysis of the outlet solution showed no Ca^{2+} to be present. Other experiments showed negligible absorbance of metals by the epoxy under experimental conditions.

Reactor Design

Two different setups were used for the experiments. Batch reaction experiments were done at 70°C at varying salinities and disc spinning rates. Marble discs were mounted on a Teflon-coated spinning shaft attached to a rotary motor. The sample assembly was then immersed in the reactive fluid

inside a 1000 ml Pyrex™ glass reactor (Figure 3.2). An impeller was attached to the shaft to ensure that the solution was well mixed and fresh reactive solution was continuously directed towards the mineral surface. NaCl solutions of 0.7 molal (28,055 ppm), 1 molal (40,078 ppm), 2 molal (80,156 ppm), and 4 molal (16,0312 ppm) ionic strengths were used for the batch experiments. Discs were spun at 300, 600 and 900 rpm (Table 3.1). Nitrogen or carbon dioxide was bubbled directly into the reactor through a Nalgene™ inlet tube. Solutions were sampled using a syringe approximately every one hour until the end of the experiment (8-10 hours). Approximately 2.2 ml solutions were taken out about 7-8 times (9-10 in a few cases) during each experiment. A total of 22-25 ml or 2.5% of the solution was lost due to sampling from the initial solution volume.

The second series of experiments were done in a mixed flow/ rotating disc reactor at 70°C, 100°C, and 150°C. The reactor setup is discussed in detail in Chapter 2. The reactant solution, contained in a Nalgene™ tank, was continuously fed into the reactor via a high pressure liquid chromatography (HPLC) pump. The 0.7 molal NaCl solutions were used for all experiments in this series (Figure 3.3). Depending on the desired pH and P_{CO_2} of the reactive fluid, carbon dioxide, or nitrogen gas was bubbled into the tank prior to and during the experiments. The disc spinning rate and solution flow rate were held constant through each experiment (Table 3.2). The effluent solution was collected for analysis after approximately four residence times (one residence time equals the reactor volume divided by the solution volumetric flow rate). Chemical analysis of

Figure 3.1 Dissolution constant k_b vs. ionic strength, based on parameterization of rate model by Zuddas and Mucci (1998)
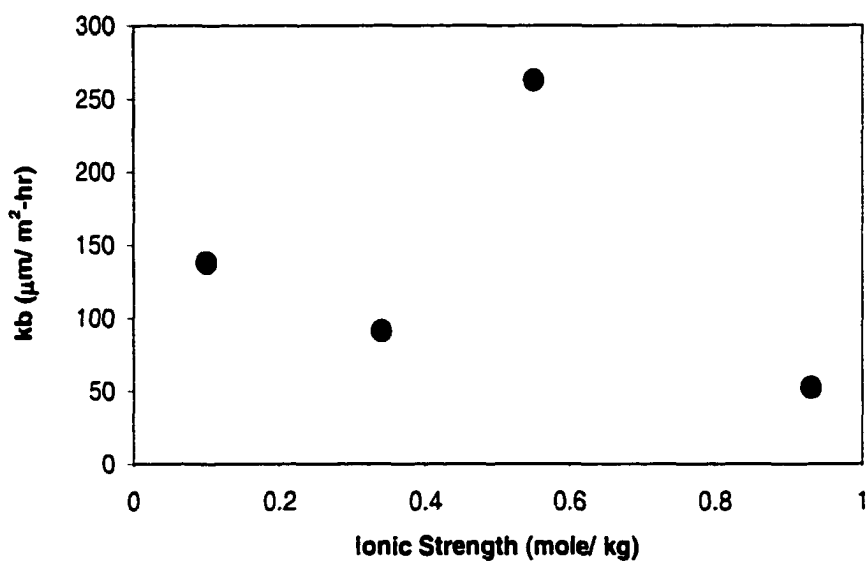
Figure 3.2 Experimental design for batch reactor experiments
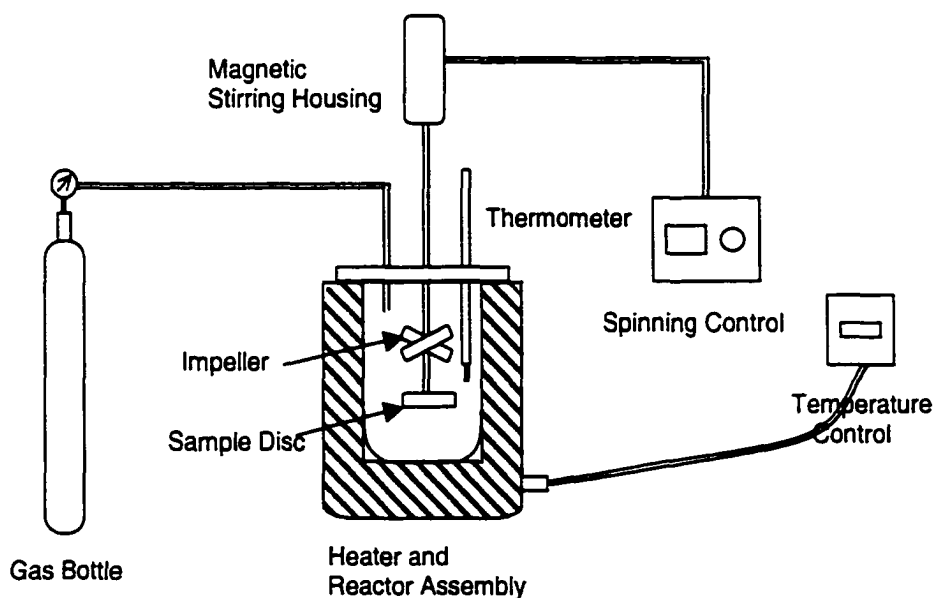
Figure 3.3 Experimental design of mixed flow/ rotating disc reactor
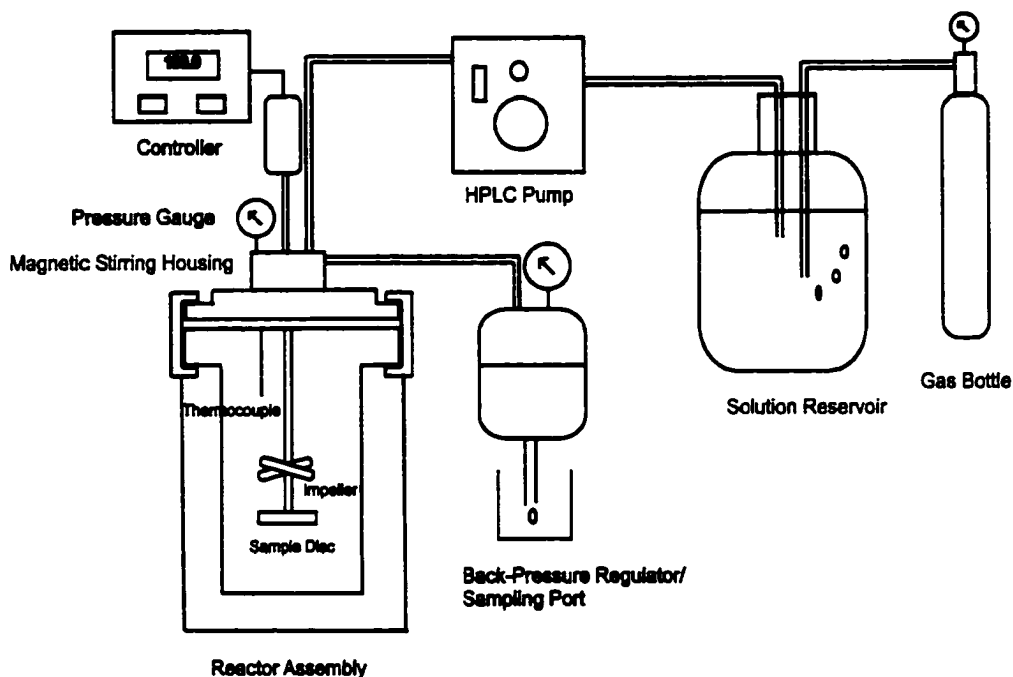
Figure 3.4   Time-concentration profiles for batch experiments in 0.7 m NaCl in N₂ atmosphere
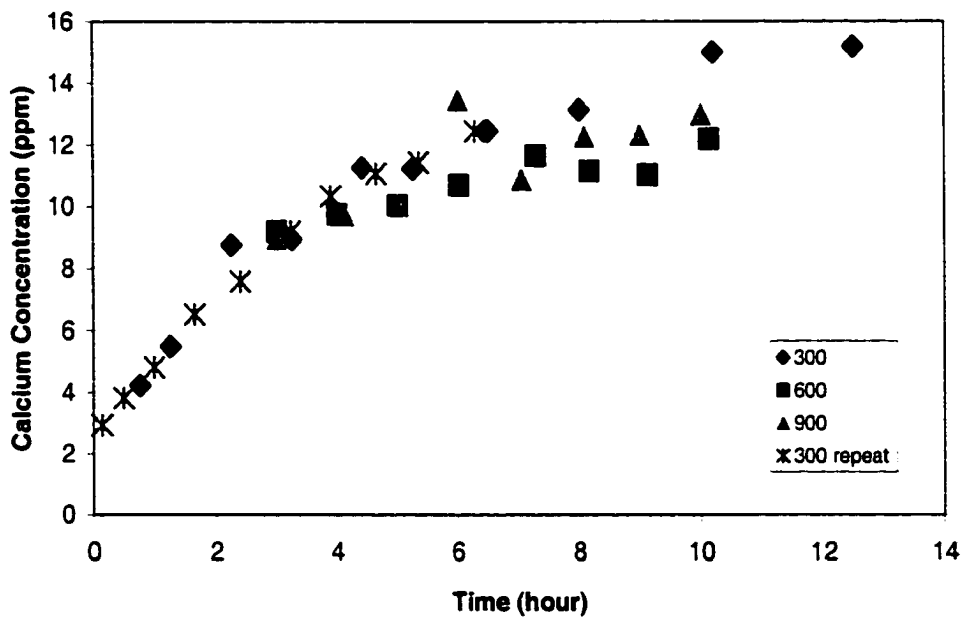
Table 3.1 Experimental matrix for saline experiments in batch reactor setting

Ionic Strength (mole/ kg)	Gas head	Spinning rate (rpm)	Temperature ($^{\circ}$C)
0.7	Nitrogen	300, 600, 900	70
	Carbon Dioxide	300, 600, 900	70
1	Nitrogen	300	70
	Carbon Dioxide	300	70
2	Nitrogen	300, 600, 900	70
	Carbon Dioxide	300, 600, 900	70
4	Nitrogen	300	70
	Carbon Dioxide	300	70

Table 3.2 Experimental matrix and dissolution rates for saline experiments in flow-through reactor setting. All experiments in this series were done using 0.7 m NaCl solution.

Experiment	Solution-Gas head	Spinning Rate (rpm)	Temperature (°C)	Dissolution Rate (mole/ cm^2-sec)
B7	0.7 m NaCl-N$_2$	300	70	1.61E-09
B8	0.7 m NaCl-N$_2$	150	70	1.38E-09
B9	0.7 m NaCl-N$_2$	400	70	2.30E-09
B10	0.7 m NaCl-N$_2$	600	70	1.78E-09
B11	0.7 m NaCl-N$_2$	900	70	2.72E-09
B12	0.7 m NaCl-N$_2$	1200	70	1.73E-09
B37	0.7 m NaCl-N$_2$	300	100	2.43E-09
B38	0.7 m NaCl-N$_2$	600	100	3.56E-09
B39	0.7 m NaCl-N$_2$	900	100	4.07E-09
B40	0.7 m NaCl-N$_2$	298	149	3.89E-09
B41	0.7 m NaCl-N$_2$	600	149	5.05E-09
B42	0.7 m NaCl-N$_2$	50	150	2.29E-09
B43	0.7 m NaCl-N$_2$	901	150	5.40E-09
B47	0.7 m NaCl-CO$_2$	300	100	1.26E-08
B48	0.7 m NaCl-CO$_2$	599	100	1.69E-08
B49	0.7 m NaCl-CO$_2$	900	100	1.83E-08
B50	0.7 m NaCl-CO$_2$	299	151	2.09E-08
B51	0.7 m NaCl-CO$_2$	600	151	2.81E-08
B52	0.7 m NaCl-CO$_2$	900	151	2.96E-08

the outlet solution for Ca^{2+} concentration was performed using standard atomic absorption techniques.

Rate Determination

Rates for flow-through experiments were determined using the following equation (Table 3.2):

$$R = \frac{(Ca^{2+}_{out} - Ca^{2+}_{in}) \cdot Flow\ rate}{Disc\ surface\ area} \quad \frac{moles/Kg \cdot Kg/sec}{cm^2} \qquad (6)$$

Rates for batch reaction experiments were determined using an integrated form of the following rate equation.

$$\partial C_{Ca}/\partial t = (A/V)\ k^+\ (1 - \Omega^{1/2})^2 \qquad (7)$$

where A/V (cm^{-1}) is the ratio of the surface area of the solid reactant and solution volume and k^+ ($mole/cm^2$-sec) is the rate coefficient.

A nonlinear rate law for surface reaction controlled rates has been expressed by the general form (Inskeep and Bloom, 1985; Shiraki and Brantley, 1995):

$$R = k\ (1 - \Omega^{1/2})^2 \qquad (8)$$

where k is the rate constant, and Ω is saturation given by the ratio of ionic activity product and solubility product for calcite. The solubility product K_{sp} is given by

$$K_{sp} = m_{Ca2+}{}^{eq} \cdot m_{CO32-}{}^{eq} \cdot \gamma_{\pm}{}^2 \qquad (9)$$

where m_i stands for molality of the subscripted species, and $\gamma_{\pm}$ is activity coefficient for Ca^{2+} (assuming $\gamma_{\pm Ca2+} \approx \gamma_{\pm CO32-}$). Rewriting $\Omega^{1/2}$ in equation (8) in terms of ionic activity product and solubility product results in

$$\Omega^{1/2} = (m_{Ca}{}^{2+} \cdot m_{CO3}{}^{2-} \cdot \gamma_{\pm}{}^2 / K_{sp})^{1/2} \qquad (10)$$

In the $CaCO_3$-CO_2-H_2O system, dissociation of bicarbonate ion occurs via reaction
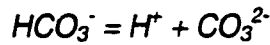
$$HCO_3^- = H^+ + CO_3^{2-}$$

for which equilibrium constant K_2 is given by

$$K_2 = a_H{}^+ \cdot a_{CO3}{}^{2-} / a_{HCO3}{}^- \qquad (11)$$

Rearranging equation (11) and rewriting in terms of molality

$$m_{CO3}{}^{2-} = m_{HCO3}{}^- \cdot \gamma_{HCO3}{}^- \cdot K_2 / (a_H{}^+ \cdot \gamma_{CO3}{}^{2-}) \qquad (12)$$

Assuming $m_{Ca}{}^{2+} = m_{HCO3}{}^-$ (valid for calcite dissolution at intermediate pH)

67

$$m_{CO_3^{2-}} = m_{Ca}^{2+} \cdot \gamma_{HCO_3^-} \cdot K_2 / (a_H^+ \cdot \gamma_{CO_3^{2-}}) \tag{13}$$

Substituting for $m_{CO_3^{2-}}$ in equation (10) results in

$$\Omega^{1/2} = m_{Ca}^{2+} \cdot \gamma_\pm \{(\gamma_{HCO_3^-} \cdot K_2) / (K_{sp} \cdot a_H^+ \cdot \gamma_{CO_3^{2-}})\}^{1/2} \tag{14}$$

Combining equation (11) at equilibrium and equation (9) gives

$$K_{sp} = (m_{Ca2+}^{eq})^2 \cdot K_2 \cdot \gamma_\pm^2 / a_H^{+\,eq} \tag{15}$$

Substituting for K_{sp} into equation (14) gives

$$\Omega^{1/2} \approx (m_{Ca2+} / m_{Ca2+}^{eq}) \cdot (a_H^{+\,eq} / a_H^+)^{1/2} \tag{16}$$

Assuming $a_H^{+\,eq} / a_H^+ \approx 1$ and substituting into equation (8) we get

$$R = k \{1 - (m_{Ca2+} / m_{Ca2+}^{eq})\}^2 \tag{17}$$

The rate law given by equation (17) is valid only if certain assumptions hold. These are

1. reactions are entirely surface reaction controlled and

2. $a_H^{+\,eq} / a_H^+ \approx 1$

As will be discussed in the results section, dissolution at 70°C is largely surface reaction controlled for these experimental conditions of ionic strength and P_{CO_2}, with one exception. Therefore, the first assumption is valid for the most

part. It is necessary to note that the second assumption may not be entirely valid for these conditions.

A concentration-time expression of rate, equivalent to equation (17), is given by

$$dC_{Ca} / dt = (A/V) \, k^+ \, \{1 - (C_{Ca2+} / C_{Ca2+}{}^{eq})\}^2 \qquad (18)$$

where A/V (cm^{-1}) is the ratio of the surface area of the solid reactant and solution volume and k^+ (mole/cm^2-sec) is the rate coefficient. Rearranging results in

$$d \, (C_{Ca2+}{}^{eq} - C_{Ca}) / dt = -(A/V) \, [k^+ / (C_{Ca2+}{}^{eq})^2] \, (C_{Ca2+}{}^{eq} - C_{Ca})^2 \qquad (19)$$

This may be rewritten in terms of Δ, the departure of solution concentration from the equilibrium concentration, i.e. $\Delta = C_{Ca2+}{}^{eq} - C_{Ca2+}$.

$$d\Delta / dt = - (A/V) \, k^+ / (C_{Ca2+}{}^{eq})^2 \, \Delta^2 \qquad (20)$$

This may be written as

$$d\Delta / dt = - k' \, . \, \Delta^2 \qquad (21)$$

where $k' = (A/V) \, k^+ / (C_{Ca2+}{}^{eq})^2$. k' is the apparent rate constant and k^+ gives the intrinsic rate constant.

Integration of equation (21) with respect to time leads to a simple linear form

$$1/\Delta_t - 1/\Delta_{t0} = k' (t - t_0) \qquad\qquad (22)$$

where Δ_{t0} is Δ at first sampling time, t_0. The concentration is expressed in mol/cm^3 and time in seconds. Experimental data represented in the above form plot along a linear trend, the slope of which gives the negative of apparent rate constant k' (Figure 3.7 – 3.9 and Figure 3.13 – 3.15). Intrinsic rate constants k^+ may be computed from the above and may be substituted in equation (8) to determine dissolution rates from batch experiments. This method of rate determination has been used for barite-water reactions in batch experiments by Sanders (1998).

RESULTS AND DISCUSSION

Batch Experiments

Time-concentration profiles for batch experiments portray the time it takes for a solution to reach equilibrium with respect to the solid in contact. As the trend plateaus off, the final concentration represents the equilibrium concentration or solubility of the mineral under the experimental conditions. In the present study, time-concentration profiles do not plateau off within the duration of the experiments. Calcite solubilities used in the rate calculations were taken from other sources (Table 3.3).

Batch experiments in an N_2 atmosphere at 70°C in 0.7 m and 2 m NaCl solutions at varying disc spinning rates do not show a marked difference in the

70

Table 3.3 Solubility constants, rate coefficients and rates determined for batch experiments. All experiments in this series were done at 70°C

Exp	Solution-Gas head	Spinning Rate (rpm)	Solubility Constant[1] (molal)	Apparent Rate Constant k'	Intrinsic Rate Constant k^+ (mole/ cm^2-sec)	Rate (mole/ cm^2 sec)
B17	0.7m NaCl-air	300	4.9E-04	143.3	3.07E-09	4.61E-12
B18	0.7 m NaCl - N_2	300	4.9E-04	156.5	3.35E-09	1.94E-12
B19	0.7 m NaCl - N_2	600	4.9E-04	51.9	1.11E-09	1.79E-12
B20	0.7 m NaCl - N_2	900	4.9E-04	89.0	1.90E-09	2.45E-12
B21	1 m NaCl - N_2	300	7.6E-04	29.1	1.50E-09	4.53E-12
B22	2 m NaCl - N_2	300	6.0E-04	33.1	1.06E-09	3.05E-12
B23	2 m NaCl - N_2	600	6.0E-04	31.6	1.01E-09	3.08E-12
B24	2 m NaCl - N_2	900	6.0E-04	31.2	1.00E-09	2.22E-12
B28	4 m NaCl - N_2	300	5.4E-04	8.6	2.24E-10	1.03E-12
B29	4 m NaCl - CO_2	300	5.9E-03	1.2	3.72E-09	2.71E-11
B30	1 m NaCl - CO_2	300	1.0E-02	0.5	4.46E-09	3.45E-11
B31	2 m NaCl - CO_2	300	8.8E-03	0.6	4.14E-09	3.18E-11
B32	2 m NaCl - CO_2	600	8.8E-03	0.6	4.14E-09	3.20E-11
B33	2 m NaCl - CO_2	900	8.8E-03	0.5	3.45E-09	2.71E-11
B34	0.7 m NaCl - CO_2	300	5.2E-03	1.4	3.37E-09	2.28E-11
B35	0.7 m NaCl - CO_2	600	5.2E-03	1.7	4.10E-09	2.49E-11
B36	0.7 m NaCl - CO_2	900	5.2E-03	2.0	4.82E-09	2.80E-11

[1] Source: 1) Report on "Comprehensive Scale Prediction Project", Atkinson 1993

2) Solubility determined using OK SCALE 98 version 1.11, Atkinson and Mecik, 1998

3) Solubility determined using PHREEQCI 2.4.2, Parkhurst and Appelo, 2001

Figure 3.5 Time-concentration profiles for batch experiments in 2 m NaCl in N_2 atmosphere
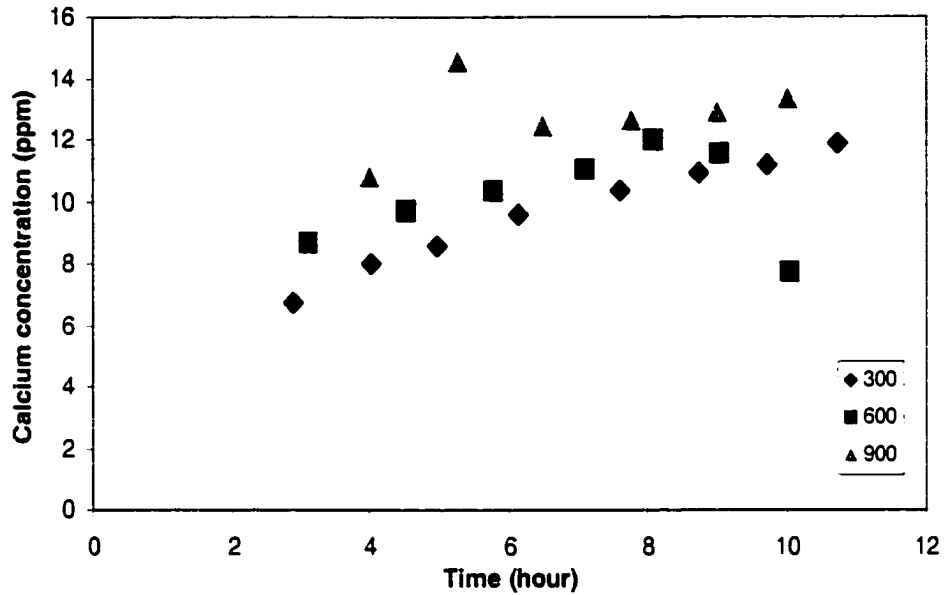
Figure 3.6 Time-concentration profiles for batch experiments in 0.7 to 4 m NaCl in N_2 atmosphere. All data at 300 rpm disc spinning rates
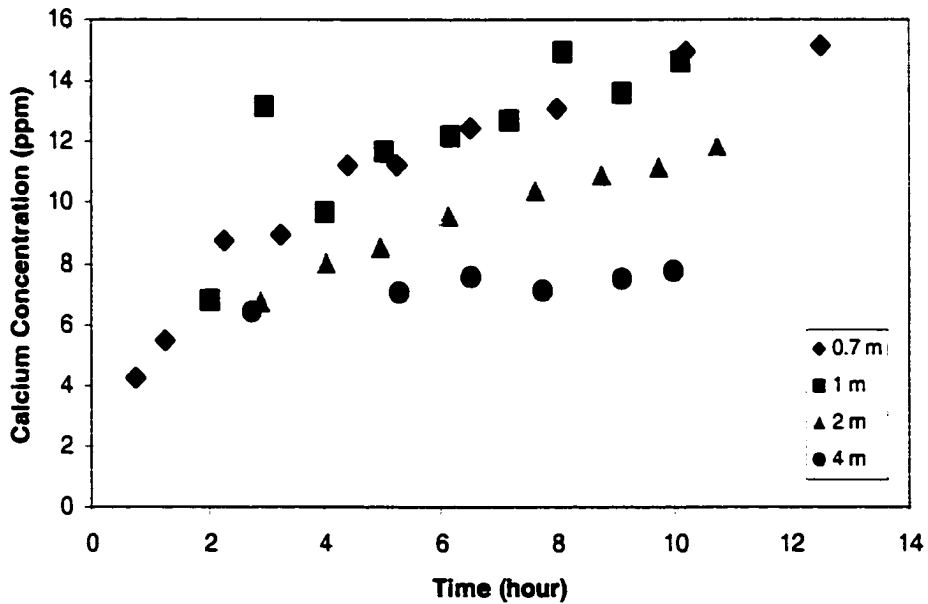
Figure 3.7 Apparent rate coefficient k' for dissolution in 0.7 m solution in N_2 atmosphere. Results are from batch experiments
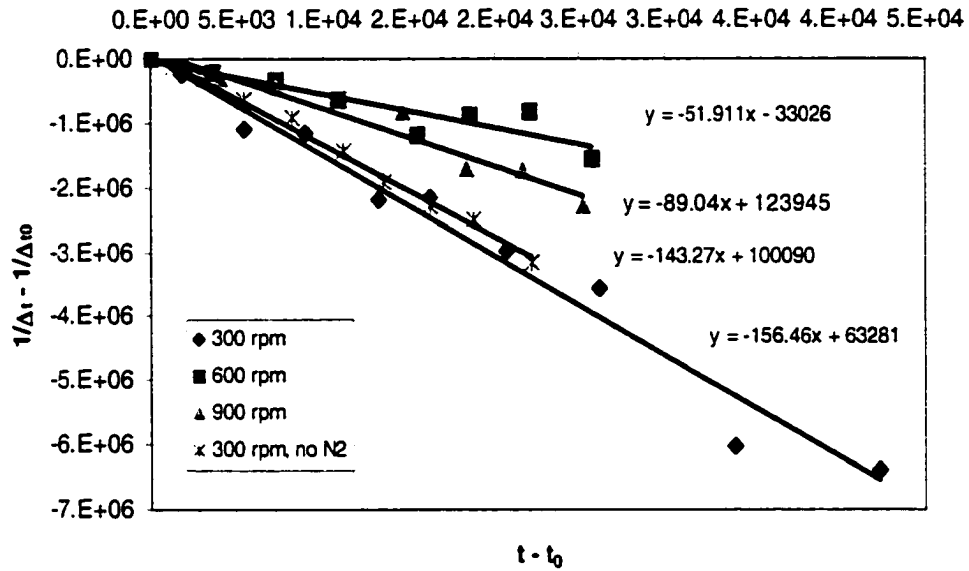
Figure 3.8 Apparent rate coefficient k' for dissolution in 2 m solution in N_2 atmosphere. Results are from batch experiments
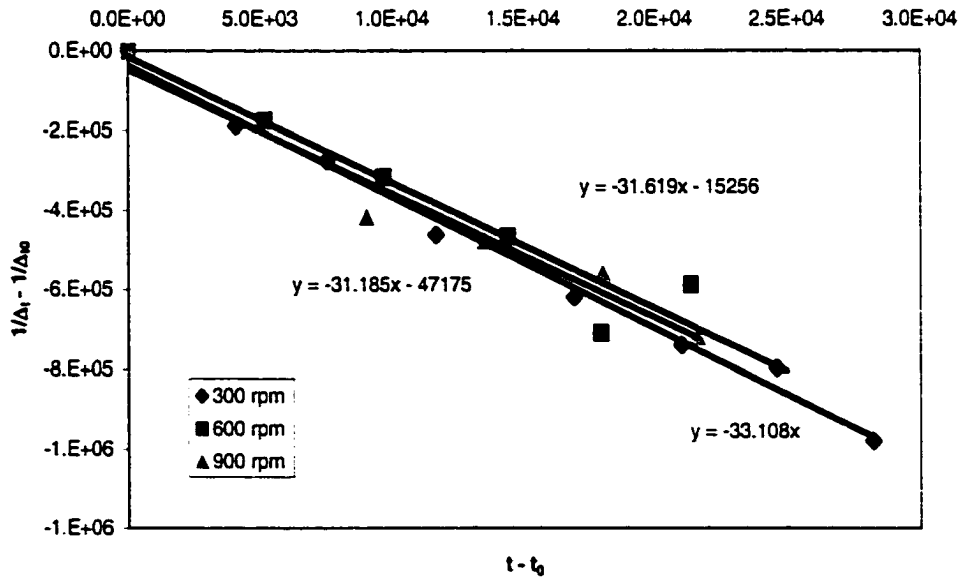
Figure 3.9 Apparent rate coefficient k' for dissolution in 0.7 m to 4 m solution in N_2 atmosphere. Results are from batch experiments
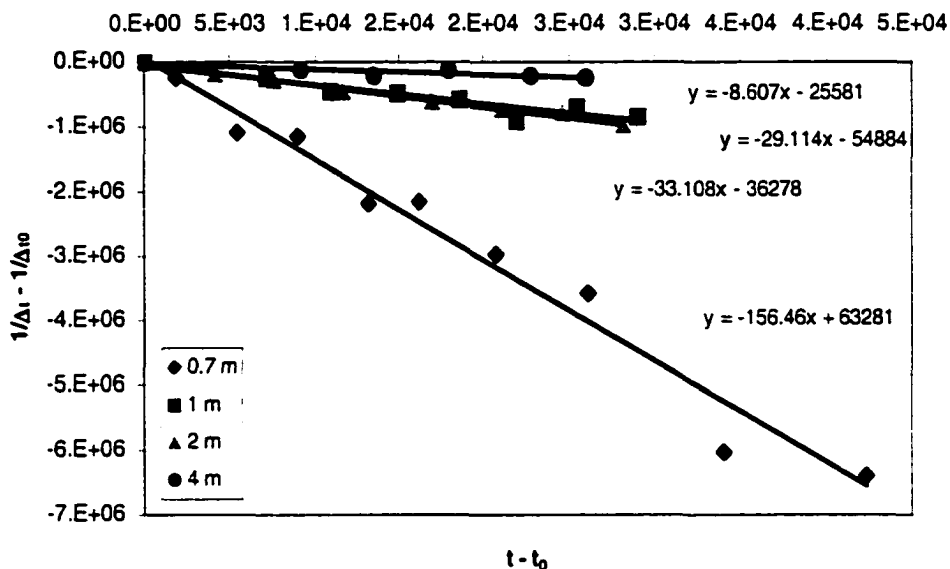
Figure 3.10 Dissolution rates at varying disc spinning rates in 0.7 m and 2 m solutions in N_2 atmosphere. Results are from batch experiments
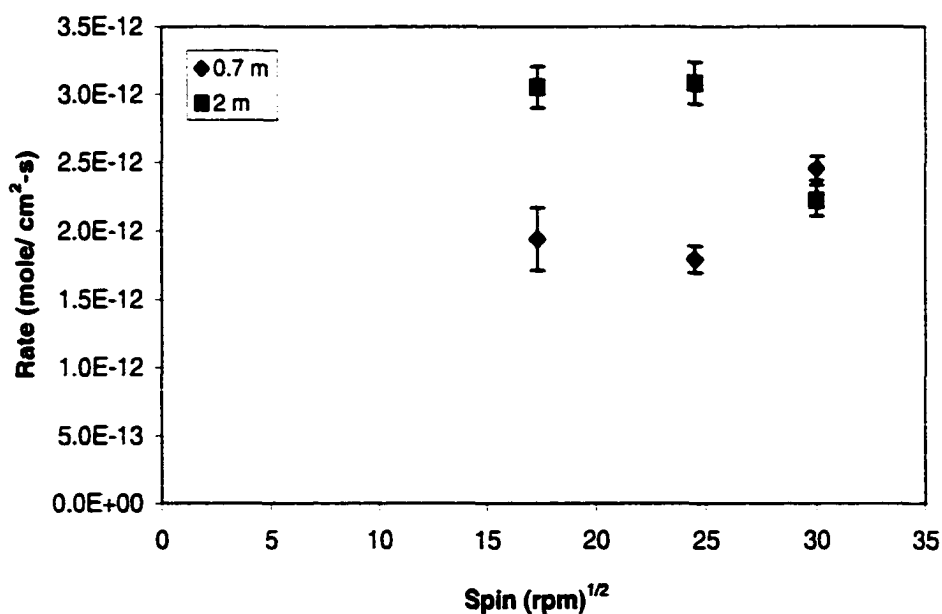
Figure 3.11 Dissolution rates and solubilities for calcite in 0.7 m to 4 m solutions in N_2 atmosphere. Rate data are for batch experiments
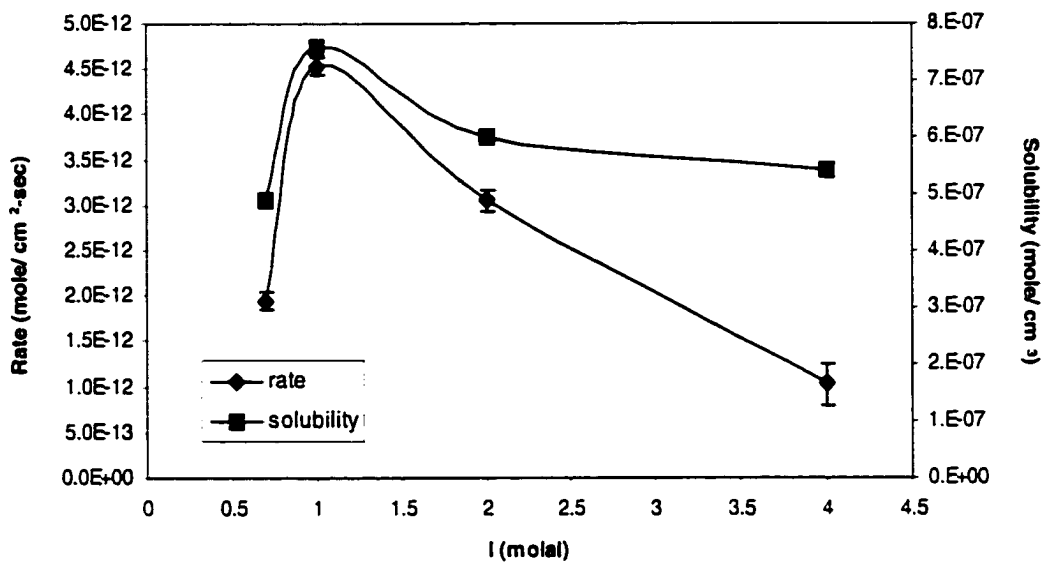
Figure 3.12 Logarithm of rate coefficient k^+ shows a near linear relation with square root of ionic strength.
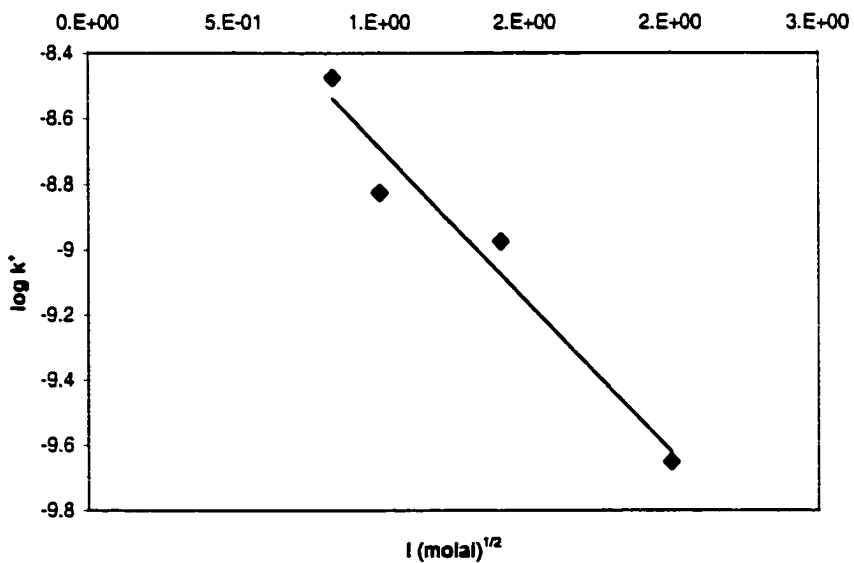
Figure 3.13 Time-concentration profiles for batch experiments in 0.7 m NaCl in CO_2 atmosphere
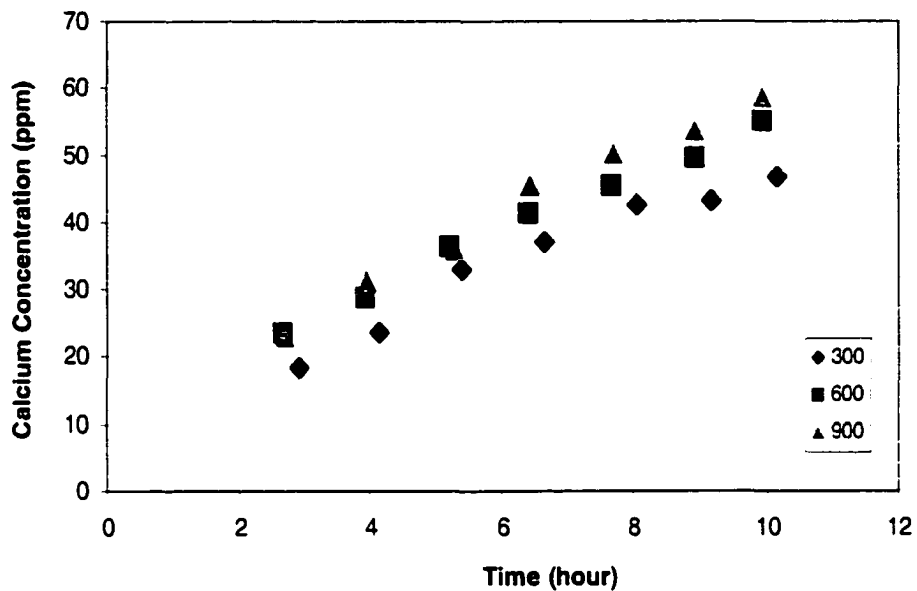
Figure 3.14 Time-concentration profiles for batch experiments in 2 m NaCl in CO_2 atmosphere
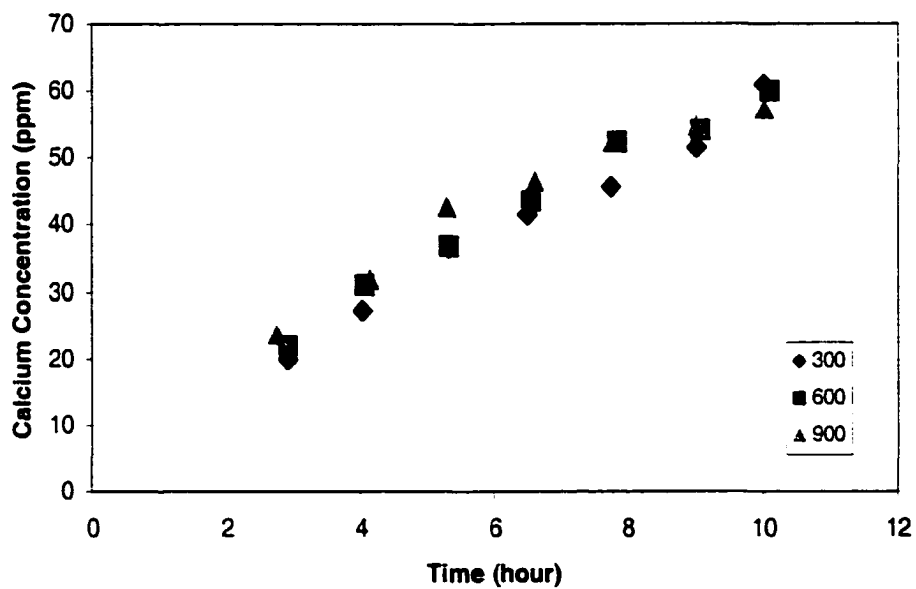
Figure 3.15 Time-concentration profiles for batch experiments in 0.7 to 4 m NaCl in CO_2 atmosphere. All data at 300 rpm disc spinning rates
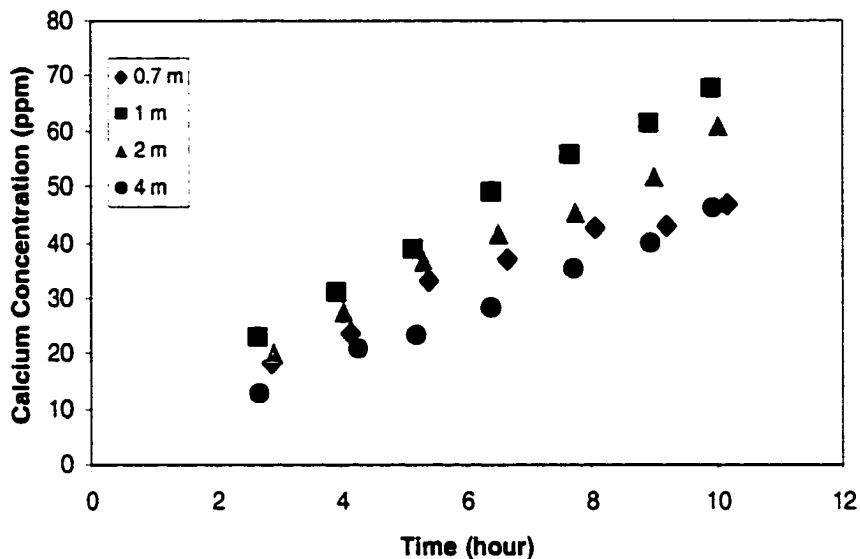
Figure 3.16 Apparent rate coefficient k' for dissolution in 0.7 m solution in CO_2 atmosphere. Results are from batch experiments
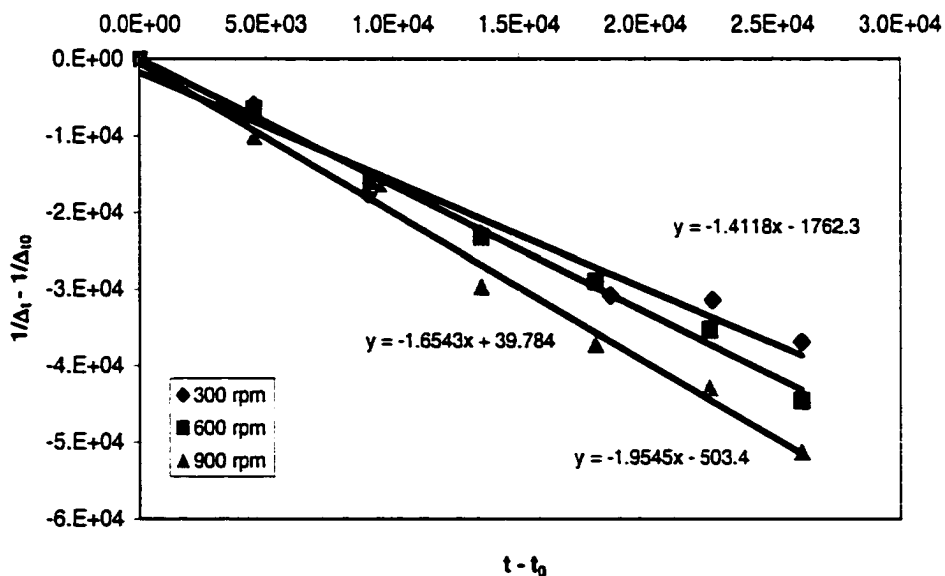
final concentrations (Figure 3.4 and Figure 3.5). This is expected since equilibrium concentrations are not functions of hydrodynamics. The influence of ionic strength on solubility is evident when concentration-time plots for dissolution in 0.7 m, 1 m, 2 m and 4 m solutions at 300 rpm disc spinning rates are compared (Figure 3.6). The solubility in 0.7 m and 1 m solutions are not appreciably different. However, solubility is seen to drop considerably as ionic strength increases to 2 m and 4 m.

The time-concentration slopes within each ionic strength series do not appear significantly different. In order to determine the effects of disc spinning on dissolution rates it is necessary to focus on the intrinsic rate coefficient k^+ in equation (20). As described previously, k^+ values were determined using the slope k' in the integrated rate form given by equation (22), i.e. the slope is obtained from $1/\Delta_t - 1/\Delta_{t0}$ vs. $(t - t_0)$. The apparent rate coefficient k' for all experiments in an N_2 atmosphere are given by the respective linear fits and k^+ values were calculated (Table 3.3, Figure 3.7 – 3.9).

To illustrate the dependence of dissolution on disc spinning rates, rate data are often plotted with respect to the square root of disc spinning rate. It has been suggested that a linear fit in such a plot represents purely transport-controlled kinetics whereas a nonlinear fit is indicative of a mixed kinetic dependence (Sjoberg and Rickard, 1984). The degree of departure from linearity is reflective of rates being dominated by other mechanisms such as surface reaction. Dissolution rates in 0.7 and 2 m solutions were calculated using equation (18) and were plotted with respect to the square root of disc spinning

rates in Figure 3.10. No systematic increase of rates is apparent, suggesting that dissolution may be independent of solution turbulence or rate of diffusional transport under these conditions. At these ionic strengths and pH, the surface reaction rates may be more important than diffusional transport. When rates and solubilities were plotted with respect to ionic strength over the range of 0.7 m to 4 m solutions, it was noted that the rates seemed to mimic the solubility behavior (Figure 3.11). The dissolution rate and solubility both increase as ionic strength increases from 0.7 m to 1 m. Rates drop significantly for higher ionic strength solutions while the solubility drops by a smaller degree. Logarithms of rate coefficients show a near linear trend when plotted with the square root of ionic strength (Figure 3.12). Based on theoretical understanding of mineral-water reactions in lower ionic strength solutions, logarithms of rate coefficients at lower ionic strength have been predicted to have a linear relation with the square root of ionic strength (Brezonik, 1994; Stumm and Morgan, 1996; Langmuir, 1997). A similar behavior is observed in this study for the higher ionic strength solutions in an N_2 atmosphere.

Time-concentration profiles for the experiments conducted under a CO_2 atmosphere all show near linear trends that do not seem to approach equilibrium during the experimental runs (Figure 3.13 – 3.15). The series in 0.7 m solutions appear to exhibit some dependence on hydrodynamics since concentrations reached by the endpoint in the experiment do show some variations with disc spinning rates. The series in 2 m solutions show no appreciable difference either in the data trend or the final concentrations reached. Similar to the N_2 case,

differences are more pronounced when concentration data are plotted for varying ionic strengths (Figure 3.15). Solubility initially goes up as the ionic strength increases from 0.7 m to 1 m. This is followed by a drop in solubility with an increase in ionic strength up to 4 m.

To determine the apparent rate coefficient k', results are plotted as $1/\Delta_t - 1/\Delta_{t0}$ against $(t - t_0)$ and the k' values were determined from the slopes (Table 3.3, Figure 3.16 to 3.18). The intrinsic rate coefficients k^+ were then calculated which allowed determination of the dissolution rates using equation (18) (Table 3.3). The experiments in 0.7 m solutions in the CO_2 atmosphere exhibit a slight dependence on the disc spinning rate indicating diffusional transport rate to have some influence on dissolution (Figure 3.19). The series in 2 m reactant solutions showed no recognizable transport control suggesting surface reaction may be more important (Figure 3.19). Again, similar to the N_2 series, rate dependence on the ionic strength shows a trend similar to that of solubility (Figure 3.20). Both rates and solubilities increase as solution ionic strength goes from 0.7 m to 1 m. This is followed by a drop in both cases as ionic strength goes up from 1 m to 4 m.

Logarithms of rate coefficients for the CO_2 series are plotted with respect to the square root of ionic strength. (Figure 3.21). All rate coefficients, except that for the 0.7 m solution, show a linear trend. It should be noted that a transport dependence was observed for dissolution in 0.7 m solutions and a CO_2 atmosphere. This suggests that the assumption of a surface reaction-controlled rate law which is used to fit the results for all experimental conditions is not

Figure 3.17 Apparent rate coefficient k' for dissolution in 2 m solution in CO_2 atmosphere. Results are from batch experiments

$y = -0.5367x - 1041.7$

$y = -0.5959x - 590.06$

300 rpm
600 rpm
900 rpm

$y = -0.6123x - 229.6$

$t - t_0$
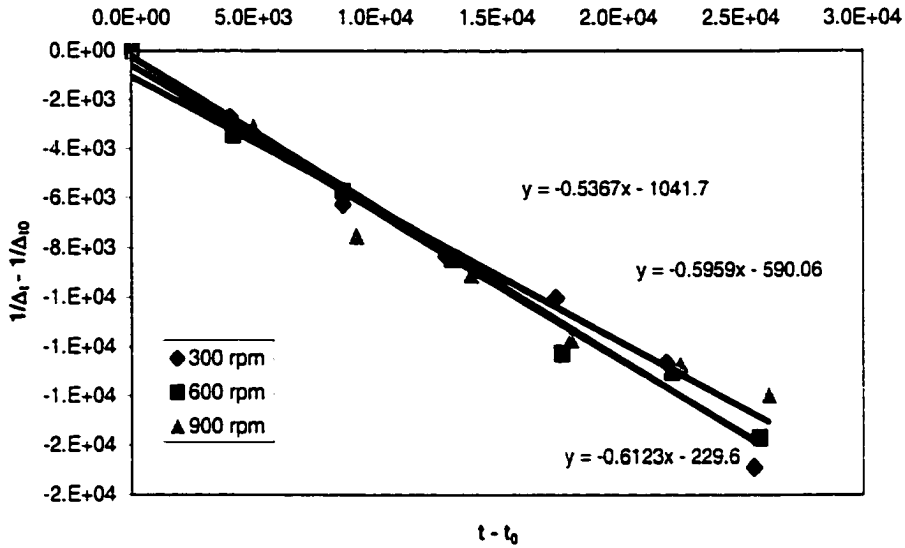
Figure 3.18 Apparent rate coefficient k' for dissolution in 0.7 m to 4 m solution in CO_2 atmosphere. Results are from batch experiments

$y = -0.5149x + 15.369$

0.7 m
1 m
2 m
4 m

$y = -0.6123x - 229.6$

$y = -1.18x + 786.75$

$y = -1.4118x - 1762.3$

$t - t_0$
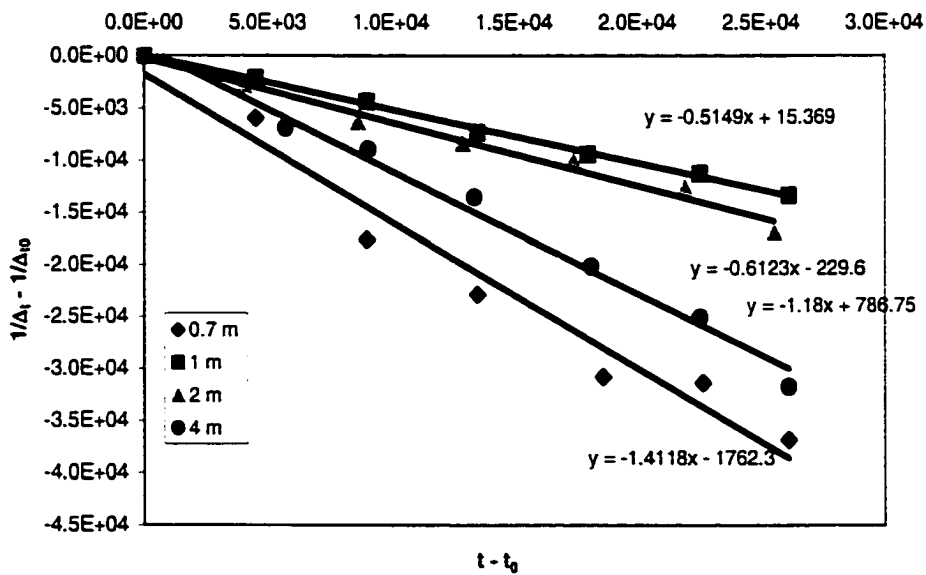
Figure 3.19 Dissolution rates at varying disc spinning rates in 0.7 m and 2 m solutions in CO_2 atmosphere. Results are from batch experiments
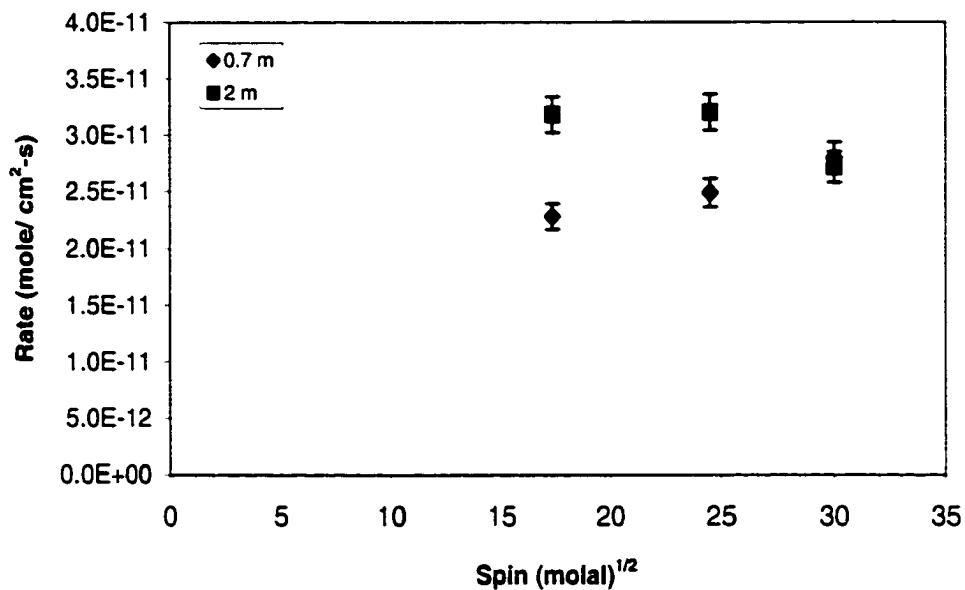
Figure 3.20 Dissolution rates and solubilities for calcite in 0.7 m to 4 m solutions in CO_2 atmosphere. Rate data are for batch experiments
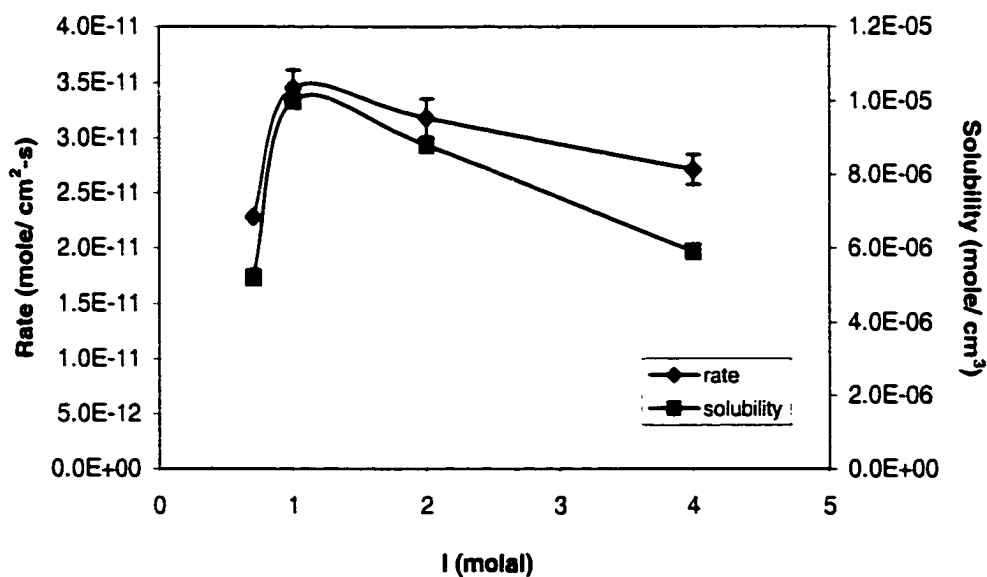
Figure 3.21 Logarithm of rate coefficient k⁺ do not show linear relation with square root of ionic strength as predicted for lower ionic strength solutions
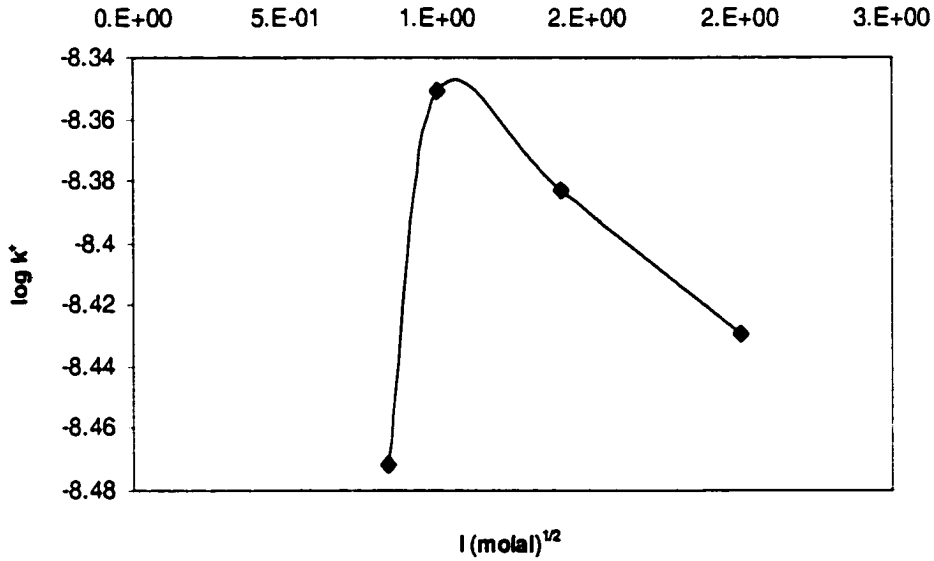
Figure 3.22 Flow-through experiments at 70, 100, and 150°C in 0.7 m NaCl solution and N_2 atmosphere. Data varying in disc spinning rates between 50 and 900 rpm. Rates reported by Sjoberg and Rickard (1984) for calcite dissolution at 62°C in 0.7 M KCl solution and N_2 atmosphere is shown for comparison
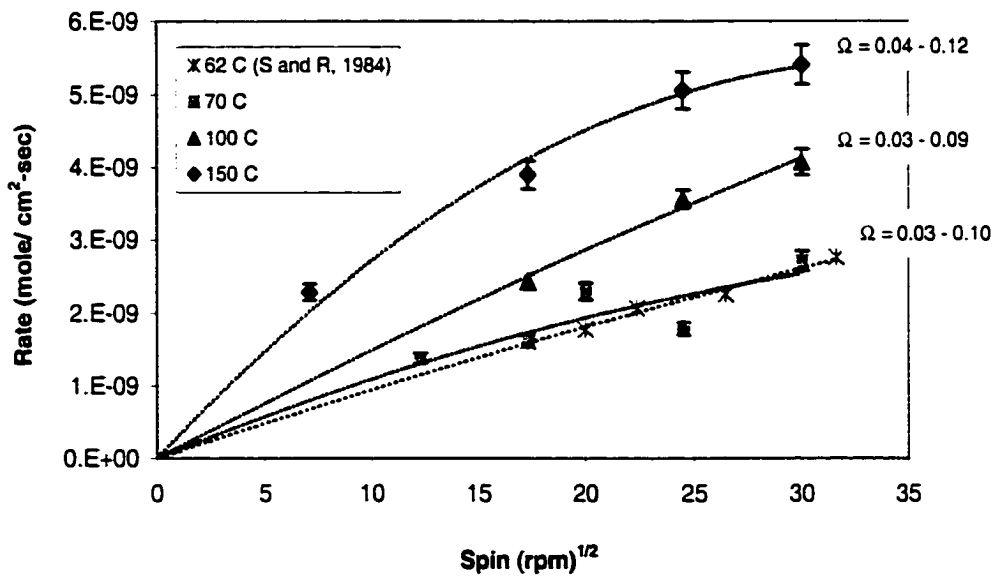
appropriate for this case. This may explain why dissolution in a 0.7 m solution and CO_2 atmosphere does not show a linear fit along with the rest of the data at similar P_{CO_2}.

Mixed Flow Experiments

The experiments performed in mixed flow reactors portray hydrodynamic, ionic strength, and temperature dependence of dissolution rates. To illustrate the effect of temperature and hydrodynamics, dissolution rates at 70°C, 100°C, and 150°C, in a N_2 atmosphere have been plotted with respect to the square root of disc spinning rates (Figure 3.22). Rates at 100°C are higher by a factor of 1.5 relative to those at 70°C, while rates at 150°C are approximately three times higher (Table 3.2). As seen in the plot, data at 70°C show some scatter and the response to disc spinning rates is not entirely clear. The relative dominance of the surface reaction rate and diffusional transport rate in controlling the overall dissolution mechanism is not evident from these results. Sjoberg and Rickard (1984) have presented dissolution data for rotating disc experiments at 62°C using Carrara marble in 0.7 M KCl solutions under a N_2 atmosphere. They have reported a mixed kinetic control under these conditions based on a nonlinear fit of rates when plotted with respect to the square root of spinning rates. It should be noted that the fit to their data appears to be linear in plots presented here, which is a function of choice of the axis scales (Figure 3.22). Based on this study, an increase in rates, in response to temperature, may be accompanied by a

84

change in the reaction mechanism from surface reaction controlled to transport controlled. Transport is the dominant dissolution mechanism at higher temperatures as rates at 100°C and 150°C show obvious response to disc spinning rates. However, the relative importance of surface reaction below 100°C is not entirely apparent from the data (Figure 3.22).

The effect of ionic strength on rates is demonstrated when dissolution rates in nonsaline solution (Chapter 2) are compared to dissolution in a 0.7 m NaCl solution at 100°C (Figure 3.23). Dissolution rates, especially those at higher spinning rates, increase more dramatically with ionic strength. This is also consistent with the observations by Zuddas and Mucci (1998). They report a sharp increase in the rate constant, and consequently rates, as the solution goes up to 0.7 m ionic strength (Figure 3.1).

Dissolution rates in a CO_2 atmosphere show a mixed kinetic dependence when plotted with respect to the square root of spinning (Figure 3.24). Rates are nearly one and a half times higher due to an increase in temperature from 100°C to 150°C (Table 3.2). Rates are almost an order of magnitude higher than dissolution in an N_2 atmosphere due to $aH_2CO_3^*$, i.e. a high concentration of dissolved CO_2.

Errors

Various factors may contribute to errors in the results. Errors in dilution may lead to inaccuracies in measured concentration values. Solution evaporation might lead to a change in concentration before and during chemical analysis. A

Figure 3.23 Dissolution in flow-through experiments at 100°C in 0.7 m NaCl solution compared with 100°C data for dissolution in nonsaline solutions. Disc spinning rates vary between 50 and 900 rpm. Both series are in N_2 atmosphere
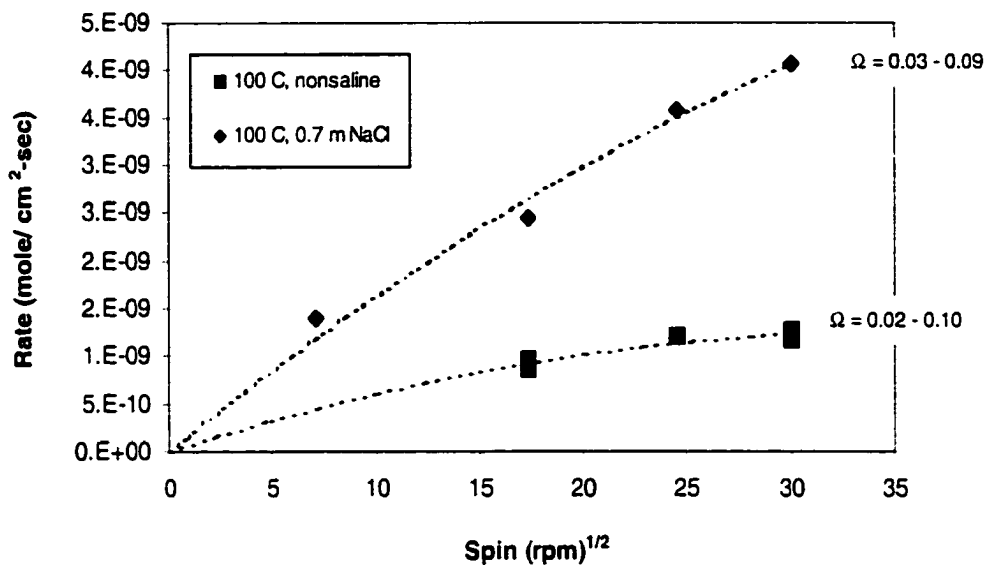
Figure 3.24 Flow-through experiments at 100, and 150°C in 0.7 m NaCl solution and CO_2 atmosphere. Data varying in disc spinning rates between 300 and 900 rpm
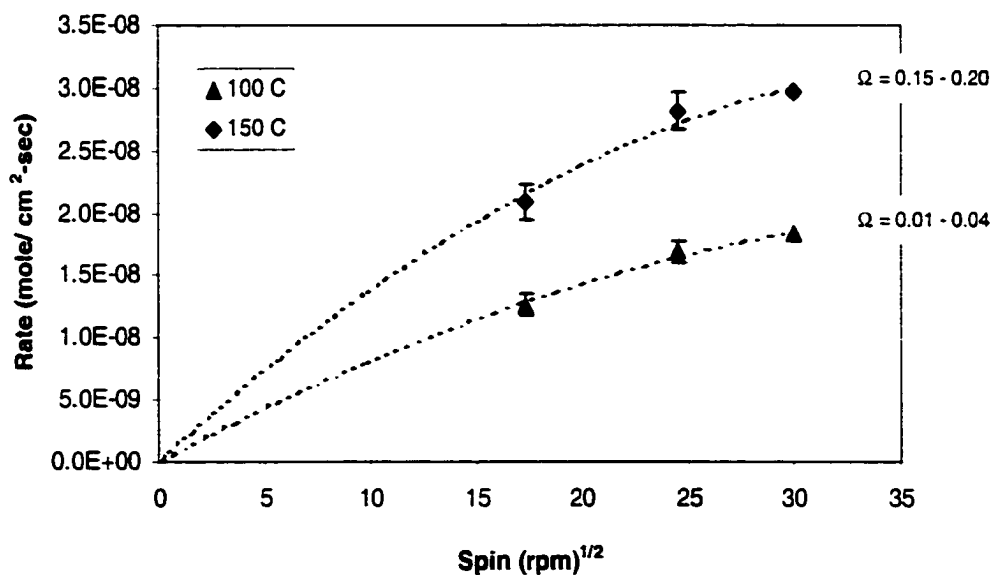
change in the solution volume may occur in the reactor due to a change in temperature as well as sampling. In addition, instrumental errors may be present in the data. A change in solution volume due to sampling, when not taken into account, will underestimate rates whereas change in concentration due to evaporation will overestimate rates. Factors such as variation in the reactive surface area between experiments due to variability in surface preparation, or variable extent of surface deterioration over the course of each experiment may also contribute to some inaccuracies. In the case of experiments performed in CO_2 atmosphere, the reactions were vigorous and discs may have suffered a greater degree of degradation at the disc edge. In these cases, solutions may have percolated through the fine cracks between the marble disc and epoxy near the disc edge. However, such damage would have been at a microscopic level since sample discs were carefully checked to ensure that there was no perceptive degradation. Based on a rough estimation (from reproducibility checks) all of the above may have contributed to a maximum of 10% total error. Error bars for 10% error are shown for all the calculated rate data (Figure 3.10, 3.11, 3.19 and 3.20).

CONCLUSIONS

Based on this study, the ionic strength does play a role in calcite dissolution rates. As seen from the batch experiments, for both the N_2 and CO_2 series, rates increase as the solution goes from dilute to 1 m ionic strength. Thereafter, rates drop with a further increase in ionic strength up to 4 m. Rates

and solubility respond to a change in ionic strength in a similar fashion. Results from mixed-flow experiments also indicate that rates increase with ionic strength up to 0.7 m.

The dissolution rate coefficient k_b as defined by Zuddas and Mucci (1998) is a function of carbonate ion concentration and is shown to drop as ionic strength drops from 0.7 m to 1 m. This is expected to result in a similar drop in dissolution rates over this range in ionic strength. But rates in this study are seen to increase between 0.7 m and 1 m.

Transport dependence for solutions at 70°C is not evident. However, dissolutions at 100°C and 150°C are distinctly influenced by the diffusional transport rate at the mineral-solution interface.

In response to a temperature increase, rates increase approximately by a factor of 1.5 and 3 between 70 °C and 100 °C and between 70 °C and 150 °C, respectively.

CHAPTER 4

Reaction-Transport Model for Calcite Scale Precipitation in Near-Wellbore Region

ABSTRACT

A model is developed that accounts for the time and space dependence of calcite precipitation. Rate expressions were fit to the experimental data over a range of physical-chemical conditions at elevated temperatures (Chapter 2 and Chapter 3). These rate equations were used in a reaction-transport model for predicting calcite scaling near oilfield production and injection wells. Solution speciation and advective transport in one spatial dimension, coupled with user defined rate laws dependent on temperature, flow conditions, solution saturation and other chemical variables, is modeled using the inbuilt capabilities of the program PHREEQC Interactive 2.4.2 (Parkhurst and Appello, 2001).

The model needs to be extended by incorporating the ionic strength dependence for calcite precipitation. This will be derived from the experiments at higher ionic strengths (Chapter 3).

INTRODUCTION

Scaling is one of the causes of formation damage or reduction in permeability of rocks in the near-wellbore region during drilling, completion, workover, injection, stimulation or production of wells. Scaling causes clogging of perforations and equipment and due to blockage in tubing and flow lines, wells may produce significantly below full potential and is of considerable concern to production engineers. Significant decline in well productivity due to formation damage leads to lost production worth billions of dollars each year worldwide (Civan 2000). To address the problem, high cost workover operations are often necessary. Calcium carbonate is one of the primary scale-forming minerals that precipitate from formation waters. Such scaling tends to decrease permeability in the near-well bore area as well as inside the pipeline by clogging the valves and other equipment (Figure 4.1 and 4.2). Scale formation is often triggered by a drop in temperature-pressure and mixing of solutions of varying chemistry during production. Identification of the mechanism and accurate prediction of scale precipitation can help engineers design more effective techniques for reducing this kind of formation damage, which can increase productivity and cost effectiveness in designing operations, and extend the life of fields. Reliable prediction can help to identify some factors that may be controlled to minimize scaling or to design effective treatment procedures.

Scale prediction models commonly used are often based only on thermodynamic considerations even though the process is not entirely under the domain of thermodynamics. For example, calcium carbonate may stay in solution

Figure 4.1 View of plug before it was subject to formation brine flooding (Courtesy www.corex.co.uk)

Figure 4.2 Plug after formation brine has been flooded through it at reservoir conditions. Scale composed of calcium carbonate has been precipitated (Courtesy www.corex.co.uk)
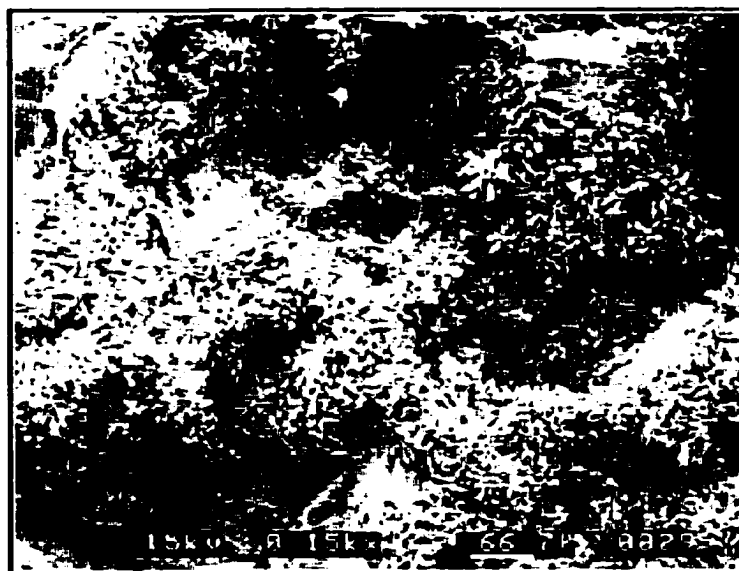
in a metastable state even after it has reached supersaturation. Thus any model based on thermodynamics alone, could make erroneous predictions. This time lag between the supersaturation and growth of the critical nuclei, also known as the induction time, is within the domain of kinetics. If the solution residence time in formation and pipelines is shorter than the induction time, scale may be altogether prevented from forming (Ostvold and Randhol, 2001). Conversely, rapid reactions can reach equilibrium in a short period of time and slow down the scale forming process as the system approaches equilibrium. Predictions based on equilibrium assumptions in this case, will lead to conservative estimates. In short, to predict scaling potential, thermodynamic calculations are used but scaling rates must be estimated using kinetic data (Zhang et al., 2001).

A rate equation fit to the experimental data from this study was used to formulate a scale prediction model. The rate equation is based on laboratory experiments conducted at elevated temperature over a range of physical and chemical conditions (Chapter 2). Relatively few studies are available in the literature on calcite-water reaction rates and rate coefficients at elevated temperatures. A 1D transport algorithm in the computer program PHREEQC Interactive 2.4.2 (Parkhurst and Appello, 2001) was used to generate a model by combining the transport effects with the kinetic reaction occurring locally to predict calcite precipitation.

Studies on kinetics have shown that mechanisms at play at the dissolution end and rate coefficients associated with the respective rate laws, may be similar to those active during mineral growth from supersaturated solutions (Shiraki and

Brantley, 1995). Models for growth by adsorption represented by linear rate equations, and growth by screw dislocations described by parabolic rate equations, have been used to predict dissolution in undersaturated solutions at similar temperature-pressure and chemical conditions. At far from equilibrium, nucleation is the dominating mechanism of growth for solutions with large supersaturations. The model developed in this study is appropriate for predicting scale precipitation at near-equilibrium conditions.

THEORETICAL BACKGROUND

Scaling, driven by a variety of mechanisms, is caused by a change in conditions and may occur at different stages of production-related activities. It may result from mixing of incompatible fluids, differing in chemistry and saturation states, and during well development operations, such as drilling and completion (Przybylinski, 1987; Amaefule et al., 1988; Civan, 2000; Civan, 2001). Injection for pressure maintenance and a better sweep efficiency, often leads to such incompatibility in fluids. Pressure and temperature changes accompanying production often cause scaling. Both mixing and pressure drop can occur during enhanced recovery processes such as water flooding, CO_2 flooding, alkaline water flooding, carbonated water flooding etc. CO_2 degassing associated with many of these processes and concomitant pressure drop can trigger the precipitation of $CaCO_3$.

Formation damage potential has been estimated based on formation specific detailed study by some investigators. In such studies, chemical and

93

mineralogical analyses were done on formation water and core samples (Demir, 1995; Haggerty and Seyler, 1997). The total dissolved solids (TDS), saturation states of scaling minerals, dissolved gas content etc. are measured or determined using geochemical programs. Based on this, formation damage potential is estimated for some typical scenarios using existing reaction path models (Bethke, 1994). For example, potential for calcite scaling is predicted in case of enhanced oil recovery processes such as acidization, water flooding, or CO_2 flooding. The effect of calcite scale deposition in the near-wellbore region has been estimated for a two-dimensional radial flow model (Satman, 1999). A calcite scale precipitation model, based on experimental rates in a synthetic formation brine, for temperatures 25 $-70°C$, and ionic strengths up to 2 m, has been proposed by Dawe and Zhang (1997) and Zhang et al. (2001). Downhole scale precipitation was predicted based on their model and was compared to the measured scale profile (Zhang et al., 2001).

METHODS

Model Development, PHREEQCI Syntax, and Assumptions

Reaction and transport processes are simulated for a solution moving through a column or 1D flow path, combined with a kinetic reaction component, using the method of finite difference. The solution domain is discretized in a series of cells as depicted in Figure 4.3. To model scale formation, PHREEQC Interactive 2.4.2 was used which can perform geochemical calculations for 1D transport in conjunction with kinetically controlled reactions (Parkhurst and

Appelo, 2001). The advection-reaction-dispersion equation governing the process is expressed as

$$\frac{\partial C}{\partial t} = -v\frac{\partial C}{\partial x} + D_L\frac{\partial^2 C}{\partial x^2} - \frac{\partial q}{\partial t} \qquad (1)$$

where C is the concentration in mol/kg water, t is time is seconds, v is the flow velocity in meter/second, x is distance in meters, q is the solid reactant in mol/kg water, D_L is the dispersion coefficient in meter^2/second given by

$$D_L = D_e + \alpha_L v \qquad (2)$$

where D_e is the effective diffusion coefficient and α_L is the dispersivity in meters. In equation (1) the term $-v \cdot \partial C/\partial t$ represents advective transport, the second term $D_L \cdot \partial^2 C/\partial x^2$ is for dispersive transport, and $\partial q/\partial t$ represents the reaction term. The assumptions implicit in the model is that v and D_L are constant for all solute species. The transport component is solved with a finite difference scheme that is forward-difference in time and centered-difference in space. With each time step, advective transport is calculated first, followed by calculations for the reactions occurring locally at each spatial discretization unit (referred to as a cell); this is followed by dispersive transport. Calculation of reactions after both advection and dispersion is done to reduce numerical dispersion (Parkhurst and Appelo, 2001). No flux of heat or change in temperature or pressure occurs during transport or reaction for the simulations performed in this study.

The 1D column is defined by a series of cells with a user-specified cell length. The total column length was set to 1 meter, divided into 20 cells, each 0.05 meter. The program allows user defined rate expressions to be used for the kinetic reactions within the cells. An input file in PHREEQCI is arranged in modules, referred to as data blocks, that allow users to define solution chemistry, mineral phases, gas components, kinetic reactions and transport parameters. The rate expressions are entered in the form of BASIC statements in data block RATES and the amount of kinetic reactant and other parameters that may evolve with reaction progress, may be specified in the KINETICS data block. The TRANSPORT data block allows users to define advection and dispersion parameters appropriate for near-wellbore conditions at which scale prediction is attempted.

The cells were initially set up at a composition undersaturated with respect to calcite. Formation brine compositions from available well data (personal communication Prof. Gordon Atkinson) were used for solution infilling or entering the column during the transport process (Table 4.1).

Discretization is necessary to eliminate numerical dispersion arising for coarse grid sizes. Initially coarser grid sizes were used to obtain results within a shorter computer time. However, the finest grid gives the closest approximation to the analytical solution. The model was run for successively fine grid sizes to ensure that final grid size was sufficiently small so as not to affect results for reactive or conservative species. Parameters such as initial solution composition, transport velocity, and total pore volume flowed through the column, were varied

Table 4.1 Formation brine chemistry

Chemistry	Formation Brine 1	Formation Brine 2
	(ppm)	(ppm)
Na^+	2992	11022
K^+	3622	0
Mg^{2+}	12	69
Ca^{2+}	676	669
Sr^{2+}	22	35
Ba^{2+}	3	0
Cl^-	8605	14187
HCO_3^-	351	1627
SO_4^{2-}	145	3420
Fe	24	0
pH	6.89	7.67

to capture the response of the model in these scenarios for a particular cell-length-transport rate combination. The model was also tested for a different brine composition to isolate the effect of changes in the infilling solution composition.

It should be noted that solutions might be saturated in other phases, which could potentially precipitate as solid phases. This may interact with calcite scaling as these solids may provide substrates for growth thereby facilitating the process. Predictions from the model may underestimate scale in such cases. On the other hand, the presence of ions such as Mg^{2+} in significant concentration, especially for Mg^{2+}/Ca^{2+} molar ratios between 0.1 to 0.5, may inhibit calcite growth rate as much as 50% (Dawe and Zhang, 1997). Estimation of scale in these cases will be overestimated.

Rate Expression

Rate equations used for the model were derived from experimental studies at elevated temperatures. The equation as derived in Chapter 2 is expressed as

$$R = k_t \, [1 - \Omega_b^{\pm} + \zeta \, \{1 - (1 + 2 \, (1 - \Omega_b^{\pm})/\zeta)^{1/2} \}] \qquad (1)$$

where R is the rate in mol/cm^2-sec, k_t $(= Dm_{eq}/\delta)$, is the rate coefficient for transport control, D represents the diffusion coefficient, m_{eq} is the mean ionic molal equilibrium concentration, δ is thickness of the hydrodynamic boundary layer, $\Omega_b^{\pm}$ is the mean ionic bulk saturation, the dimensionless parameter ζ is

given by $Dmeq/2\delta k^+$, and k^+ is the second order rate coefficient for surface reaction control.

The rate equation fit to saline experiments is:

$$R = k \left(\Omega^{1/2} - 1\right)^2 \qquad\qquad (2)$$

where R is the rate in mol/cm^2-sec, $\Omega = aCa^{2+} \cdot aCO_3^{2-} / K_{sp}$, (i.e. ratio of the ion activity product for calcium and carbonate ions to the solubility product of calcite), k is the rate constant derived for various ionic strengths, P_{CO_2} and disc spinning rates in saline experiments conducted in this study (Table 3.3, Chapter 3).

RESULTS AND DISCUSSION

Model Validation

PHREEQCI results are compared with analytical solutions for conservative chloride ion concentration and shows excellent agreement (Figure 4.4). This provides a unique solution that agrees with the numerical solution for certain boundary conditions.

Discretization of grid size, i.e. simulation runs using a finer grid size gave nearly identical results, indicating artificial dispersion is either absent or negligible in the numerical solution. Figure 4.5a shows calcite saturation modeled using a finer grid size of 0.05 meter compared to outputs with 0.17 meter grid size shown in Figure 4.5b.

Figure 4.3 Schematic representation of near-wellbore region for which scale precipitation is modeled
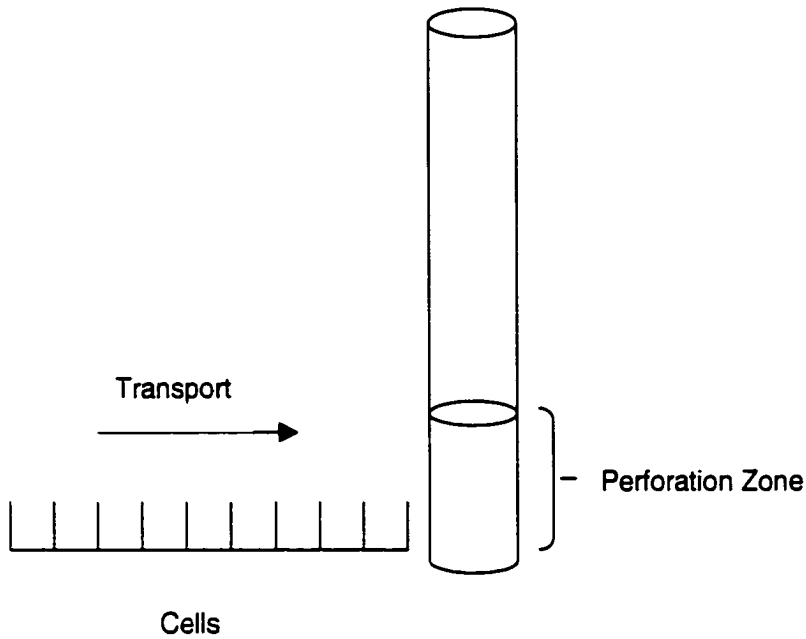
Figure 4.4 Analytical solution (solid line) for 1D transport model at constant boundary condition is compared with PHREEQCI calculation for Cl⁻ ion concentrations (symbols) that is conservative through reaction and transport
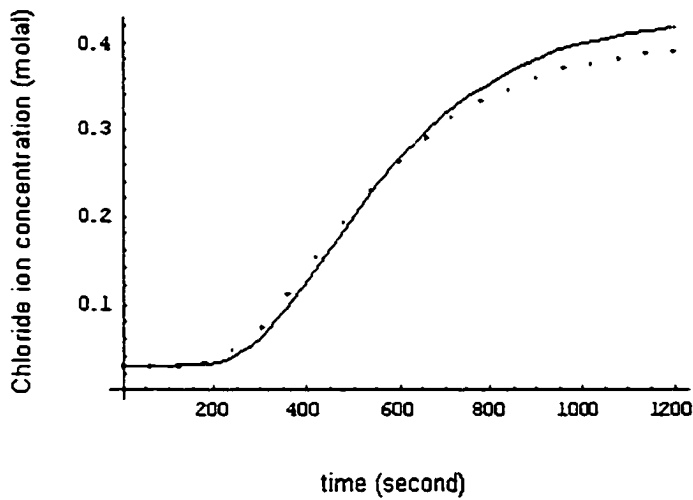
Figure 4.5 Grid size refined to 0.05 meter cells to check degree of numerical dispersion (a). Results are similar to the runs with coarser grid at 0.167 meter cells (b)

a.

b.
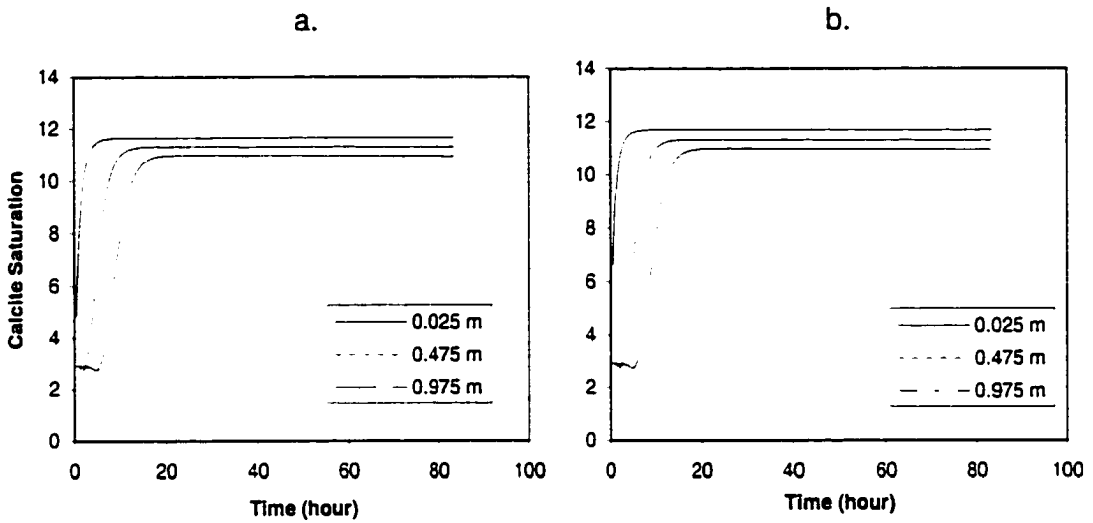
Figure 4.6 CaCO₃ concentrations in solution as it evolves in time due to one-dimensional transport coupled with kinetic reactions
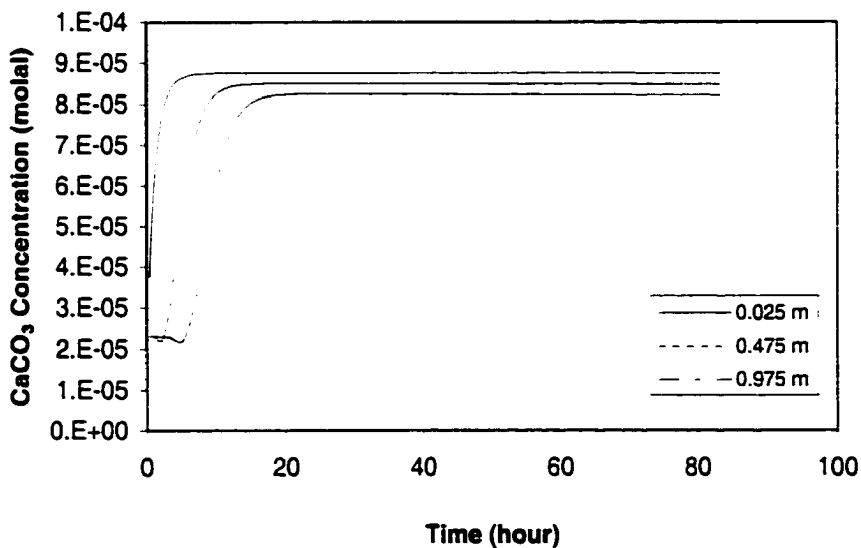
Model Output

Breakthrough curves show that a maximum concentration was reached within the first 20 hours as indicated in a calcite concentration vs. time plot (Figure 4.6). Three series in the plot represent variable distances from the upstream end of the column. The total calcite precipitated shows a steady increase throughout the run (Figure 4.7a). The volume of calcite precipitated is also shown in a spatial plot where precipitation amount is represented in terms of distance from the upstream (proximal with respect to the source) end of the column (Figure 4.7b). A decrease in scale precipitation is observed with increasing distance. This is expected as the solution is increasingly depleted in calcium carbonate as it moves further along the path. In reality, the bottom of the production borehole will probably suffer from more severe clogging as solution at this end will be more saturated in scale forming ions compared to the segment of the borehole towards the top, which receives a less concentrated solution. The evolution of Pco_2 and ionic strength with time, shows a plateauing off within the first 20 hours as with the calcite concentration profile (Figure 4.6, 4.8 and 4.9). As mentioned earlier, the solution residence time is especially significant in geochemical reactions where kinetics may be important. The effect of variation in residence time is reflected in the modeling results for runs at a slower transport rate (Figure 4.10). A slower transport rate signifies a longer residence time for the moving solution. This allows for a larger volume of calcite to be precipitated from the supersaturated brine.

Figure 4.7 Calcite precipitated as a result of coupled 1D transport and kinetic reaction in time and space.

a.

b.
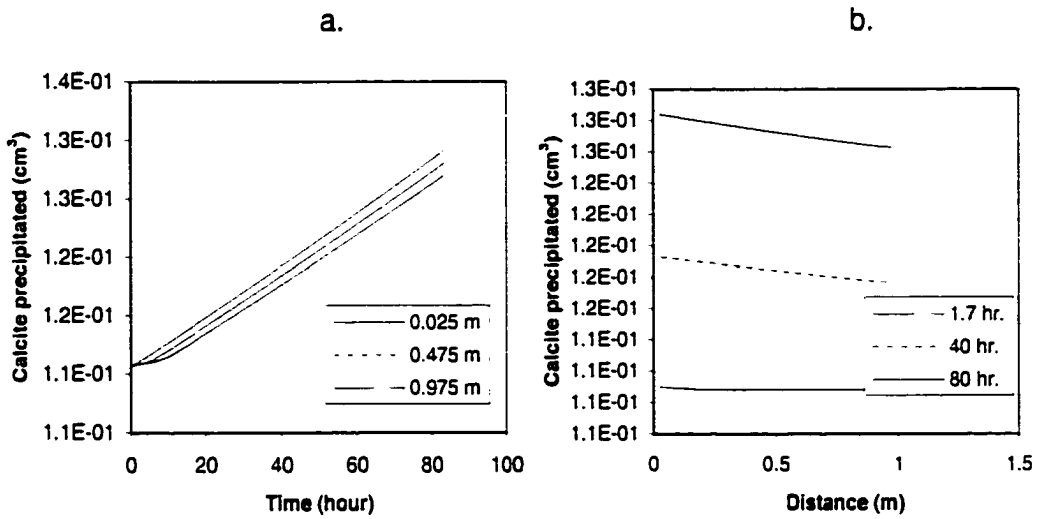
Figure 4.8 Pco₂ profile evolving in time as a result of calcite transport and reaction.
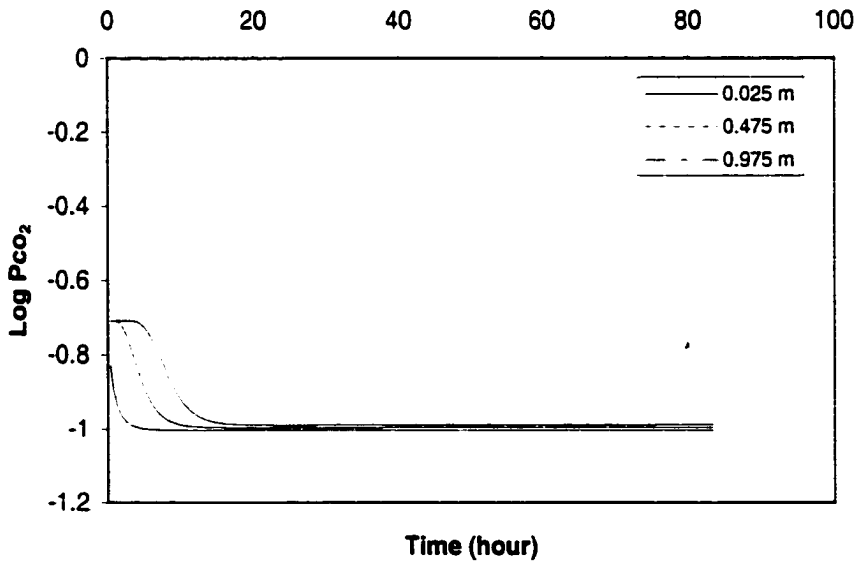
Figure 4.9 Ionic strength profiles evolving in time as a result of calcite transport and reaction.
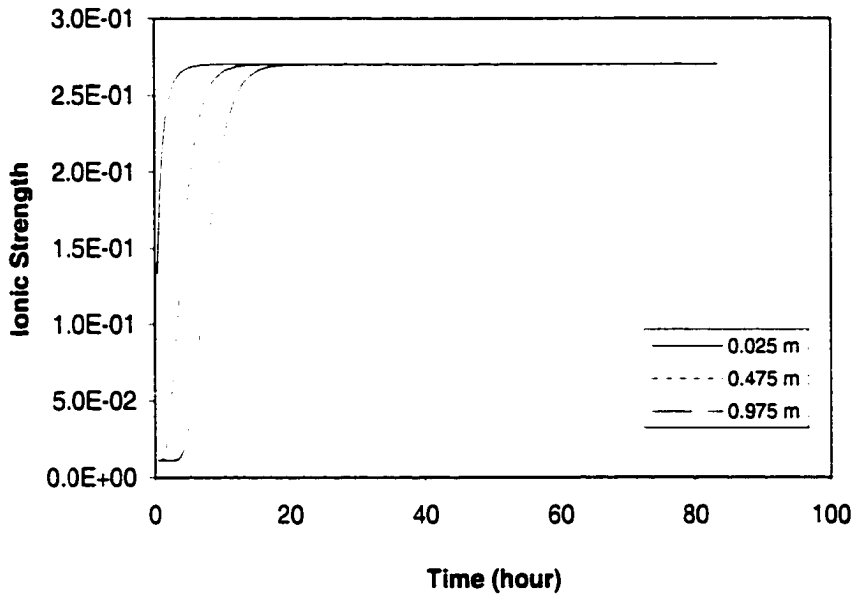
Figure 4.10 1/3 flow velocity allows more residence time and more reaction time, resulting in larger mass of calcite scale precipitation
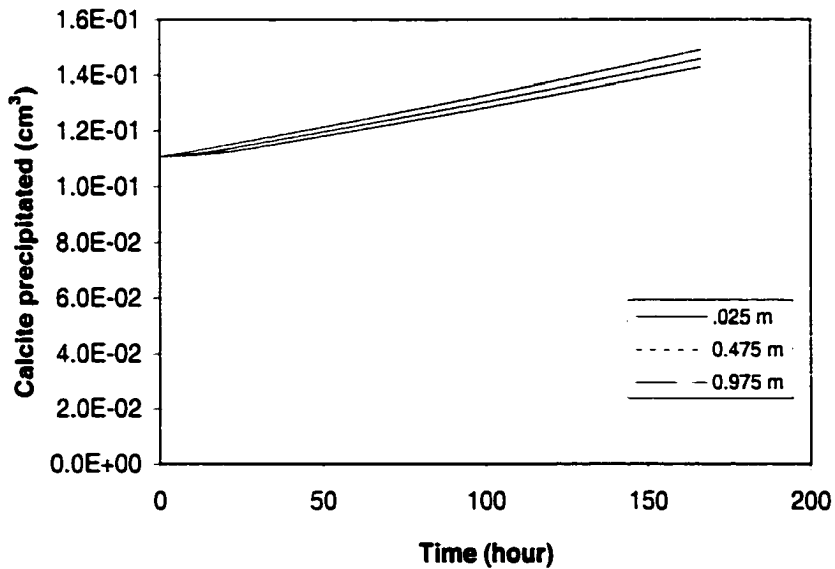
The rate law derived from the results of batch experiments at 70°C, in 0.7 m NaCl solution, was used to predict scale precipitation for the same brine composition. Predicted rates seem to be somewhat lower than that predicted by the other rate equation derived from experiments at 100°C (Figure 4.7a and Figure 4.11). This may be due to the temperature dependence of calcite kinetics embedded in the two rate equations, as elevated temperatures enhance reaction kinetics. The model results for a different brine composition show a somewhat reduced precipitation although initial Ca^{2+} concentration in the two solutions were not markedly different. This may be due to the variability in other species present in the two solutions (Figure 4.12 and Figure 4.13). Solutions with a higher concentration of ions such as Sr^{2+}, Mg^{2+}, Ba^{2+} may also be saturated in carbonates other than calcite, such as strontianite ($SrCO_3$), dolomite ($CaMg(CO_3)_2$, magnesite ($MgCO_3$) and witherite ($BaCO_3$) depleting CO_3^{2-} available for calcite. On the other hand solution with higher SO_4^{2-} content may precipitate minerals such as anhydrite ($CaSO_4$) at the cost of calcite, as Ca^{2+} needed for calcite saturation is reduced.

CONCLUSIONS

Scale formation is a problem well-recognized by production engineers in oil and gas fields. A number of models have been proposed and used for prediction of scales in the near-wellbore or downhole conditions, but many do not take into account the kinetic aspects in the process. Instead, they are based only on assumptions of thermodynamic equilibrium. It has been shown that the

Figure 4.11 Modeling runs using rate equation fitted to data from experiments done at 70°C in 0.7 m NaCl solution.
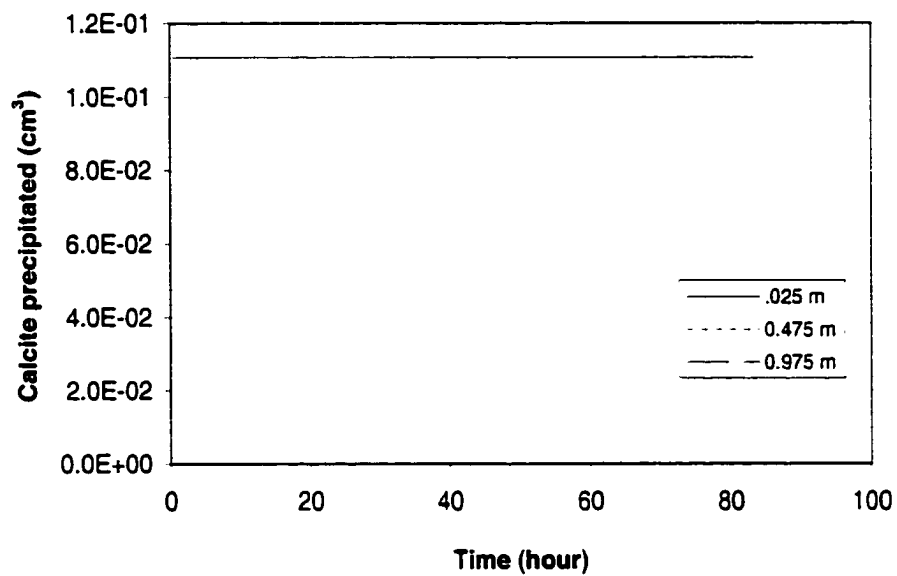
Figure 4.12 Modeling results for a brine composition from a different formation
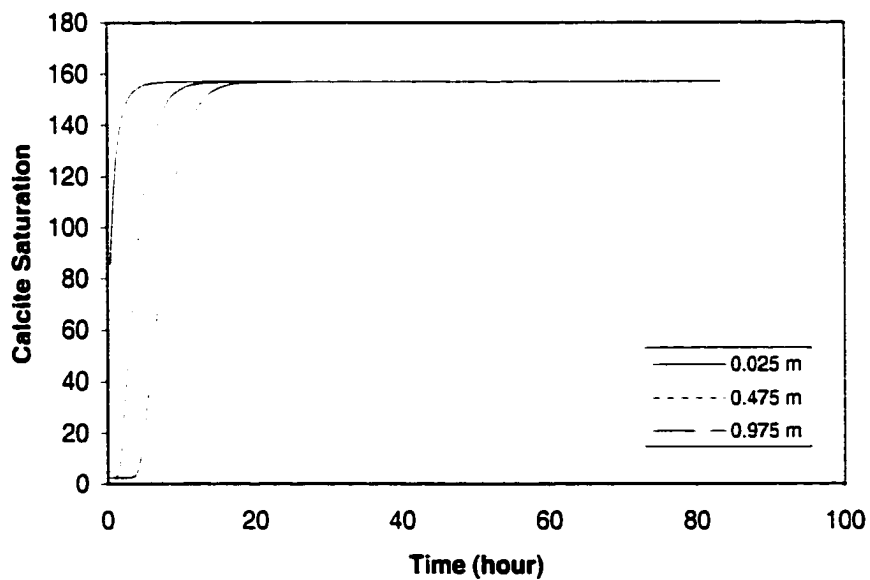
Figure 4.13 Modeling results for a brine composition from a different formation. Calcite scale precipitated is somewhat lower
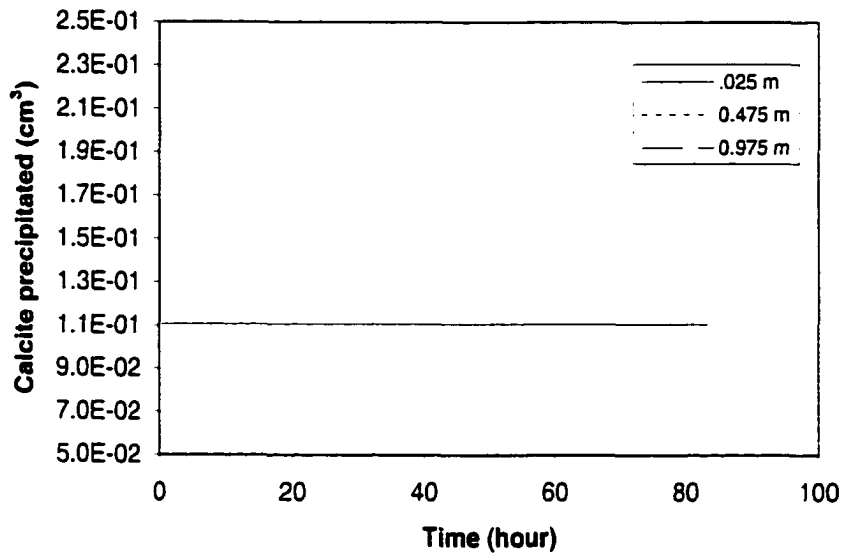
solutions in wellbores often reach saturation and yet do not precipitate scale in the formation or in the wellbore within the solution residence time (Ostvold and Randhol, 2001). This underlines the importance of taking kinetics into consideration. Even those employing a kinetic approach may be using parameters valid only for lower temperatures since few studies are available for calcite reaction at elevated temperature-pressure.

The present model is a simplistic formulation of a scale prediction model that includes kinetic considerations parameterized by experiments at elevated temperatures. Oilfield brine is a complex solution with numerous dissolved species that may inhibit or otherwise interfere with the kinetics modeled in this study. There are also a number of dissolved gases present in production brine that change the redox condition of the solution or degas due to a pressure drop to trigger scale formation during production operations. The brines modeled here are relatively low ionic strength solutions. In order to simulate calcite reaction in higher ionic strength brines, a series of experiments were conducted in simple $NaCl-CaCO_3-CO_2-H_2O$ systems. The rate parameters depicting the ionic strength dependence will be incorporated in later work.

Formation properties such as porosity of the reservoir in the near-wellbore region need to be taken into account to make this prediction meaningful for a specific formation. It is assumed that the formation is homogeneous over the spatial and temporal scale of the model. Petrophysical properties such as porosity and permeability are assumed to be high and connectivity through the pores is not significantly reduced over the time scale of the model. Young and

underconsolidated hydrocarbon reservoirs, such as those in the deep water Gulf of Mexico, may be appropriate for application of such models.

The current model provides some insights and a framework on which a more robust scale prediction model may be built in future. Experimental studies on dissolution could also provide insight into developing effective treatment of calcite scale and help in scale management planning.

APPENDIX B

Table 4.B.1 PHREEQCI output

Input file: Z:\SSARKAR\AAAResearch\PHREEQC 2.4.2\North Sea Scale\ Brine1.pqi
Output file: Z:\SSARKAR\AAAResearch\PHREEQC 2.4.2\North Sea Scale\ Brine1.pqo
Database file: C:\Program Files\USGS\Phreeqc Interactive 2.4.2 Alpha\ phreeqc.dat

```
-------------------
Reading data base.
-------------------

        SOLUTION_MASTER_SPECIES
        SOLUTION_SPECIES
        PHASES
        EXCHANGE_MASTER_SPECIES
        EXCHANGE_SPECIES
        SURFACE_MASTER_SPECIES
        SURFACE_SPECIES
        RATES
        END
------------------------------------
Reading input data for simulation 1.
------------------------------------

        DATABASE C:\Program Files\USGS\Phreeqc Interactive 2.4.2 Alpha\phreeqc.dat
        SOLUTION 0 Brine from Production Water
            temp      100
            pH        6.89
            pe        4
            redox     pe
            units     mol/kgw
            density   1.023
            Na        0.13
            K         0.093
            Ca        0.017
            Cl        0.243
            C         0.006
            S(6)      0.002
            water     1 # kg
        END
------------------------------------
Beginning of initial solution calculations.
------------------------------------

Initial solution 0.    Brine from Production Water

-----------------------------Solution composition----------------------------

        Elements           Molality         Moles

        C                  6.000e-003      6.000e-003
        Ca                 1.700e-002      1.700e-002
        Cl                 2.430e-001      2.430e-001
        K                  9.300e-002      9.300e-002
        Na                 1.300e-001      1.300e-001
        S(6)               2.000e-003      2.000e-003

----------------------------Description of solution----------------------------

                                  pH  =    6.890
                                  pe  =    4.000
                    Activity of water  =    0.992
                       Ionic strength  =    2.699e-001
                   Mass of water (kg)  =    1.000e+000
               Total alkalinity (eq/kg)  =    5.205e-003
```

110

```
                    Total CO2 (mol/kg)  =  6.000e-003
                   Temperature (deg C)  =  100.000
               Electrical balance (eq)  =  4.795e-003
   Percent error, 100*(Cat-|An|)/(Cat+|An|)  =  0.95
                            Iterations  =  9
                               Total H  =  1.110173e+002
                               Total O  =  5.553125e+001


-----------------------Distribution of species-----------------------

                                                 Log       Log       Log
            Species        Molality   Activity  Molality  Activity  Gamma

            OH-            6.514e-006 4.179e-006  -5.186    -5.379   -0.193
            H+             1.699e-007 1.288e-007  -6.770    -6.890   -0.120
            H2O            5.551e+001 9.917e-001  -0.004    -0.004    0.000
C(-4)          0.000e+000
            CH4            0.000e+000 0.000e+000  -74.627   -74.600   0.027
C(4)           6.000e-003
            HCO3-          4.324e-003 2.994e-003  -2.364    -2.524   -0.160
            CO2            9.763e-004 1.039e-003  -3.010    -2.983    0.027
            CaHCO3+        3.840e-004 2.659e-004  -3.416    -3.575   -0.160
            NaHCO3         1.410e-004 1.501e-004  -3.851    -3.824    0.027
            CaCO3          8.834e-005 9.400e-005  -4.054    -4.027    0.027
            NaCO3-         7.959e-005 5.542e-005  -4.099    -4.256   -0.157
            CO3-2          7.067e-006 1.626e-006  -5.151    -5.789   -0.638
Ca             1.700e-002
            Ca+2           1.623e-002 3.914e-003  -1.790    -2.407   -0.618
            CaHCO3+        3.840e-004 2.659e-004  -3.416    -3.575   -0.160
            CaSO4          2.969e-004 3.159e-004  -3.527    -3.500    0.027
            CaCO3          8.834e-005 9.400e-005  -4.054    -4.027    0.027
            CaOH+          7.181e-009 5.001e-009  -8.144    -8.301   -0.157
            CaHSO4+        1.442e-009 1.004e-009  -8.841    -8.998   -0.157
Cl             2.430e-001
            Cl-            2.430e-001 1.573e-001  -0.614    -0.803   -0.189
H(0)           1.216e-025
            H2             6.079e-026 6.469e-026  -25.216   -25.189   0.027
K              9.300e-002
            K+             9.260e-002 5.996e-002  -1.033    -1.222   -0.189
            KSO4-          3.978e-004 2.770e-004  -3.400    -3.557   -0.157
            KOH            1.504e-009 1.600e-009  -8.823    -8.796    0.027
Na             1.300e-001
            Na+            1.296e-001 8.912e-002  -0.888    -1.050   -0.163
            NaSO4-         2.167e-004 1.509e-004  -3.664    -3.821   -0.157
            NaHCO3         1.410e-004 1.501e-004  -3.851    -3.824    0.027
            NaCO3-         7.959e-005 5.542e-005  -4.099    -4.256   -0.157
            NaOH           4.259e-009 4.532e-009  -8.371    -8.344    0.027
O(0)           4.023e-023
            O2             2.011e-023 2.140e-023  -22.696   -22.670   0.027
S(6)           2.000e-003
            SO4-2          1.089e-003 2.311e-004  -2.963    -3.636   -0.673
            KSO4-          3.978e-004 2.770e-004  -3.400    -3.557   -0.157
            CaSO4          2.969e-004 3.159e-004  -3.527    -3.500    0.027
            NaSO4-         2.167e-004 1.509e-004  -3.664    -3.821   -0.157
            HSO4-          3.064e-008 2.134e-008  -7.514    -7.671   -0.157
            CaHSO4+        1.442e-009 1.004e-009  -8.841    -8.998   -0.157


--------------------------Saturation indices--------------------------

            Phase          SI log IAP  log KT

            Anhydrite     -0.72   -6.04   -5.32  CaSO4
            Aragonite      0.97   -8.20   -9.17  CaCO3
            Calcite        1.07   -8.20   -9.27  CaCO3
            CH4(g)       -71.24 -106.68  -35.44  CH4
            CO2(g)        -1.00  -19.57  -18.56  CO2
            Gypsum        -1.20   -6.05   -4.85  CaSO4:2H2O
            H2(g)        -21.78  -21.78    0.00  H2
            H2O(g)         0.04   -0.00   -0.04  H2O
```

111

```
        Halite              -3.57    -1.85    1.72   NaCl
        O2(g)              -19.44    43.55   62.99   O2


-------------------
End of simulation.
-------------------


------------------------------------
Reading input data for simulation 2.
------------------------------------

        SOLUTION 1-20 Solution Initially filling Column
            temp      100
            pH        6.5
            pe        4
            redox     pe
            units     mol/kgw
            density   1
            Ca        0.005
            C         0.005
            water     1 # kg
        END
-------------------------------------------------
Beginning of initial solution calculations.
-------------------------------------------------


Initial solution 1.    Solution Initially filling Column

-------------------------------Solution composition--------------------------

        Elements            Molality        Moles

        C                  5.000e-003    5.000e-003
        Ca                 5.000e-003    5.000e-003

-------------------------------Description of solution------------------------

                               pH =    6.500
                               pe =    4.000
                 Activity of water =    1.000
                    Ionic strength =    1.105e-002
                 Mass of water (kg) =   1.000e+000
             Total alkalinity (eq/kg) = 2.378e-003
                 Total CO2 (mol/kg) =   5.000e-003
               Temperature (deg C) = 100.000
             Electrical balance (eq) = 7.022e-003
  Percent error, 100*(Cat-|An|)/(Cat+|An|) =  56.08
                        Iterations =    9
                           Total H = 1.110154e+002
                           Total O = 5.551917e+001


-------------------------Distribution of species-------------------------

                                              Log      Log      Log
            Species       Molality  Activity  Molality Activity Gamma

            OH-          1.953e-006 1.716e-006  -5.709  -5.765  -0.056
            H+           3.530e-007 3.162e-007  -6.452  -6.500  -0.048
            H2O          5.551e+001 9.998e-001  -0.000  -0.000   0.000
C(-4)              0.000e+000
            CH4          0.000e+000 0.000e+000 -71.192 -71.191   0.001
C(4)               5.000e-003
            HCO3-        2.746e-003 2.430e-003  -2.561  -2.614  -0.053
            CO2          2.047e-003 2.053e-003  -2.689  -2.688   0.001
            CaHCO3+      1.829e-004 1.619e-004  -3.738  -3.791  -0.053
            CaCO3        2.326e-005 2.332e-005  -4.633  -4.632   0.001
            CO3-2        8.759e-007 5.375e-007  -6.058  -6.270  -0.212
Ca                 5.000e-003
            Ca+2         4.794e-003 2.937e-003  -2.319  -2.532  -0.213
```

112

```
      CaHCO3+        1.829e-004  1.619e-004    -3.738    -3.791    -0.053
      CaCO3          2.326e-005  2.332e-005    -4.633    -4.632     0.001
      CaOH+          1.750e-009  1.541e-009    -8.757    -8.812    -0.055
H(0)          7.776e-025
      H2             3.888e-025  3.898e-025   -24.410   -24.409     0.001
O(0)          1.195e-024
      O2             5.977e-025  5.992e-025   -24.223   -24.222     0.001


------------------------------Saturation indices------------------------------

      Phase            SI  log IAP  log KT

      Aragonite       0.36    -8.80    -9.17  CaCO3
      Calcite         0.46    -8.80    -9.27  CaCO3
      CH4(g)        -67.83  -103.27   -35.44  CH4
      CO2(g)         -0.71   -19.27   -18.56  CO2
      H2(g)         -21.00   -21.00     0.00  H2
      H2O(g)          0.04    -0.00    -0.04  H2O
      O2(g)         -20.99    42.00    62.99  O2


-------------------
End of simulation.
-------------------


---------------------------------------
Reading input data for simulation 3.
---------------------------------------

      TITLE Our rate equation, units changed from cm to m
            Pco2 taken from speciation, not predefined
            solubility = mCaeq is calculated for this solution
      RATES
          Calcite_2
      start
      10 sat = SR("Calcite")
      20 IF (M <= 0 AND sat < 0) THEN GOTO 300
      30 t = 1
      40 IF M0 > 0 THEN t = M/M0
      50 IF t = 0 THEN t = 1
      60 area = PARM( 1 ) * t ^PARM( 2 )
      70 spin = 300
      80 meq = 2.19e-3
      90 pco2 = SI("CO2(g)")
      100 dprime = 3.488e-9
      110 kt = dprime * meq * (spin)^(1/2)
      120 k2 = 2.179e-4
      130 k3 = 9.409e-4
      140 kplus = k2 * pco2 + k3
      150 zeta = dprime * meq/(2*kplus)
      160 mibs = sat^0.5
      170 rem NOTE BELOW that "mibs -1" replaces "1-mibs"
      180 rf = - kt * (mibs - 1 + zeta * (1 - (1 + 2 * (mibs - 1 )/ zeta)^(1/2)))
      190 rate = area * rf
      200 moles = rate * TIME
      210 rem Do not Dissolve more Calcite than present
      220 IF (moles > M) THEN moles = M
      230 IF (moles >= 0) THEN GOTO 300
      240 rem Do not Precipitate more Ca or C(4) than present
      250 temp = TOT("Ca")
      260 mc = TOT("C(4)")
      270 IF mc < temp THEN temp = mc
      280 IF -moles > temp THEN moles = -temp
      300 SAVE moles
      end
      KINETICS 1-20
      Calcite_2
          formula  CaCO3  1
          m        0.003
          m0       0.003
```

```
            parms    5 0.6
            tol      1e-008
        steps        1 in 1 steps # seconds
        step_divide 1
        runge_kutta 3
        SELECTED_OUTPUT
            file              Brine1.sel
            simulation        false
            state             false
            time              false
            pe                false
            molalities        CaCO3
            saturation_indices   Calcite  Halite  CO2(g)
            kinetic_reactants    Calcite_2
        USER_PUNCH
        headings Ionic_Strength Time Total_time
        start
        10 punch MU
        20 punch TIME
        30 punch TOTAL_TIME
        end
        TRANSPORT
            cells                20
            shifts               200
            time_step            1500 # seconds
            flow_direction       forward
            boundary_conditions  flux flux
            lengths              20*0.05
            dispersivities       20*0.05
            correct_disp         true
            diffusion_coefficient 0
            print_cells          20
            print_frequency      20
            warnings             true
        PRINT
            echo_input           false
-----
TITLE
-----

 Our rate equation, units changed from cm to m
      Pco2 taken from speciation, not predefined
      solubility = mCaeq is calculated for this solution

------------------------------------
Beginning of transport calculations.
------------------------------------


--------------------------------
Equilibrating initial solutions
--------------------------------

Using solution 20.    Solution Initially filling Column

----------------------------Solution composition----------------------------

        Elements           Molality        Moles

        C                  5.000e-003  5.000e-003
        Ca                 5.000e-003  5.000e-003

----------------------------Description of solution----------------------------

                            pH  =    6.500      Charge balance
                            pe  =    4.000      Adjusted to redox equilibrium
            Activity of water  =    1.000
                Ionic strength  =    1.105e-002
            Mass of water (kg)  =    1.000e+000
        Total alkalinity (eq/kg)  =    2.978e-003
```

114

```
                   Total CO2 (mol/kg)  =  5.000e-003
                   Temperature (deg C)  = 100.000
               Electrical balance (eq)  =  7.022e-003
Percent error, 100*(Cat-|An|)/(Cat+|An|)  =  56.08
                        Iterations  =   0
                           Total H  = 1.110154e+002
                           Total O  = 5.551917e+001


-------------------------Saturation indices-----------------------------

       Phase           SI log IAP  log KT

       Aragonite      0.36   -8.80   -9.17  CaCO3
       Calcite        0.46   -8.80   -9.27  CaCO3
       CH4(g)       -67.83 -103.27  -35.44  CH4
       CO2(g)        -0.71  -19.27  -18.56  CO2
       H2(g)        -21.00  -21.00    0.00  H2
       H2O(g)         0.04   -0.00   -0.04  H2O
       O2(g)        -20.99   42.00   62.99  O2


Transport step 1-20.

Using mix 20.
Using kinetics 20.    Kinetics defined in simulation 3.


       2.750e-001 Solution 19      Solution after simulation 3.
       0.000e+000 Solution 21      Solution Initially filling Column
       7.250e-001 Solution 20      Solution after simulation 3.



       Time step: 1500 seconds

       Rate name     Delta Moles Total Moles   Reactant       Coefficient

       Calcite_2     1.358e-006  3.016e-003  CaCO3                    1

--------------------------Solution composition---------------------------

       Elements       Molality     Moles

       C             5.570e-003  5.570e-003
       Ca            1.210e-002  1.210e-002
       Cl            1.443e-001  1.443e-001
       K             5.523e-002  5.523e-002
       Na            7.720e-002  7.720e-002
       S             1.188e-003  1.188e-003

--------------------------Description of solution------------------------

                           pH  =   6.700      Charge balance
                           pe  =   7.734      Adjusted to redox equilibrium
                Activity of water  =   0.995
                    Ionic strength  =  1.649e-001
                 Mass of water (kg)  =  1.000e+000
             Total alkalinity (eq/kg)  =  4.253e-003
                  Total CO2 (mol/kg)  =  5.570e-003
                   Temperature (deg C)  = 100.000
               Electrical balance (eq)  =  5.699e-003
Percent error, 100*(Cat-|An|)/(Cat+|An|)  =   1.87
                        Iterations  =   2
                           Total H  = 1.110165e+002
                           Total O  = 5.552627e+001


-------------------------Saturation indices-----------------------------

       Phase           SI log IAP  log KT
```

```
          Anhydrite         -0.91   -6.23   -5.32  CaSO4
          Aragonite          0.66   -8.51   -9.17  CaCO3
          Calcite            0.76   -8.51   -9.27  CaCO3
          CH4(g)           -99.46 -134.90  -35.44  CH4
          CO2(g)            -0.86  -19.42  -18.56  CO2
          Gypsum            -1.38   -6.23   -4.85  CaSO4:2H2O
          H2(g)            -28.87  -28.87    0.00  H2
          H2O(g)             0.04   -0.00   -0.04  H2O
          H2S(g)           -99.63 -132.61  -32.98  H2S
          Halite            -3.98   -2.26    1.72  NaCl
          O2(g)             -5.26   57.74   62.99  O2
          Sulfur           -75.92 -103.74  -27.83  S


Transport step 21-40.

Using mix 20.
Using kinetics 20.    Kinetics defined in simulation 3.


Mixture 20.

          2.750e-001 Solution 19       Solution after simulation 3.
          0.000e+000 Solution 21       Solution Initially filling Column
          7.250e-001 Solution 20       Solution after simulation 3.

Kinetics 20.   Kinetics defined in simulation 3.

          Time step: 1500 seconds

          Rate name     Delta Moles Total Moles  Reactant      Coefficient

          Calcite_2      2.304e-006  3.057e-003  CaCO3                    1

-----------------------------Solution composition----------------------------

          Elements        Molality      Moles

          C             5.946e-003  5.946e-003
          Ca            1.686e-002  1.686e-002
          Cl            2.412e-001  2.412e-001
          K             9.230e-002  9.230e-002
          Na            1.290e-001  1.290e-001
          S             1.985e-003  1.985e-003

---------------------------Description of solution---------------------------

                                    pH =     6.865   Charge balance
                                    pe =     7.552   Adjusted to redox equilibrium
                      Activity of water =     0.992
                         Ionic strength =     2.679e-001
                      Mass of water (kg) =    1.000e+000
              Total alkalinity (eq/kg) =     5.095e-003
                  Total CO2 (mol/kg) =     5.946e-003
                  Temperature (deg C) =   100.000
               Electrical balance (eq) =     4.812e-003
Percent error, 100*(Cat-|An|)/(Cat+|An|) =     0.96
                           Iterations =     2
                              Total H = 1.110173e+002
                              Total O = 5.553102e+001

---------------------------Saturation indices--------------------------------

          Phase           SI log IAP  log KT

          Anhydrite        -0.73   -6.05   -5.32  CaSO4
          Aragonite         0.94   -8.23   -9.17  CaCO3
          Calcite           1.04   -8.23   -9.27  CaCO3
          CH4(g)          -99.44 -134.88  -35.44  CH4
```

116

```
        CO2(g)        -0.99 -19.55  -18.56  CO2
        Gypsum        -1.20  -6.05   -4.85  CaSO4:2H2O
        H2(g)        -28.83 -28.83    0.00  H2
        H2O(g)         0.04  -0.00   -0.04  H2O
        H2S(g)       -99.71 -132.69 -32.98  H2S
        Halite        -3.58  -1.86    1.72  NaCl
        O2(g)         -5.33  57.66   62.99  O2
        Sulfur       -76.03 -103.86 -27.83  S
```

Transport 41-60.

Using mix 20.
Using kinetics 20.   Kinetics defined in simulation 3.

Mixture 20.

```
    2.750e-001 Solution 19        Solution after simulation 3.
    0.000e+000 Solution 21        Solution Initially filling Column
    7.250e-001 Solution 20        Solution after simulation 3.
```

Kinetics 20.   Kinetics defined in simulation 3.

Time step: 1500 seconds

Rate name	Delta Moles	Total Moles	Reactant	Coefficient
Calcite_2	2.344e-006	3.104e-003	CaCO3	1

-----------------------------Solution composition----------------------------

Elements	Molality	Moles
C	5.952e-003	5.952e-003
Ca	1.695e-002	1.695e-002
Cl	2.430e-001	2.430e-001
K	3.299e-002	3.299e-002
Na	1.300e-001	1.300e-001
S	2.000e-003	2.000e-003

---------------------------Description of solution----------------------------

```
                              pH =   6.868     Charge balance
                              pe =   7.552     Adjusted to redox equilibrium
             Activity of water =   0.992
                Ionic strength =   2.698e-001
           Mass of water (kg) =   1.000e+000
        Total alkalinity (eq/kg) =   5.109e-003
             Total CO2 (mol/kg) =   5.952e-003
             Temperature (deg C) = 100.000
          Electrical balance (eq) =   4.795e-003
Percent error, 100*(Cat-|An|)/(Cat+|An|) =   0.95
                     Iterations =   2
                        Total H = 1.110173e+002
                        Total O = 5.553110e+001
```

----------------------------Saturation indices-------------------------------

Phase	SI	log IAP	log KT	
Anhydrite	-0.72	-6.04	-5.32	CaSO4
Aragonite	0.94	-8.23	-9.17	CaCO3
Calcite	1.04	-8.23	-9.27	CaCO3
CH4(g)	-99.46	-134.90	-35.44	CH4
CO2(g)	-0.99	-19.55	-18.56	CO2
Gypsum	-1.20	-6.05	-4.85	CaSO4:2H2O
H2(g)	-28.84	-28.84	0.00	H2
H2O(g)	0.04	-0.00	-0.04	H2O

```
        H2S(g)          -99.73 -132.71  -32.98  H2S
        Halite           -3.57   -1.85    1.72  NaCl
        O2(g)            -5.32   57.67   62.99  O2
        Sulfur          -76.05 -103.87  -27.83  S


Transport step 61-80.


Using mix 20.
Using kinetics 20.    Kinetics defined in simulation 3.

Mixture 20.

        2.750e-001 Solution 19       Solution after simulation 3.
        0.000e+000 Solution 21       Solution Initially filling Column
        7.250e-001 Solution 20       Solution after simulation 3.

Kinetics 20.   Kinetics defined in simulation 3.

        Time step: 1500 seconds

        Rate name      Delta Moles Total Moles   Reactant      Coefficient

        Calcite_2       2.365e-006  3.151e-003   CaCO3                    1

-----------------------------Solution composition------------------------------

        Elements        Molality      Moles

        C             5.952e-003  5.952e-003
        Ca            1.695e-002  1.695e-002
        Cl            2.430e-001  2.430e-001
        K             9.300e-002  9.300e-002
        Na            1.300e-001  1.300e-001
        S             2.000e-003  2.000e-003

----------------------------Description of solution----------------------------

                                  pH  =   6.868       Charge balance
                                  pe  =   7.562       Adjusted to redox equilibrium
                    Activity of water =   0.992
                       Ionic strength =   2.698e-001
                   Mass of water (kg) =   1.000e+000
               Total alkalinity (eq/kg) =   5.109e-003
                     Total CO2 (mol/kg) =   5.952e-003
                   Temperature (deg C) = 100.000
              Electrical balance (eq) =   4.795e-003
Percent error, 100*(Cat-|An|)/(Cat+|An|)  =   0.95
                           Iterations =   2
                              Total H  = 1.110173e+002
                              Total O  = 5.553110e+001


----------------------------Saturation indices---------------------------------

        Phase           SI log IAP  log KT

        Anhydrite       -0.72   -6.04   -5.32  CaSO4
        Aragonite        0.94   -8.23   -9.17  CaCO3
        Calcite          1.04   -8.23   -9.27  CaCO3
        CH4(g)         -99.55 -134.98  -35.44  CH4
        CO2(g)          -0.99  -19.55  -18.56  CO2
        Gypsum          -1.20   -6.05   -4.85  CaSO4:2H2O
        H2(g)          -28.86  -28.86    0.00  H2
        H2O(g)           0.04   -0.00   -0.04  H2O
        H2S(g)         -99.82 -132.80  -32.98  H2S
        Halite          -3.57   -1.85    1.72  NaCl
        O2(g)           -5.28   57.71   62.99  O2
        Sulfur         -76.11 -103.94  -27.83  S
```

118

Transport step 81-100.

Using mix 20.
Using kinetics 20.   Kinetics defined in simulation 3.

Mixture 20.

        2.750e-001 Solution 19   Solution after simulation 3.
        0.000e+000 Solution 21   Solution Initially filling Column
        7.250e-001 Solution 20   Solution after simulation 3.

Kinetics 20.   Kinetics defined in simulation 3.

        Time step: 1500 seconds

        Rate name   Delta Moles Total Moles   Reactant   Coefficient

        Calcite_2   2.385e-006 3.198e-003   CaCO3   1

---------------------------Solution composition----------------------------

        Elements   Molality   Moles

        C   5.951e-003 5.951e-003
        Ca   1.695e-002 1.695e-002
        Cl   2.430e-001 2.430e-001
        K   9.300e-002 9.300e-002
        Na   1.300e-001 1.300e-001
        S   2.000e-003 2.000e-003

---------------------------Description of solution--------------------------

                                 pH =   6.867   Charge balance
                                 pe =   7.564   Adjusted to redox equilibrium
                    Activity of water =   0.992
                          Ionic strength =   2.698e-001
                       Mass of water (kg) =   1.000e+000
                  Total alkalinity (eq/kg) =   5.108e-003
                      Total CO2 (mol/kg) =   5.951e-003
                    Temperature (deg C) = 100.000
                  Electrical balance (eq) =   4.795e-003
Percent error, 100*(Cat-|An|)/(Cat+|An|) =   0.95
                            Iterations =   2
                               Total H = 1.110173e+002
                               Total O = 5.553110e+001

---------------------------Saturation indices------------------------------

        Phase   SI log IAP log KT

        Anhydrite   -0.72   -6.04   -5.32 CaSO4
        Aragonite   0.94   -8.23   -9.17 CaCO3
        Calcite   1.04   -8.23   -9.27 CaCO3
        CH4(g)   -99.56 -134.99 -35.44 CH4
        CO2(g)   -0.99 -19.55 -18.56 CO2
        Gypsum   -1.20   -6.05   -4.85 CaSO4:2H2O
        H2(g)   -28.86 -28.86   0.00 H2
        H2O(g)   0.04   -0.00   -0.04 H2O
        H2S(g)   -99.83 -132.81 -32.98 H2S
        Halite   -3.57   -1.85   1.72 NaCl
        O2(g)   -5.27   57.72   62.99 O2
        Sulfur   -76.12 -103.94 -27.83 S

Transport step 101-120.

119

```
Using mix 20.
Using kinetics 20.     Kinetics defined in simulation 3.

Mixture 20.

        2.750e-001 Solution 19        Solution after simulation 3.
        0.000e+000 Solution 21        Solution Initially filling Column
        7.250e-001 Solution 20        Solution after simulation 3.

Kinetics 20.    Kinetics defined in simulation 3.

        Time step: 1500 seconds

        Rate name       Delta Moles Total Moles   Reactant       Coefficient

        Calcite_2        2.405e-006  3.246e-003   CaCO3                      1

-------------------------------Solution composition----------------------------

        Elements          Molality      Moles

        C               5.951e-003  5.951e-003
        Ca              1.695e-002  1.695e-002
        Cl              2.430e-001  2.430e-001
        K               9.300e-002  9.300e-002
        Na              1.300e-001  1.300e-001
        S               2.000e-003  2.000e-003

----------------------------Description of solution----------------------------

                                 pH  =   6.867      Charge balance
                                 pe  =   7.569      Adjusted to redox equilibrium
                  Activity of water  =   0.992
                    Ionic strength   =   2.698e-001
               Mass of water (kg)    =   1.000e+000
             Total alkalinity (eq/kg) =   5.107e-003
               Total CO2 (mol/kg)    =   5.951e-003
               Temperature (deg C)   = 100.000
             Electrical balance (eq) =   4.795e-003
Percent error, 100*(Cat-|An|)/(Cat+|An|) =   0.95
                      Iterations   =   2
                         Total H  = 1.110173e+002
                         Total O  = 5.553110e+001

----------------------------Saturation indices---------------------------------

        Phase             SI log IAP  log KT

        Anhydrite        -0.72   -6.04   -5.32  CaSO4
        Aragonite         0.94   -8.23   -9.17  CaCO3
        Calcite           1.04   -8.23   -9.27  CaCO3
        CH4(g)          -99.60 -135.03  -35.44  CH4
        CO2(g)           -0.99  -19.55  -18.56  CO2
        Gypsum           -1.20   -6.05   -4.85  CaSO4:2H2O
        H2(g)           -28.87  -28.87    0.00  H2
        H2O(g)            0.04   -0.00   -0.04  H2O
        H2S(g)          -99.87 -132.85  -32.98  H2S
        Halite           -3.57   -1.85    1.72  NaCl
        O2(g)            -5.25   57.74   62.99  O2
        Sulfur          -76.15 -103.97  -27.83  S

Transport step 121-140.

Using mix 20.
Using kinetics 20.     Kinetics defined in simulation 3.

Mixture 20.
```

```
        2.750e-001 Solution 19        Solution after simulation 3.
        0.000e+000 Solution 21        Solution Initially filling Column
        7.250e-001 Solution 20        Solution after simulation 3.

Kinetics 20.   Kinetics defined in simulation 3.

        Time step: 1500 seconds

        Rate name      Delta Moles Total Moles   Reactant         Coefficient

        Calcite_2      2.426e-006  3.295e-003    CaCO3                       1

-------------------------Solution composition-----------------------------

        Elements          Molality      Moles

        C              5.950e-003  5.950e-003
        Ca             1.695e-002  1.695e-002
        Cl             2.430e-001  2.430e-001
        K              9.300e-002  9.300e-002
        Na             1.300e-001  1.300e-001
        S              2.000e-003  2.000e-003

-------------------------Description of solution---------------------------

                                  pH  =    6.867      Charge balance
                                  pe  =    7.555      Adjusted to redox equilibrium
                    Activity of water =    0.992
                       Ionic strength =    2.698e-001
                   Mass of water (kg) =    1.000e+000
              Total alkalinity (eq/kg) =   5.106e-003
                   Total CO2 (mol/kg) =    5.950e-003
                  Temperature (deg C) =  100.000
               Electrical balance (eq) =   4.795e-003
Percent error, 100*(Cat-|An|)/(Cat+|An|) =    0.95
                          Iterations  =    2
                             Total H  = 1.110173e+002
                             Total O  = 5.553110e+001

-------------------------Saturation indices--------------------------------

        Phase          SI  log IAP  log KT

        Anhydrite     -0.72   -6.04   -5.32  CaSO4
        Aragonite      0.94   -8.23   -9.17  CaCO3
        Calcite        1.04   -8.23   -9.27  CaCO3
        CH4(g)       -99.48 -134.92  -35.44  CH4
        CO2(g)        -0.99  -19.55  -18.56  CO2
        Gypsum        -1.20   -6.05   -4.85  CaSO4:2H2O
        H2(g)        -28.84  -28.84    0.00  H2
        H2O(g)         0.04   -0.00   -0.04  H2O
        H2S(g)       -99.75 -132.73  -32.98  H2S
        Halite        -3.57   -1.85    1.72  NaCl
        O2(g)         -5.31   57.68   62.99  O2
        Sulfur       -76.06 -103.89  -27.83  S

Transport step 141-160.


Using mix 20.
Using kinetics 20.     Kinetics defined in simulation 3.

Mixture 20.

        2.750e-001 Solution 19        Solution after simulation 3.
        0.000e+000 Solution 21        Solution Initially filling Column
        7.250e-001 Solution 20        Solution after simulation 3.

Kinetics 20.   Kinetics defined in simulation 3.
```

Time step: 1500 seconds

Rate name	Delta Moles	Total Moles	Reactant	Coefficient
Calcite_2	2.446e-006	3.343e-003	CaCO3	1

---------------------------Solution composition---------------------------

Elements	Molality	Moles
C	5.950e-003	5.950e-003
Ca	1.695e-002	1.695e-002
Cl	2.430e-001	2.430e-001
K	9.300e-002	9.300e-002
Na	1.300e-001	1.300e-001
S	2.000e-003	2.000e-003

---------------------------Description of solution---------------------------

$$
\begin{aligned}
pH &= 6.867 \quad \text{Charge balance} \\
pe &= 7.574 \quad \text{Adjusted to redox equilibrium} \\
\text{Activity of water} &= 0.992 \\
\text{Ionic strength} &= 2.698e-001 \\
\text{Mass of water (kg)} &= 1.000e+000 \\
\text{Total alkalinity (eq/kg)} &= 5.105e-003 \\
\text{Total CO2 (mol/kg)} &= 5.950e-003 \\
\text{Temperature (deg C)} &= 100.000 \\
\text{Electrical balance (eq)} &= 4.795e-003 \\
\text{Percent error, } 100*(Cat-|An|)/(Cat+|An|) &= 0.95 \\
\text{Iterations} &= 2 \\
\text{Total H} &= 1.110173e+002 \\
\text{Total O} &= 5.553110e+001
\end{aligned}
$$

---------------------------Saturation indices---------------------------

Phase	SI	log IAP	log KT	
Anhydrite	-0.72	-6.04	-5.32	CaSO4
Aragonite	0.94	-8.23	-9.17	CaCO3
Calcite	1.04	-8.23	-9.27	CaCO3
CH4(g)	-39.63	-135.06	-35.44	CH4
CO2(g)	-0.99	-19.55	-18.56	CO2
Gypsum	-1.20	-6.05	-4.85	CaSO4:2H2O
H2(g)	-28.88	-28.88	0.00	H2
H2O(g)	0.04	-0.00	-0.04	H2O
H2S(g)	-39.90	-132.88	-32.98	H2S
Halite	-3.57	-1.85	1.72	NaCl
O2(g)	-5.24	57.75	62.99	O2
Sulfur	-76.17	-104.00	-27.83	S

Transport step 161-180.

Using mix 20.
Using kinetics 20.   Kinetics defined in simulation 3.

Mixture 20.

        2.750e-001 Solution 19   Solution after simulation 3.
        0.000e+000 Solution 21   Solution initially filling Column
        7.250e-001 Solution 20   Solution after simulation 3.

Kinetics 20.   Kinetics defined in simulation 3.

        Time step: 1500 seconds

Rate name	Delta Moles	Total Moles	Reactant	Coefficient

```
        Calcite_2        2.466e-006  3.393e-003   CaCO3                        1

------------------------------Solution composition----------------------------

        Elements          Molality       Moles

        C               5.950e-003  5.950e-003
        Ca              1.695e-002  1.695e-002
        Cl              2.430e-001  2.430e-001
        K               9.300e-002  9.300e-002
        Na              1.300e-001  1.300e-001
        S               2.000e-003  2.000e-003

-----------------------------Description of solution---------------------------

                              pH  =    6.867    Charge balance
                              pe  =    7.563    Adjusted to redox equilibrium
                 Activity of water  =   0.992
                     Ionic strength  =  2.698e-001
                   Mass of water (kg)  =  1.000e+000
              Total alkalinity (eq/kg)  =  5.104e-003
                  Total CO2 (mol/kg)  =  5.950e-003
                   Temperature (deg C)  = 100.000
              Electrical balance (eq)  =  4.795e-003
    Percent error, 100*(Cat-|An|)/(Cat+|An|)  =   0.95
                         Iterations  =    2
                            Total H  = 1.110173e+002
                            Total O  = 5.553110e+001

---------------------------Saturation indices--------------------------------

        Phase            SI  log IAP  log KT

        Anhydrite       -0.72   -6.04   -5.32  CaSO4
        Aragonite        0.94   -8.23   -9.17  CaCO3
        Calcite          1.04   -8.23   -9.27  CaCO3
        CH4(g)         -99.54 -134.98  -35.44  CH4
        CO2(g)          -0.99  -19.55  -18.56  CO2
        Gypsum          -1.20   -6.05   -4.85  CaSO4:2H2O
        H2(g)          -28.86  -28.86    0.00  H2
        H2O(g)           0.04   -0.00   -0.04  H2O
        H2S(g)         -99.81 -132.79  -32.98  H2S
        Halite          -3.57   -1.85    1.72  NaCl
        O2(g)           -5.28   57.71   62.99  O2
        Sulfur         -76.10 -103.93  -27.83  S

Transport step 181-200.


Using mix 20.
Using kinetics 20.    Kinetics defined in simulation 3.

Mixture 20.

        2.750e-001 Solution 19      Solution after simulation 3.
        0.000e+000 Solution 21      Solution Initially filling Column
        7.250e-001 Solution 20      Solution after simulation 3.

Kinetics 20.   Kinetics defined in simulation 3.

        Time step: 1500 seconds

        Rate name      Delta Moles Total Moles   Reactant        Coefficient

        Calcite_2       2.487e-006  3.442e-003   CaCO3                        1

-----------------------------Solution composition-----------------------------

        Elements          Molality       Moles
```

```
C              5.949e-003  5.949e-003
Ca             1.695e-002  1.695e-002
Cl             2.430e-001  2.430e-001
K              9.300e-002  9.300e-002
Na             1.300e-001  1.300e-001
S              2.000e-003  2.000e-003
```

------------------------Description of solution------------------------

```
                          pH =    6.866      Charge balance
                          pe =    7.571      Adjusted to redox equilibrium
        Activity of water  =    0.992
            Ionic strength  =    2.698e-001
         Mass of water (kg)  =    1.000e+000
     Total alkalinity (eq/kg) =    5.103e-003
        Total CO2 (mol/kg)  =    5.949e-003
       Temperature (deg C)  =  100.000
     Electrical balance (eq)  =    4.795e-003
Percent error, 100*(Cat-|An|)/(Cat+|An|)  =    0.95
                   Iterations  =    2
                      Total H  = 1.110173e+002
                      Total O  = 5.553109e+001
```

------------------------Saturation indices------------------------

```
        Phase          SI  log IAP  log KT

        Anhydrite    -0.72   -6.04   -5.32  CaSO4
        Aragonite     0.94   -8.23   -9.17  CaCO3
        Calcite       1.04   -8.23   -9.27  CaCO3
        CH4(g)      -99.60 -135.04  -35.44  CH4
        CO2(g)       -0.99  -19.55  -18.56  CO2
        Gypsum       -1.20   -6.05   -4.85  CaSO4:2H2O
        H2(g)       -28.97  -28.97    0.00  H2
        H2O(g)        0.04   -0.00   -0.04  H2O
        H2S(g)      -99.87 -132.85  -32.98  H2S
        Halite       -3.57   -1.85    1.72  NaCl
        O2(g)        -5.25   57.74   62.99  O2
        Sulfur      -76.15 -103.98  -27.83  S
```

```
------------------
End of simulation.
------------------
```

```
-----------------------------------
Reading input data for simulation 4.
-----------------------------------
```

```
-----------
End of run.
-----------
```

CHAPTER 5

Calcite Dissolution Rates at Elevated Temperatures using a Surface Complexation Model

ABSTRACT

Several rate equations (Nilsson and Sternbeck, 1999) involving surface complexes participating in the dissolution reaction are tested for calcite dissolution at elevated temperatures. The surface densities of $\equiv CaCO_3^-$, $\equiv CaHCO_3^0$, $\equiv CaOH_2^+$, $\equiv CO_3^-$, $\equiv CO_3Ca^+$, $\equiv CO_3H^0$, $\equiv CaOH^0$, and $\equiv CaO^-$ are predicted using a surface complexation model proposed by Van Cappelen et al. (1993) for calcite reaction in aqueous solutions. Dissolution rates are predicted for all of the nonsaline solutions in the laboratory experiments at elevated temperatures. The models do not fit this data very well as evident from the negative signs for several of the rate constants. Further investigations into identifying the complexes that will adequately describe rates at elevated temperatures are recommended.

INTRODUCTION

Calcite dissolution and growth kinetics have been well-studied at surface temperatures and pressures, addressing various aspects of physical and chemical parameters that influence calcite-fluid reaction rates (Berner and

Morse, 1974; Plummer et al., 1978, 1979; Morse, 1983; Sjoberg and Rickard, 1984; Busenberg and Plummer, 1986; Chou et al., 1989; Arakaki and Mucci, 1995; Shiraki and Brantley, 1995; Dreybrodt et al., 1996, Davis et al., 2000). It has been emphasized that chemical processes taking place at the interface between the mineral lattice and bulk solution play a key role in such reactions (Morse, 1986). A closer look at reactions occurring at the molecular level indicates the presence of surface complexes generated during the course of the reaction and distributed in both the bulk solution and at the mineral-fluid interface. These complexes form an intermediate step in the overall reaction. One approach in the investigation of reaction kinetics has been to include surface complexations in mechanistic rate laws describing dissolution or growth of minerals (Van Cappellen et al., 1993; Nilsson and Sternbeck, 1999).

Integrating reaction rates with surface complexation is significant because it would permit an interpretation of calcite reaction in terms of actual surface species acting as intermediaries or "activated complexes" in the reaction steps. The observed differences in rates as a function of carbon dioxide partial pressures could be explained in terms of variation in densities of the surface complexes. A surface complexation-based rate law would allow separation of pH and P_{CO_2} effects on the overall reaction.

In this part of the study, solution and surface speciations were done for the various solutions in the experiments at elevated temperatures (Chapter 2). The surface densities of complexes were determined based on a surface complexation model for carbonate minerals proposed by Van Cappellen et al.

126

(1993). The geochemical program PHREEQC Interactive 2.4.2 (Parkhurst and Appelo, 2001) was used for simulating the solution speciation, participating reactions, and surface complexation. It uses heterogeneous mass action equations and mole balance equations for the surface sites. In addition, other equations for surface charge and surface electrostatic potential are also considered in the program. The rate data and the surface densities were fit to a surface complexation-based rate equation and rate constants were determined using multiple linear regression.

THEORETICAL BACKGROUND

Based on a vast number of studies on calcite reaction kinetics, it is recognized that in addition to temperature and pressure, the solution pH, P_{CO_2}, ionic strength, saturation state, hydrodynamic condition and presence of inhibiting inorganic species or organic ligands all play an important role in calcite dissolution (Plummer et al., 1978; Morse, 1983; Sjoberg and Rickard, 1984; Chou et al., 1989; Dreybrodt et al., 1996, Davis et al., 2000). Different approaches have been adopted for defining rate laws to describe calcite-water reaction behavior. In some studies rates were determined as a function of the degree of saturation (Nancollas and Reddy, 1971; Morse, 1978; Neilsen, 1983; Mucci, 1986). Elementary reaction-based rate laws arrive at overall rates as a combined result of elementary reactions involved at the molecular level (Plummer et al., 1978, 1979; Busenberg and Plummer, 1986). In yet another approach, elementary reaction-based models have been extended to include the

role of surface-complexation in rate determination (Van Cappellen et al., 1993; Nilsson and Sternbeck, 1999). Surface complexation accompanying the reactions occurring in the bulk solutions, have been studied for carbonates and other minerals. It has been argued that a kinetic description of dissolution rate of metal oxides, silicates and carbonates significantly improves when cast in terms of surface speciation (Schindler and Stumm, 1987; Stumm and Weiland, 1990; Davis and Kent, 1990; Dzombak and Morel, 1990; Van Cappellen et al., 1993; Arakaki and Mucci, 1995; Nilsson and Sternbeck, 1999).

Surface Speciation Model

The theory of surface speciation suggests that ions react chemically with specific surface hydroxyl groups having passed through an interfacial electric field at the surface (Dzombak and Morel, 1990). The electric field may be positive or negative due to chemical reactions occurring at the surface. The reactions at the surface are considered analogous to the formation of complexes in the bulk solution that are described by mass action law equations. It must be noted, however, that equilibrium constants in the two cases are not the same. The difference between the equilibrium constants is a reflection of the variable electrostatic energy of interaction caused by a variable charge at the surface. An exponential coulombic correction factor, derived from EDL (electrostatic double layer) theory is included in the surface complexation equations to account for this electrostatic effect (Dzombak and Morel, 1990). This model assumes an

128

electrostatic double layer, i.e. two layers at the surface—one planar surface layer and a diffuse layer of counterions. Of the two commonly described surface complexation models, Van Cappellen et al. (1993) used the *constant-capacitance* model proposed by Schindler and coworkers (Schindler and Kamber, 1968; Stumm et al., 1970; Schindler and Gamsjager, 1972). This has an ionic strength dependence and implies a constant capacitance between the two layers, for modeling surface speciation of calcite.

Using x-ray photoelectron spectroscopic techniques it has been possible to detect the formation of a hydrated mineral layer at the freshly exposed mineral surface (Stipp and Hochella, 1991). Using low-energy electron diffraction (LEED) it was observed that water molecules essentially form a monolayer, which does not penetrate deep into the lattice. A water molecule is dissociated and adsorbed to a freshly exposed mineral surface in which the cation site is hydroxylated and the anion is protonated as $\equiv CaOH^o$ and $\equiv CO_3H^o$ ($\equiv$ symbol is used to indicate that the species is a surface complex). Based on these observations, a surface complexation model for the chemical structure and reactivity at the mineral-solution interface was presented for carbonate minerals by Van Cappellen et al. (1993). According to the model several different complexes form as a result of reactions between species such as $\equiv CO_3H^o$, $\equiv CaOH^0$, Ca^{2+}, H^+ and CO_2. It was shown that $\equiv CO_3^-$, $\equiv CaHCO_3^0$, and $\equiv CaCO_3^-$ dominated the surface of calcite between pH 6 – 9, at high P_{CO_2}. As P_{CO_2} decreases, the concentrations of $\equiv CaHCO_3^0$ and $\equiv CaCO_3^-$ decrease relative to $\equiv CaOH_2^+$.

129

It was suggested that hydration processes influence surface electrical charge and calcite reactivity. In turn, calcite reaction rates may also be expressed in terms of density of the surface-complexes. Three important parameters— pH, P_{CO_2} and saturation states, which are key controls on formation of surface-complexes, are also the key governing elements for calcite dissolution rates.

METHODS

Bulk solution speciation and surface speciation associated with calcite dissolution in aqueous solutions at 100°C were modeled using PHREEQC Interactive 2.4.2 (Parkhurst and Appelo, 2001). Various solutions used in the dissolution experiments in this study were reacted with calcite. The solution chemistry, reactions, mineral phases, and gas phases are all defined in various modules, referred to as data blocks within the input file. s_Ca and s_CO$_3$ are defined as the surface binding sites in the SURFACE data block. ≡CaOH° and ≡CO$_3$H° are specified as the primary surface species in the SURFACE_MASTER_SPECIES data block.

The reactions that govern surface complexation and the analog bulk solution reactions in the $CaCO_3$-H_2O-CO_2 system, according to the model proposed by Van Cappellen et al. (1993), are listed in Table 5.1. Equilibrium constants, K_{eq}, for the bulk solution reactions at 100°C were used as proxies for the corresponding surface reactions. This is considered valid since the K_{eq}

130

reported for bulk and surface reactions at 25°C are close approximations of each other (Table 5.2).

The K_{eq} for the bulk solution at 100°C were computed from the ionic activity products for the respective reactions. The activities for the individual species in each reaction were determined from speciation calculations performed using PHREEQCI. To check the accuracies of the equilibrium constants computed by this method, a few of these were evaluated by other independent calculations. The temperature dependence of K_{eq} is described by the general equation (Maier and Kelly, 1932; Plummer and Busenberg, 1982)

$$Log\ K_{eq} = A + BT + C/T + D\ log\ T + ET^2$$

where A, B, C, D, and E are constants and T is the temperature in °K. For example, K_{eq} at 100°C for the reaction $H_2CO_3 = HCO3^- + H^+$ was calculated using this equation. Magnitudes of the above constants were taken from Plummer and Busenberg (1982). Computation based on PHREEQCI speciation gave an identical value for this reaction.

RESULTS AND DISCUSSION

The variation in the densities of surface complexes with pH has been predicted using a complexation model proposed by Van Cappellen et al. (1993). The overall distribution of complexes at 25°C could be reproduced well using PHREEQCI (Figure 5.1). This provides a basis for using PHREEQCI as a

131

Table 5.1 Surface complexation and analog bulk solution reactions for $CaCO_3$-CO_2-H_2O system (Van Cappellen et al., 1993)

	Surface Reactions	Analog Bulk Reactions
1	$\equiv CO_3H^0 = \equiv CO_3^- + H^+$	$H_2CO_3^* = HCO_3^- + H^+$
2	$\equiv CO_3H^0 + Ca^{2+} = \equiv CO_3Ca^+ + H^+$	$H_2CO_3^* + Ca^{2+} = CaHCO_3^+ + H^+$
3	$\equiv CaOH_2^+ + H^+ = \equiv CaOH^+ + H_2O$	$Ca(OH)_2^0 + H^+ = CaOH^+ + H_2O$
4	$\equiv CaOH^0 = \equiv CaO^- + H^+$	$Ca(OH)_2^0 + H_2O = Ca(OH)_3^- + H^+$
5	$\equiv CaOH^0 + CO_2 = \equiv CaHCO_3^0$	$CaOH^+ + CO_2 = CaHCO_3^-$
6	$\equiv CaOH^0 + CO_2 = \equiv CaCO_3^- + H^+$	$CaOH^+ + CO_2 = CaCO_3^0 + H^+$

Table 5.2 Log K for surface reactions (s) and analog bulk solution reactions (b) are close approximations at 25°C. Bulk solution K at 100°C are used as proxy for respective surface reaction constants

Surface Reactions		Log K at 25°C	Log K at 100°C
$\equiv CO_3H^0 = \equiv CO_3^- + H^+$	(1)	-4.9 (s) -4.1 (b)	-6.43
$\equiv CO_3H^0 + Ca^{2+} = \equiv CO_3Ca^+ + H^+$	(2)	-2.8 (s) -2.8 (b)	-5.06
$\equiv CaOH_2^+ + H^+ = \equiv CaOH^+ + H_2O$	(3)	12.2 (s) 11.0 (b)	12.27
$\equiv CaOH^0 = \equiv CaO^- + H^+$	(4)	-17.0 (s) -17.0 (b)	-16.25
$\equiv CaOH^0 + CO_2 = \equiv CaHCO_3^0$	(5)	6.0 (s) 5.8 (b)	7.71
$\equiv CaOH^0 + CO_2 = \equiv CaCO_3^- + H^+$	(6)	-2.6 (s) -2.4 (b)	0.37

132

Figure 5.1 Surface densities of complexes at 25°C and Pco_2 3.3 x 10^{-4} atm (Van Cappellen et al., 1993) using PHREEQCI
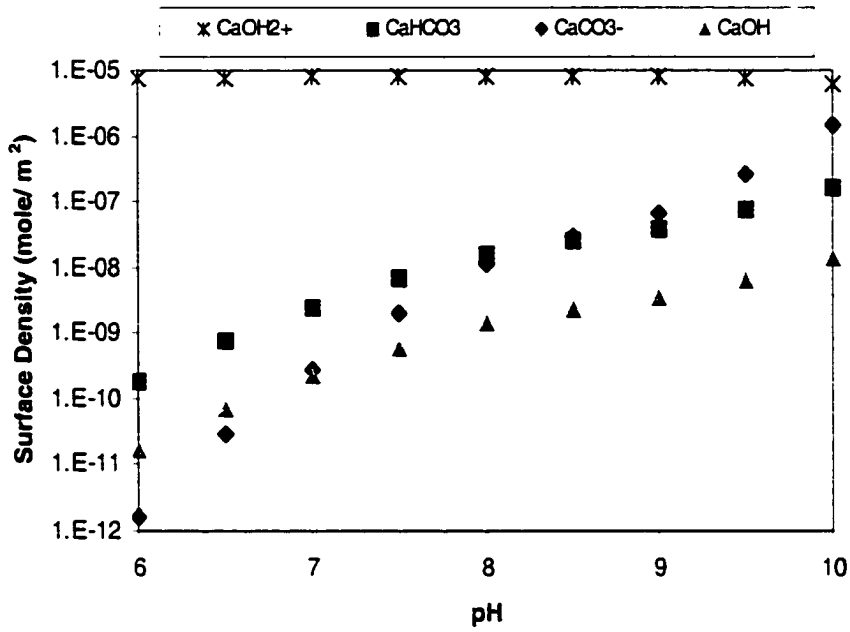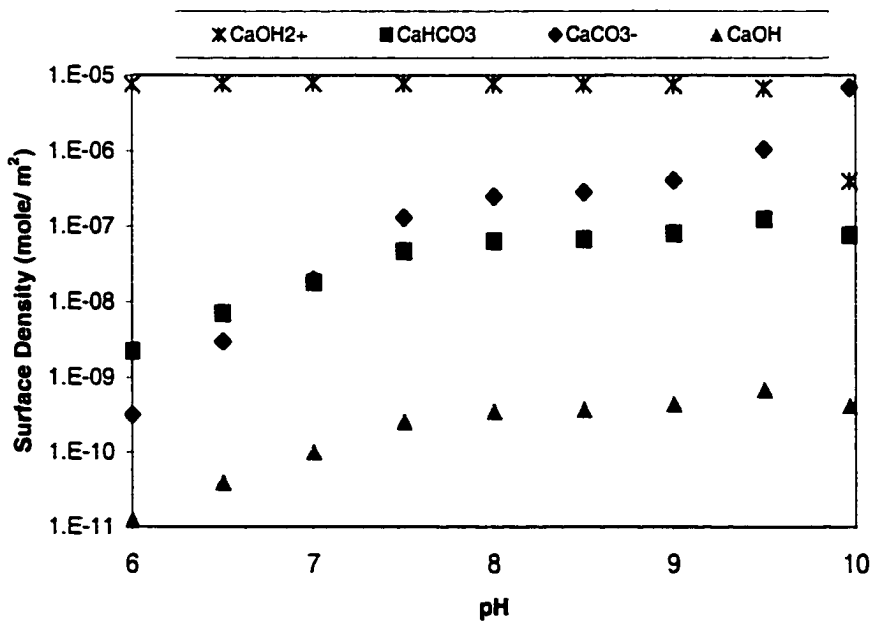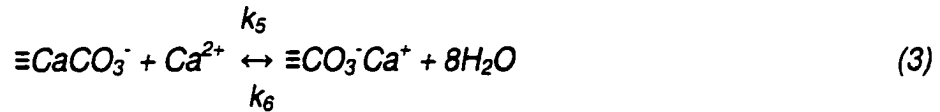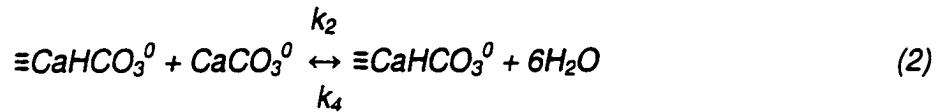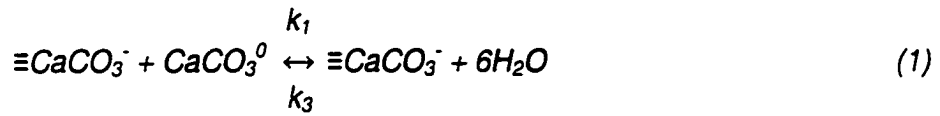

Figure 5.2 Surface densities of complexes at 100°C and Pco_2 3.3 x 10^{-4} atm using PHREEQCI

modeling tool for capturing aspects of surface complexation at elevated temperatures. The surface densities of complexes at 100°C are shown for comparison in Figure 5.2.

A previous study suggested that $\equiv CaHCO_3^0$, $\equiv CaCO_3^-$, and $\equiv CO_3Ca^+$ were the chief surface complexes that participate in calcite-water reaction via the following reversible reactions (Nilsson and Sternbeck, 1999).

$$\equiv CaCO_3^- + CaCO_3^0 \overset{k_1}{\underset{k_3}{\longleftrightarrow}} \equiv CaCO_3^- + 6H_2O \qquad (1)$$

$$\equiv CaHCO_3^0 + CaCO_3^0 \overset{k_2}{\underset{k_4}{\longleftrightarrow}} \equiv CaHCO_3^0 + 6H_2O \qquad (2)$$

$$\equiv CaCO_3^- + Ca^{2+} \overset{k_5}{\underset{k_6}{\longleftrightarrow}} \equiv CO_3^-Ca^+ + 8H_2O \qquad (3)$$

The above reactions describe calcite growth and dissolution where k_1, k_2 and k_5 are the rate constants for the forward reactions representing growth, whereas k_3, k_4 and k_6 are the backward reaction constants representing dissolution. It should be noted that the surface complexes occurring on the right and left hand side are not the same. These are reactions occurring at the mineral surface describing species that are incorporated into bulk lattice (in case of growth) or escape into bulk solution (in case of dissolution). For example, $\equiv CaCO_3^-$ on the left hand side escape into bulk lattice as $CaCO_3^0$ is incorporated.

134

The $\equiv CaCO_3^-$ on the right hand side are converted into soluble $CaCO_3^0$ following hydrolysis (Nilsson and Sternbeck, 1999).

Combining the above reactions that presumably dominate complexation in the $CaCO_3$-H_2O-CO_2 system, the following rate equation may be formulated to predict dissolution rate:

$$Rate = -k_1 \cdot (CaCO_3^0) \cdot \{\equiv CaCO_3^-\} - k_2 \cdot (CaCO_3^0) \cdot \{\equiv CaHCO_3^0\} + k_3 \cdot \{\equiv CaCO_3^-\} + k_4 \cdot \{\equiv CaHCO_3^0\} - k_5 \cdot (Ca^{2+}) \cdot \{\equiv CaCO_3^-\} + k_6 \cdot \{\equiv CO_3Ca^-\} \tag{4}$$

where ( ) denotes activity of the species in bulk solution and { } denotes the surface densities of the complexes. Rate data (Chapter 2) and the surface densities determined using PHREEQCI were fit to the above rate equation and rate constants were determined using a multiple linear regression tool available in spreadsheet programs. The linear regression analysis was performed by using the least squares method. The rate (dependent variable) in equation (4) is a linear function of the surface densities of complexes and activities of species in the bulk solution (independent variables). The coefficients k_1 through k_6 were determined from the regression analysis.

Data from this study do not fit the above model very well. Results were better when only reaction (1) and (2) were considered. Attempts by Nilsson and Sternbeck (1999) to fit their data by considering only reaction (1) and (2) also resulted in a negative value for one of the rate coefficients. This suggested the possible role of other complexes and reactions in controlling the overall rate.

135

Inclusion of reaction (3) resulted in a better description of their rates. However, the fit to the present rates was worse when reaction (3) was included.

An alternative to equation (3) also has been suggested that assumes $\equiv CaOH_2^+$ may be the relevant complex instead of $\equiv CO_3^- Ca^+$ based on data fit for calcite growth experiments. Of the two models, the one using $\equiv CaOH_2^+$ better fits data from this study (Table 5.3 and Figure 5.3).

CONCLUSIONS

The model fit to results from this study was able to predict dissolution rates well. However negative signs for some of the rate constants calls for a better understanding of the mechanisms assumed here. The rate equation and the complexes that are assumed to be key to rate determination may not be the most appropriate description of reactions occurring at the experimental conditions. Alternative rate equations have been suggested including a different set of complexes— $\equiv CO_3^-$, $\equiv CO_3H^0$, and $\equiv Ca^+$ that adequately describe calcite dissolution and precipitation at similar conditions (Arakaki and Mucci, 1995). In view of this attempt, it appears that further investigations are necessary to recognize the set of complexes that satisfactorily describe rates at elevated temperatures.

Table 5.3 Rate constants and rates predicted using a rate model involving complexation species $\equiv CaCO_3^-$, $\equiv CaHCO_3^0$, and $\equiv CaOH_2^+$

Rate Constant (mmolal/ hr)		Observed Rates (mmolal/ m^2-hr)	Predicted Rates (mmolal/m^2-hr)
k1	-3.14E+23	1.91E+01	-5.29E+01
k2	2.63E+24	3.87E+02	3.17E+02
k3	-2.48E+18	3.80E+01	5.29E+01
k4 .	2.02E+19	8.61E+00	8.61E+00
k5	1.42E+19	3.44E+01	7.99E+01
k6	6.11E+15	1.31E+02	1.72E+02

FIGURE 5.3 Observed vs. predicted rates
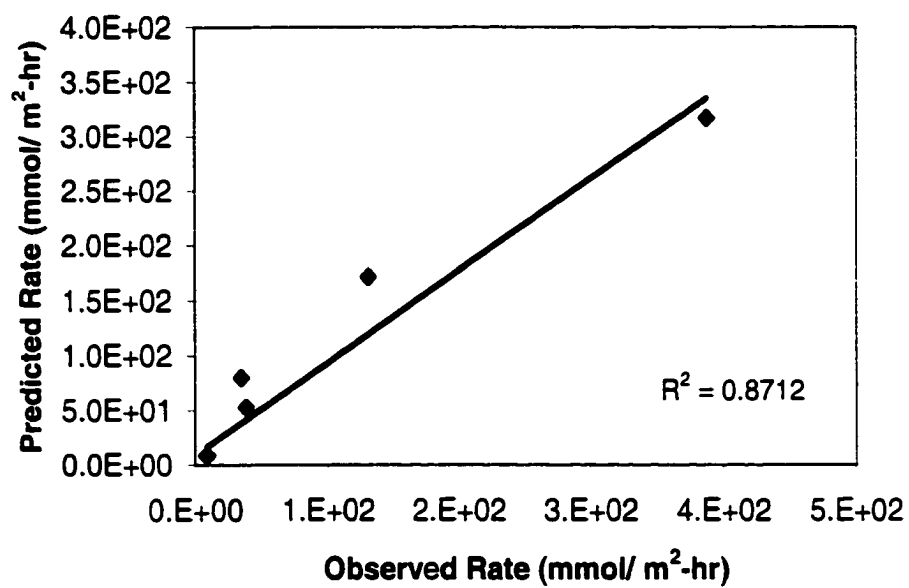
REFERENCES

Alkattan M., Oelkers E. H., Dandurand J. L., and Schott J. (1998) An experimental study of calcite and limestone dissolution rates as a function of pH from -1 to 3 and temperature from 25 to 80°C. *Chem. Geol.* **151**, 199-214.

Amaefule J. O., Kersey D. G., Norman D. L., and Shannon P. M. (1988) Advances in formation damage assessment and control strategies. CIM 88-39-65 paper, Proceedings of the 39th Annual Technical Meeting of Petroleum Society of CIM and Canadian Gas Processors Association, June 12-16, Calgary, Alberta, 16 p.

Arakaki T. and Mucci A. (1995) A continuous and mechanistic representation of calcite reaction-controlled kinetics in dilute solutions at 25°C and 1 atm total pressure. *Aquatic Geochem.* **1**, 105-130.

Atkinson G. (1993) *Comprehensive Scale Prediction Project, Phase II, Progress Report No. 4 – Final Report*, Department of Chemistry, University of Oklahoma.

Atkinson G. and Mecik M (1998) OK SCALE 98 version 1.11, for Windows 98, Department of Chemistry, University of Oklahoma.

Badiozamani K., Mackenzie F. T., and Thorstenson, D. C. (1977) Experimental carbonate cementation: salinity, temperature, and vadose-phreatic effects. *J. Sediment. Petrol.* **47**, 529-542.

Berner R. A. and Morse J. W. (1974) Dissolution kinetics of calcium carbonate in seawater IV. Theory of calcite dissolution. *Amer. J. Sci.* **274**, 1173-1186.

Berner R. A. (1995) Chemical weathering and its effects on atmospheric CO_2 and climate. In *Chemical Weathering Rates of Silicate minerals* (ed. A.F. White and S.L. Brantley), *Rev. Mineral.* **31**, 565-583.

Bethke C. M. (1994) *The Gechemist's Workbench*^{TM}*, version 2.0, A Users Guide to RXN, Act2, Tact, React, and Gtplot.* University of Illinois.

Bischoff J. L. (1968) Kinetics of calcite nucleation: magnesium ion inhibition and ionic strength catalysis. *J. Geophys. Res.* **73**, 3315-3322.

Blum A. E. and Lasaga A. C. (1987) Monte Carlo Simulations of surface reaction rate laws. In *Aquatic Surface Chemistry* (ed. W. Stumm) pp. 255-292. Wiley.

Brady P. V., Krumhansl J. L., and Papenguth H. W. (1996) Surface complexation clues to dolomite growth. *Geochim. Cosmochim. Acta.* **60**, 727-731.

Brezonik P. L. (1994) *Chemical Kinetics and process Dynamics in Aquatic Systems*. Lewis Publishers.

Brown C. A., Compton R. G., and Narramore C. A. (1993) The kinetics of calcite dissolution/precipitation. *J. Colloid Interface Sci.* **160**, 372-379.

Busenberg E. and Plummer L. N. (1986) A comparative study of the dissolution and crystal growth kinetics of calcite and aragonite. In *Studies in diagenesis* (ed. F. A. Mumpton); *USGS Bull.* **1578**, 139-168.

Casey W. H. (1987) Heterogeneous kinetics and diffusion boundary layers: the example of reaction in a fracture. *J. Geophys. Res.* **92**, 8007-8013.

Castellan G. W. (1971) *Physical Chemistry*. Addison-Wesley Publishing Company.

Chen Y., Wang X., Sha Q., and Zhang N. (1979) Experimental studies on the system of $Ca^{2+}-Mg^{2+}-HCO_3^--H_2O$ at room temperature at room temperature and pressure. *Sci Geol Sin.* **1**, 22-36.

Chou L., Garrels R. M., and Wollast R. (1989) Comparative study of kinetics and mechanisms of dissolution of carbonate minerals. *Chem. Geol.* **78**, 269-

282.

Civan F. (2000) *Reservoir Formation Damage: Fundamentals, Modeling, Assessment and Mitigation.* Gulf Publishing Co.

Civan F. (2001) Scale effect on porosity and permeability: kinetics, model and correlation. *American Institute of Chemical Engineers.* **47**, 271-288.

Compton R. G. and Daly P. J. (1984) The dissolution kinetics of iceland spar single crystals. *J. Colloid Interface Sci.* **101**, 159-166.

Compton R. G. and Daly P. J. (1987) The dissolution/ precipitation kinetics of calcium carbonate: An assessment of various kinetic equations using a rotating disc method. *J. Colloid Interface Sci.* **115**, 493-498.

Compton R. G. and Pritchard K. L (1990) The dissolution of calcite at pH >7: Kinetics and mechanism. *Phil. Trans. Royal Soc. London Ser. A Math. Phys. Sci.* **330**, 47-70.

Compton R. G., Pritchard K. L., and Unwin P. R. (1989) The dissolution of calcite in acid waters. Mass transport vs. surface control. *Freshwater Biol.* **22**, 285-288.

Compton R. G. and Unwin P. R. (1990) The dissolution of calcite in aqueous solution at pH < 4: Kinetics and mechanism. *Phil. Trans. Royal Soc. London Ser. A Math. Phys. Sci.* **330**, 1-46.

Davies, C. W. and Jones, A. L. (1955) The precipitation of silver chloride from aqueous solutions: Parts 2-4. *Trans. Faraday Soc.*, **51**, 812-829.

Davis J. A. and Kent D. B. (1990) Surface complexation modeling in aqueous geochemistry. In *Mineral-water interface geochemistry* (ed. M. F. Hochella and A. F. White): *Rev. Mineral 23.* pp. 177-260.

Davis K. J., Dove P. M., and De Y. J. (2000) The role of Mg (super 2+) as an impurity in calcite growth, *Science*, **290**, 5494, 1134-1137.

Dawe R. A. and Zhang Yuping (1997) Kinetics of calcium carbonate scaling using observations from glass micromodels. *Journal of Petroleum Science and Engineering.* **18**, 179-187.

Dove P. M. and Hochella M. F., Jr. (1993) Calcite precipitation mechanisms and inhibition by orthophosphate: In situ observations by scanning force microscopy. *Geochim. Cosmochim. Acta.* **57**, 705-714.

Dreybrodt W. and Buhmann, D. (1991) A mass transfer model for dissolution and

precipitation of calcite from solutions in turbulent motion, *Chem. Geol.* **90**, 107-122.

Dreybrodt W., Lauckner J., Zaihua L., Svensson U., and Buhmann D. (1996) The kinetics of the reaction $CO_2 + H_2O = HCO_3^-$ as one of the rate limiting steps for the dissolution of calcite in the system H_2O-CO_2-$CaCO_3$. *Geochim. Cosmochim. Acta* **60**, 3375-3381.

Dzombak D. A. and Morel F. M. M. (1990) *Surface Complexation Modeling: hydrous ferric oxide.* J. Wiley & Sons.

Haggerty D. J. and Seyler B. (1997) Investigation of Formation Damage from Mud Cleanout Acids and Injection Waters in Aux Vases Sandstone Reservoirs, Department of Natural Resources, Illinois State Geological Survey, *Illinois Petroleum Series*, **152**.

Harvie C. E., Moller N., and Weare J. H. (1984) the prediction of mineral solubilities in natural waters: The Na-K-Mg-Ca-H-Cl-SO_4-OH-HCO_3-CO_3-CO_2-H_2O system to high ionic strengths at 25°C. *Geochim. Cosmochim. Acta* **48**, 723-751.

He, S. and Morse J. W. (1993) The carbonic acid system and calcite solubility in aqueous Na-K-Ca-Mg-Cl-SO_4 solutions from 0 to 90°C. *Geochim.*

Cosmochim. Acta **57**, 3533-3554.

Herman J. S. (1982) The dissolution kinetics of calcite, dolomite and dolomite rocks in carbon dioxide-water system. Ph. D. Thesis., Pennsylvania State University, University Park, Pa. (unpublished)

Inskeep W. P. and Bloom P. R. (1985) An evaluation of rate equations for calcite precipitation kinetics at P_{CO_2} less than 0.01 atm and pH greater than 8. *Geochim. Cosmochim. Acta.* **49**, 2165-2180.

Inskeep W. P. and Bloom P.R. (1986) Kinetics of calcite precipitation in the presence of water soluble organic ligands. *Soil Sci. Soc. Amer. J.* **50**, 1167-1172.

Kazmierczak T. F., Tomson M. B., and Nancollas G. H. (1982) Crystal growth of calcium carbonate: A controlled composition kinetic study. *J. Phys. Chem.* **86**, 103 - 107.

Kharaka Y. K., Gunter W. D., Aggarwal P. K., Perkins E. H., and DeBraal J. D. (1988) SOLMINEQ88: A Computer Program Code for Geochemical Modeling of Water-Rock Interactions. *USGS Water Resources Investigation Report.* **88-4227**.

Kile D. E., Eberl D. D., Hoch A. R,. and Reddy, M. M. (2000) An assessment of calcite crystal growth mechanisms based on crystal size distributions, *Geochim. Cosmochim. Acta.* **64,** 17, 2937-2950.

Langmuir D. (1997) *Aqueous Environmental Geochemistry.* Prentice Hall.

Lasaga A. C. (1981) Transition state theory, in Kinetics of Geochemical Processes, (ed. A.C. Lasaga and R. J. Kirkpatrick); *Rev. Mineral,* p. 135-169.

Lasaga A. C. (1995) Fundamental approaches in describing mineral dissolution and precipitation rate. *Rev. Mineral.* **31,** 23-86.

Lebron I. and Suarez D. L. (1998) Kinetics and mechanisms of precipitation of calcite as affected by P_{CO_2} and organic ligands at 25°C. *Geochim. Cosmochim. Acta.* **62,** 405-416.

Liu, S. T., Nancollas, G. H. (1971) The kinetics of dissolution of calcium sulfate dihydrate, *J. Inorg. Nucl. Chem.* **33,** 2311-2316.

Lund K., Fogler, H. S., McCune C. C., and Ault, J. W. (1975) Acidization: II. The dissolution of calcite in hydrochloric acid. *Chem. Eng. Sci.* **30,** 825-835.

MacInnis I. and Brantley S.L. (1992) The role of dislocations and surface

morphology in calcite dissolution. *Geochim. Cosmochim. Acta.* **56**, 1113-1126.

Maier C. G. and Kelly K. K. (1932) An equation for the representation of high temperature heat content data. *J. Amer. Chem. Soc* **54**, 3243-3246.

Millero F.J. (1979) The thermodynamics of the carbonate system in seawater, *Geochim. Cosmochim. Acta.* **43**, 1651-1661.

Morse J. W. (1978) Dissolution kinetics on calcium carbonate in sea water VI. The near equilibrium dissolution kinetics of calcium carbonate-rich deep sea sediments. *Amer. J. Sci.* **278**, 344-353.

Morse J. W. (1983) The kinetics of calcium carbonate dissolution and precipitation. In *Carbonates: Mineralogy and Chemistry* (ed. R.J. Reeder), *Rev. Mineral.* **11**, 227-264.

Morse J. W. (1986) The surface chemistry of calcium carbonate minerals in natural waters: An overview. *Marine Chemistry* **20**, 91-112.

Mucci, A. (1986) Growth kinetics and composition of magnesian calcite overgrowths precipitated from seawater: Quantitative influence of orthophosphate ions. *Geochim. Cosmochim. Acta.* **50**, 2255-2265.

Murphy W., Oelkers E., and Lichtner P. (1989) Surface reaction versus diffusion control of mineral dissolution and growth rates in geochemical processes. *Chem. Geol.* **78**, 357-380.

Nancollas G. H. and Reddy M. M. (1971) The crystallization of calcium carbonate II. Calcite growth mechanism. *J. Colloid Interface Sci.* **10**, 215-252.

Nielsen A. E. (1983) Precipitates: Formation coprecipitation and agin. In *Treatise on Analytical Chemistry* (ed. I.M. Kolthoff and P.J. Elving) pp. 269-347. Wiley.

Nilsson Ö. and Sternbeck J. (1999) A mechanistic model for calcite crystal growth using surface speciation. *Geochim. Cosmochim. Acta.* **63**, 217-225.

Ostvold T. and Randhol P. (2001) Kinetics of CaCO3 scale formation: the influence of temperature, supersaturation and ionic composition. SPE 68302 paper, SPE Third International Symposium on Oilfield Scale, Jan 30-31, Aberdeen, UK.

Pabalan R. T. and Pitzer K. S. (1987) Thermodynamics of concentrated electrolyte mixtures and the prediction of mineral solubilities to high

temperatures for mixtures in the system $Na-K-Mg-Cl-SO_4-OH-H_2O$. *Geochim. Cosmochim. Acta* **51**, 2429-2443.

Parkhurst D. (1995) PHREEQC— A computer program for speciation, reaction-path, advective-transport, and inverse geochemical calculations, *USGS Water Resources Investigations Report* **95-4227**.

Parkhurst D. L. and Appelo C. A. J. (2001) PHREEQC Interactive (Version 2)— A Computer Program for Speciation, Batch-Reaction, One-Dimensional Transport, and Inverse Geochemical calculations. http://wwwbrr.cr.usgs.gov/projects/GWC_coupled/phreeqci/

Patterson C. S., Slocum G. H., Busey R. H., and Mesmer R. E., (1982) Carbonate equilibria in hydrothermal systems: First ionization of carbonic acid in NaCl media to 300°C. *Geochim. Cosmochim. Acta* **46**, 1653-1663.

Patterson C. S., Busey R. H., and Mesmer R. E., (1984) Second ionization of carbonic acid in NaCl media to 250°C. *J. Soln. Chem.* **13**, 647-660.

Pitzer K. S. (1987) Thermodynamic model for aqueous solutions of liquid-like density. In *Thermodynamic modeling of geological materials: Minerals, fluids and melts* (ed. I. S. E. Carmichael and H. P. Eugster); *Reviews in Mineralogy* **17**, 97 – 142.

Plummer L. N. and Busenberg E. (1982) The solubilities of calcite, aragonite and vaterite in CO_2-H_2O solutions between 0 and 90°C, and an evaluation of the aqueous model for the system $CaCO_3$-CO_2-H_2O. *Geochim. Cosmochim. Acta.* **46,** 1011-1040.

Plummer L. N., Wigley T. M. L., and Parkhurst D. L. (1978) The kinetics of calcite dissolution in CO_2: Water systems at 5-60°C and 0.0-1.0 atm CO_2. *Amer. J. Sci.* **278,** 179-216.

Plummer L. N., Wigley T. M. L., and Parkhurst D. L. (1979) Critical review of the kinetics of calcite dissolution and precipitation. Chemical Modeling in Aqueous Systems (ed. E.A. Jeune). *American Chemical Society Symposium Series* **93,** 537-573.

Przybylinski, J (1987) The role of bicarbonate ion in calcite scale formation. SPE 13547, Oilfield Geothermal Chemistry, Arizona April 9-11.

Raines M. A. and Dewers T. A. (1997) Mixed transport/ reaction control of gypsum dissolution kinetics in aqueous solutions and initiation of gypsum karst. *Chem. Geol.* **140,** 29-48.

Reddy M. M. and Nancollas G. H. (1973) Calcite crystal growth inhibitions by

phosphonates. *Desalination.* **12**, 61-73.

Reddy M. M., Plummer L. N., and Busenberg E. (1981) Crystal growth of calcite from calcium bicarbonate solutions at constant P_{CO2} and 25°C: A test of a calcite dissolution model. *Geochim. Cosmochim. Acta.* **45**, 1281-1289.

Rickard D. T. and Sjoberg E. L. (1983) Mixed control of calcite dissolution rates. *Amer. J. Sci.* **283**, 815-830.

Sanders W. E. (1998) *Rate and Mechanism of Barite Mineralization at Zodletone Mountain, Southwestern Oklahoma,* Masters Thesis. University of Oklahoma.

Satman A., Ugur Z., and Onur M. (1999) The effect of calcite deposition on geothermal well inflow performance. *Geothermics* **28**, 425-444.

Schindler P. W. and Stumm W. (1987) The surface chemistry of oxides, hydroxides, and oxide minerals. In *Aquatic Surface Chemistry* (ed. W. Stumm). pp. 83-110. J. Wiley & Sons.

Schott J., Brantley S., Crerar D., Guy C., Borcsik M., Willaime C. (1989) Dissolution kinetics of strained calcite. *Geochim. Cosmochim. Acta.* **53**, 373-382.

Shiraki R. and Brantley S. L. (1995) Kinetics of near-equilibrium calcite precipitation at 100°C: An evaluation of elementary-reaction based and affinity-based rate laws. *Geochim. Cosmochim. Acta.* **59**, 1457-1471.

Sjoberg E. L. and Rickard D. T. (1984) Temperature dependence of calcite dissolution kinetics between 1 and 62°C at pH 2.7 to 8.4 in aqueous solutions. *Geochim. Cosmochim. Acta.* **48**, 485-493.

Stipp S. L. and Hochella M. F, Jr. (1991) Structure and bonding environments at the calcite surface observed with X-ray photoelectron spectroscopy (XPS) and low energy electron diffraction (LEED). *Geochim. Cosmochim. Acta.* **55**, 1723-1736.

Stumm W. and Morgan J. J. (1996) *Aquatic Chemistry, Chemical Equilibria and rates in Natural Waters.* John Wiley and Sons, Inc.

Stumm W. and Wieland E. (1990) Dissolution of oxide and silicate minerals: Rates depend on surface speciation. In *Aquatic Surface Chemistry* (ed. W. Stumm). pp. 367-400. J. Wiley & Sons.

Talman S. J., Wiwchar B., Gunter W. D., and Scarge C. M. (1990) Dissolution kinetics of calcite in the H_2O-CO_2 system along the steam saturation curve

to 210°C. In *Fluid-Mineral Interaction* (ed. R. J. Spencer and I. M. Chou); *Geochem. Soc. Spec.* **2**, 41-55.

Teng H. H., Dove P. M., and De, Y. J. (2000) Kinetics of calcite growth: surface processes and relationships to macroscopic rate laws, *Geochim. Cosmochim. Acta.* **64**, 13, 2255-2266.

Van Cappellen P., Charlet L., Stumm W., and Wersin P. (1993) A surface complexation model of the carbonate mineral-aqueous solution interface. *Geochim. Cosmochim. Acta.* **57**, 3505-3518.

Walter L M. (1986) Relative efficiency of carbonate dissolution and precipitation during diagenesis: A progress report on the role of solution chemistry. *J. Sediment Petrol.* **56**, 1-11.

Wollast R. (1990) Rate and mechanism of dissolution of carbonates in the system $CaCO_3$-$MgCO_3$. In *Aquatic Chemical Kinetics* (ed. Stumm W.) pp. 431-445. Wiley.

Zhang Y, Shaw H., Farquhar, R., Dawe R. (2001) The kinetics of carbonate scaling— application for the prediction of downhole carbonate scaling, *Journal of Petroleum Science and Engineering* **29**, 85-95.

Zhong S. and Mucci A. (1989) Calcite and aragonite precipitation from seawater solutions of various salinities: Precipitation rates and overgrowth compositions. *Chem. Geol.* **78**, 283-299.

Zuddas P. and Mucci A. (1994) Kinetics of calcite precipitation from seawater: I. A classical chemical kinetics description for strong electrolyte solutions. *Geochim. Cosmochim. Acta* **58**, 4353-4362.

Zuddas P. and Mucci A. (1998) Kinetics of calcite precipitation from seawater: II The influence of the ionic strength. *Geochim. Cosmochim. Acta.* **62**, 757-766.